UNIVERSITY OF NAPLES FEDERICO II
School of Polytechnic and Basic Sciences

Department of Structures for Engineering and Architecture

PH.D. PROGRAMME IN STRUCTURAL, GEOTECHNICAL AND SEISMIC ENGINEERING - XXIX CYCLE
COORDINATOR: PROF. LUCIANO ROSATI

FABIANA DE SERIO
Ph.D. Thesis

MASONRY STRUCTURES MODELLED AS ASSEMBLIES OF RIGID BLOCKS

TUTORS: PROF. ING. MARIO PASQUINO
PROF. ARCH. MAURIZIO ANGELILLO

2017

Acknowledgements

During the course of my studies, I have had the privilege of knowing an exceptional life mentor: I would like to express my deepest gratitude to Professor Mario Pasquino, who guided me since my bachelor's degree, and then gave me the opportunity to make this PhD experience possible, assisting me professionally and, especially, humanly.

My biggest gratitude goes to an extraordinary Professor, Maurizio Angelillo, who believed in me and motivated my interest in the matter, with his invaluable advice, knowledges and unwavering guidance. It was because of his intuitions and persistent help that the development of this dissertation has been possible.

A special 'thank you' goes to Professor Antonio Gesualdo and my colleague Antonino Iannuzzo, our cooperation and friendship was particularly inspiring and cheering during these years.

I am profoundly grateful to the Coordinator of this PhD course, Professor Luciano Rosati, for his support during these three years and for the interest showed in my research.

In addition, I would also like to sincerely thank the reviewers of my PhD thesis, Professor Santiago Huerta and Professor Elio Sacco, their opinion and compliments have been very important to me, representing a big encouragement to continue in the field of scientific research.

I am extremely grateful for the loving care of my adorable husband Alessandro, for following me closely during this work experience, for his invaluable presence and constant encouragement and help, even when being far away.

I cannot forget my dear friends Mara, Silvia and Maria Grazia, for giving me all their love and comfort and for being always there when I needed it.

Above all, I want to thank my wonderful parents, for their countless sacrifices to see me happy, for their support and encouragement throughout my studies; and my lovely brother and sister for their affection and esteem towards me.

Without these people this thesis would not have been completed.

Fabiana De Serio

Abstract

The broad topic of the present work is Statics and Kinematics of masonry structures made of monolithic blocks, that is rigid bodies submitted to unilateral constraints, loaded by external forces, and undergoing small displacements. Specifically, in this work, we study the effect, in term of internal forces, of specified loads, by using given settlements/eigenstrains to trigger special regimes of the internal forces.

Although our main scope here is the analysis of masonry structures made of monolithic pieces, and whose blocks are not likely to break at their inside, the theory we use applies also to general masonry structures, such as those made of bricks or small stones. Such structures may actually fracture everywhere at their inside, forming rigid blocks in relative displacement among each other. If the partition of the structure is fixed in advance, we may search the displacement field **u**, which is a possible solution of a displacement type boundary value problem, by minimizing the potential energy $\wp$ of the loads, over the finite dimensional set of the rigid displacements of the blocks. Actually, the functional $\wp$ is linear in **u**, then, if the supports of the strain singularities, i.e. the potential fractures, are fixed in advance, the minimization of $\wp$ reduces to the minimization of a linear functional under linear unilateral and bilateral constraints.

This simple theory, based essentially on Heyman's model for masonry, is applied to cantilevered stairs, or, more precisely, to spiral stairs composed of monolithic steps with an open well. In the present work, a case study, the triple helical stair of the convent of San Domingos de Bonaval is analysed, by employing a discrete model.

The convent of San Domingos de Bonaval, founded by St. Dominic de Guzman in 1219, is located in the countryside of San Domingos, in the Bonaval district of Santiago de Compostela. The majority of the buildings of the convent which are still standing, were built between the end of XVII and the beginning of XVIII centuries in Baroque style by Domingo de Andrade. A triple helical stair of outstanding beauty and structural boldness was also built by Andrade to connect the cloister with the stairs of the main building. This extraordinary triple helical staircase consists of three separate inter-woven coils, composed of 126 steps each. The three separate ramps lead to different stories and only one of them comes to the upper viewpoint. The steps are made of a whole stone piece of granite; they are built in into the outer cylindrical wall for a length of 0.3 m, and set in an inner stone rib. The steps do not apparently join (or even touch) each other but at their very end.

A likely set of given settlements of the constraints is imposed on the structure, and the corresponding piecewise rigid displacement is found by minimizing the potential energy. Then the dual static problem is dealt with, by identifying the equilibrium of the individual steps and of the entire structure.

The whole calculation procedure is carried out with the programming language Matlab. After a comparative analysis of the results, in particular with reference to the internal forces and internal moments diagrams (torsional and flexural moments, axial and shear forces) for all the steps, a possible explanation of the reason why such bold structure is standing safely, is given.

Keywords: *masonry, unilateral materials, helical stairs, rigid blocks, settlements.*

Summary

Chapter 1

OVERVIEW ON MASONRY STRUCTURES

1.1 Prologue

Old masonry constructions

Advances in materials science have made possible the design of materials based on the functional optimization of the mechanical properties. Through the modern homogenization technique, which describes the material behaviour at a macroscopic level, taking into account the material properties at micro or mesoscopic level, it is possible to functionally tuning the macroscopic properties of materials.

Nowadays, it is also possible to represent the plasticity of materials, by quantifying the dislocation of their component crystals, and to simulate the propagation and nucleation of fractures in brittle materials.

In this context of progress and innovation, and where attention to seismic safety is in continuous growth and development, masonry buildings are perceived by most of the modern technicians as old and unreliable constructions, due to the inherent weakness of material when compared to the strength and reliability of modern materials.

However, when we are faced with a masonry construction, as an arch, a tower or a dome, we are inevitably impressed and fascinated by its undeniable expressive force, which leads us to preserve and keep it, as unquestionable heritage for the community [1].

Besides, as Heyman observes [2], "the fact remains that two severe earthquakes only slightly damaged Hagia Sophia (Fig. 1.1), and the bombardments of the Second World War often resulted in a medieval cathedral left standing in the ruins of a modern city. At a much less severe level of disturbance, the continual shifts and settlements of foundations experienced over the centuries seem to cause to the masonry structures no real distress", giving evidence that masonry constructions exhibit an extraordinary stability.

Heyman notes that ancient and medieval structures are characterized by low stresses, so that they work at a stress level which is one or two orders of magnitude below the

crushing strength of the material. This condition, combined with correct proportions and geometry, may explain the survival of these kind of structures through the centuries.

Masonry constructions are, indeed, massive structures (Fig. 1.2) and their safety and stability are mainly provided by geometry and geometric proportions of the building (Fig. 1.3) (so that structural forces may be adequately accommodated), while strength plays a secondary role ([2], [3]).

These concepts were clear to old master masons, who had an intuitive understanding of forces and resulting stresses, consolidated through successive experiences, trials and errors, and whose knowledge has been handed down over time, for centuries, verbally or by drawing (Fig. 1.4).

Fig. 1.1: Interior of the basilica of Hagia Sophia (Istanbul)

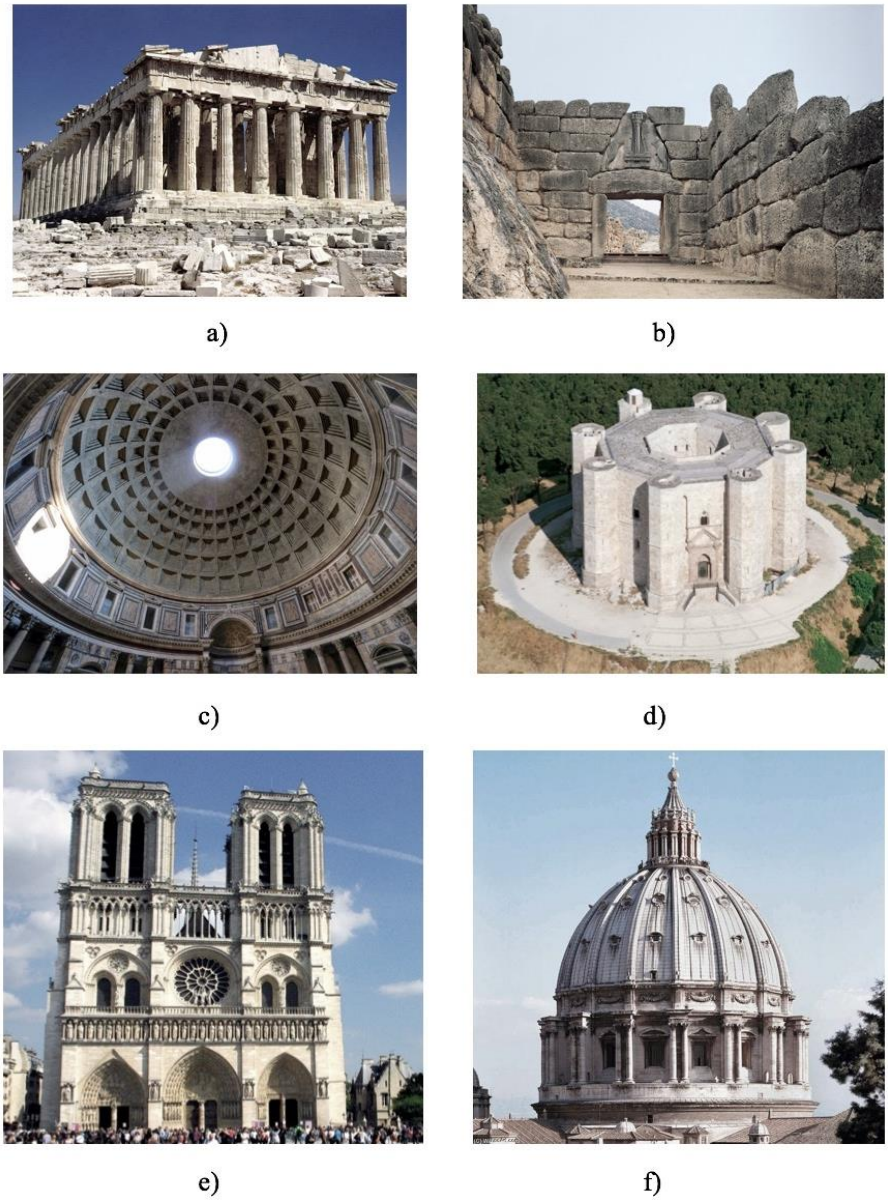

Fig. 1.2: Examples of masonry constructions a) Parthenon (Atene, Greece); b) Lion Gate (Micene, Greece); c) Pantheon (Rome); d) Castel of the Mountain (Andria, Italy); e) Notre Dame Cathedral (Paris); f) St. Peter's dome (Rome)

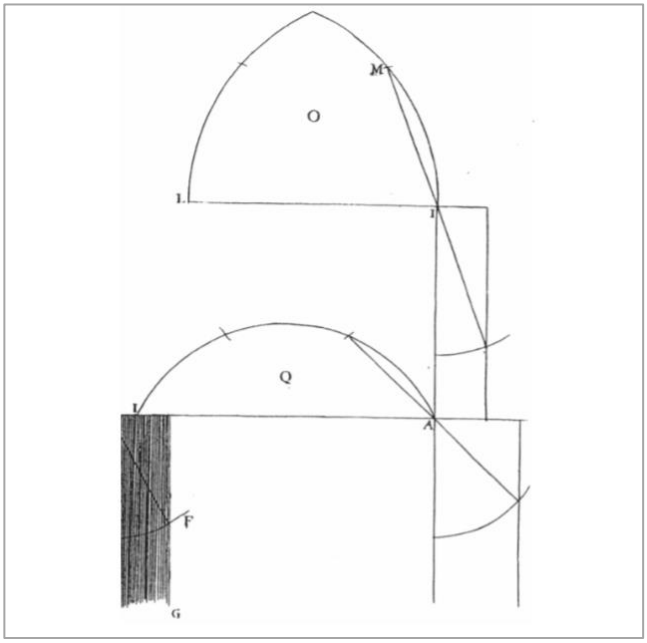

Fig. 1.3: An example of rules of proportion: Derand's rule for buttress design [4], [5]

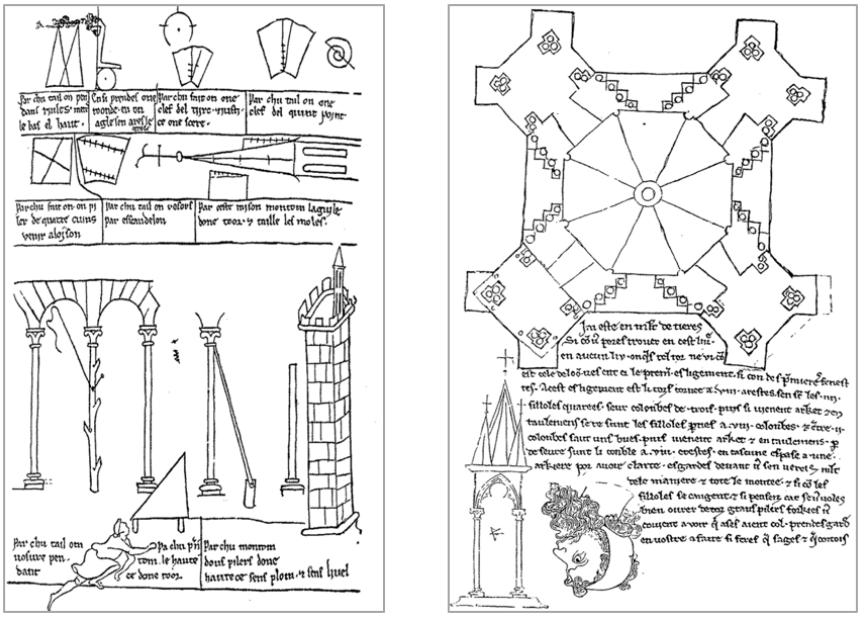

Fig. 1.4: Pages of sketchbook of Villard de Honnecourt (from Willis 1859) [2]

Unilateral behaviour

The statics of a masonry element can be compared to the equilibrium of cables, as both the cable and the masonry element are composed by a material that can be modelled as *unilateral.* A typical demonstration of this association can be recognized in Gaudì's masterpieces: Gaudì hung chains of various lengths close to each other, arranging them so as to achieve the desired result (Fig. 1.5a); then he put a mirror below the built structure, in order to perceive the effect from the bottom upwards and exploited this to realize his architectural works. Among these, the most famous is the Sagrada Familia, in Barcelona (Fig. 1.5b).

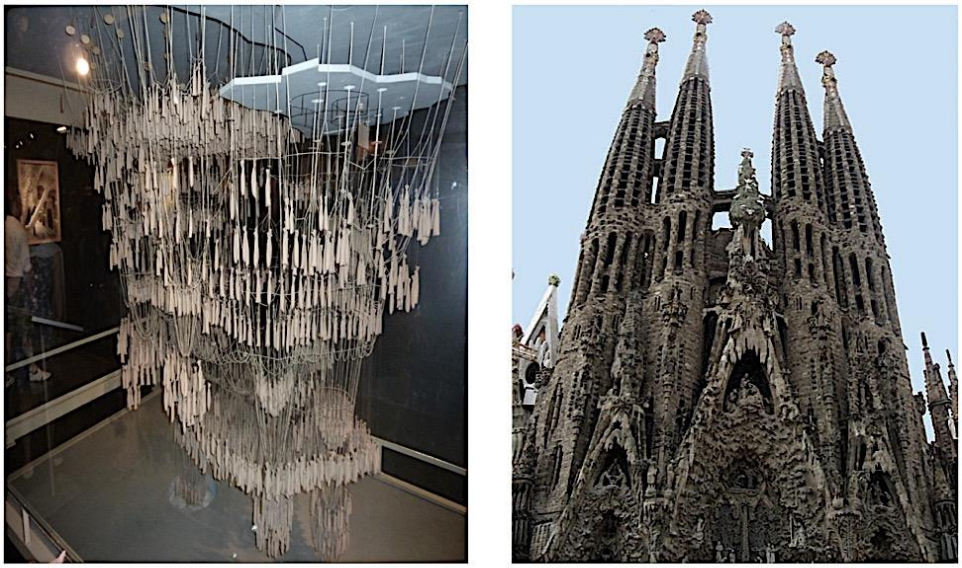

a) b)

Fig. 1.5: Sagrada Familia, Gaudì (Barcelona):
a) Catenary model; b) View of the frontal façade

Since ancient times, masonry buildings were built by relying on the material's compressive strength only. Masonry is, indeed, an elastic-brittle composite material, characterized by a very low tenacity and cohesion compared to the acting forces; both mortar and blocks, although sometimes of poor quality, exhibit a very low tensile strength, which varies based on how the blocks are relatively positioned among each other and how the mortar adheres to the blocks. Therefore, it seems safer to neglect tensile strength for these materials, and to assume a unilateral behaviour, in the sense that masonry material is incapable to resist tensile forces; the cable behaves in the opposite way, being able to withstand traction and no compression (Fig. 1.6).

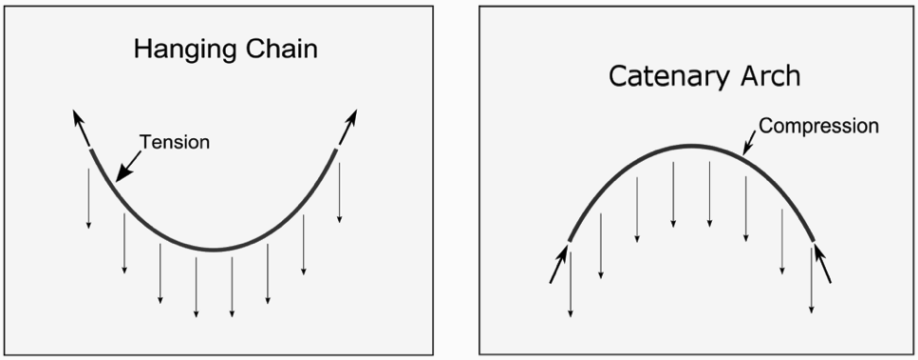

Fig. 1.6: Unilateral behaviour for cables and masonry elements

Quality of masonry

Masonry is a composite material made of blocks and mortar. The size and the nature of the blocks can be very different from one type of masonry to another (see [1], [6]), but what it must be understood is that the way in which the stones are put in place is not random. Indeed, any masonry structural element is not a bunch of individual elements arranged casually, but rather a collection of well-organized units. The science of cutting and organizing the stone pattern in masonry is called strereotomy (see [7]).

In real masonry structures, one can usually identify large planar joints (e.g. horizontal joints in walls) through which large compressive forces are exerted and where, due to friction, sliding is not possible; on planes across which the transmission of compressive forces is feeble or absent (e.g. vertical planes in walls), the stones are interlocked so as to contrast sliding.

The basic idea is that the main objective of the construction apparatus, realized through stone cutting geometry (stereotomy) and proper block disposition, is to avoid sliding. For example, in a wall, sliding is contrasted by interlocking along vertical planes and by friction on horizontal planes.

The model of Heyman

A simple way to describe the behaviour described above, is due to Heyman with his model [8], condensed into three basic assumptions: the material is not capable to transmit any tensile force; fractures, which are of pure detachment, occur without sliding; the material is rigid in compression.

Heyman's model is a valuable tool for the analysis of masonry structures, based on their unilateral behaviour. For an arch, for example, the unilateral behaviour of masonry gives, as an effect, the thrusts in correspondence of the abutments.

1.2 The masonry arch and the line of thrust

Thrust

The essential elements of masonry constructions can be understood by studying arches. These structures, which were invented some 6000 years ago in Mesopotamia, are usually composed by individual voussoir stones in mutual contrast among each other. In the manual *"La pratica del fabbricare"*, written by Carlo Formenti (see [9]), the arches are defined as curved structures, whose pieces maintain equilibrium through mutual contrast (Fig. 1.7b). These blocks, subject to the force of gravity, transmit inclined forces whose line of action is contained within the masonry, and whose vertical component increases from the keystone to the springings, while the horizontal component remains constant (Fig. 1.7a). Then, an inclined force, called thrust force, is transmitted down to the springings, and must be resisted by the buttresses.

Thrust line

The arch is in equilibrium if the thrust, transmitted by the stones, is contained within the geometry of the arch; thus, a set of compressive stress equivalent to the thrust is obtained, and the locus of the points of application of the thrust is called *line of thrust*. Since the arch is a statically redundant structure, it can be in equilibrium under infinite states of internal stress and usually there exist infinite regimes of internal compression.

The line of thrust is exactly the opposite of the equilibrated funicular polygon of a cable that maintains the equilibrium among the same forces, as discovered by Hooke and hidden in his famous anagram "*Ut pendet continuum flexile, sic stabit contiguum rigidum inversum*" (1675), in which he recognized the mathematical correspondence between the suspension bridge and the masonry arch (Fig. 1.8).

In the centuries that followed, Hooke's idea has been used to understand the arch behaviour through new graphical tools, in particular by using the graphical analysis in order to determine possible equilibrium states. A compendium of old and new results on masonry arches, can be found in [7] and [10]. A real case, which demonstrates this type of equilibrium, can be observed for example in the Trevi's arch (Fig. 1.9), where, in the analysis, a distributed effect of the weight of the stone, rather than concentrated, is assumed.

For a stone voussoir arch, it is possible to obtain an equilibrium solution of pure compressive forces, by imagining that the weight of each voussoir is supported by two compressive forces, which act through the contact surfaces between adjacent blocks (Fig. 1.7b).

The line of thrust can be determined mathematically by solving a differential equation of the type $y''=q/H$, where y is the y-coordinate of the line of thrust, q is the given load per unit projected length and H is the horizontal thrust. A simple case is described in [11], where the second order equation of the thrust line and the value of the thrust in an arch, are obtained for some simple examples. The thrust is the main feature of the arches and vaults, determining their structural behaviour, and, according to the thrust value, the structures that support them must be designed.

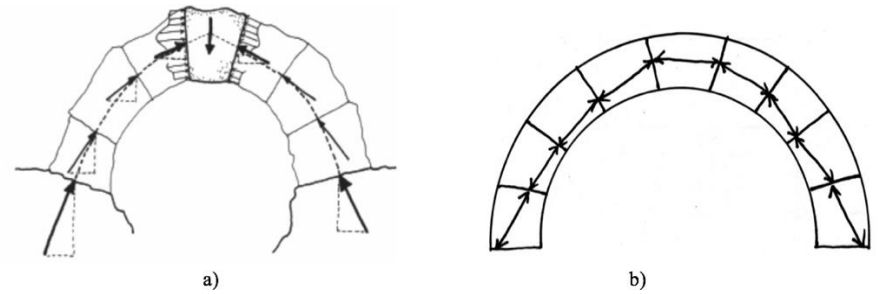

Fig. 1.7: Masonry arch:
a) Etruscan voussoir arch (Durm, 1885) [12]; b) Mutual contrast effect in voussoir arch

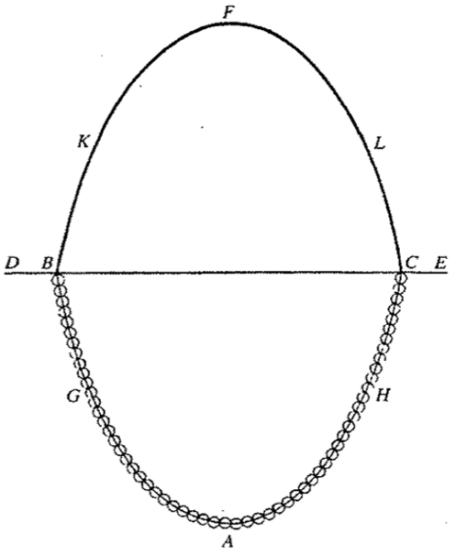

Fig. 1.8: Hooke's hanging chain [2]

Fig. 1.9: Trevi's arch

Remark 1. In [11], some differences between the equilibrium of cables and the equilibrium of arches are pointed out:

1. the cable is a 1d structure that changes its geometry in order to satisfy the equilibrium with the external loads, while the arch is a 2d structure that, maintaining unchanged its initial shape, search inside itself a pressure line in equilibrium with the external loads;
2. for a cable, of fixed length, there is only one equilibrium geometry, while for an arch there are infinite possible pressure lines;
3. the unilateral condition for the cable is expressed by imposing that the axial force is a tensile force and that this axial force is tangent to the cable, regarded as a 1d structure, while for the arch it is required that the axial force is a compressive force and also that the pressure line is point by point inside the contour of the arch.

Safety of the arch

Therefore, in the case of a masonry arch, it is possible to find an admissible equilibrium solution if one of the infinite lines of thrust can be found, compatible with the unilateral assumption of the material, namely entirely contained within the masonry. There exists a minimum thickness, able to contain only one thrust line. On the basis of this minimum value, a geometric safety coefficient can be introduced, thanks to which it is possible to assess the safety of the structure against collapse [2].

Rules of proportions

The aim of masonry architecture has always been to ensure that the arch would remain upright and that the buttresses could absorb the thrust safely, in order to guarantee the life of the building for centuries or millennia. In this context, one wonders how the design rules were formulated, since the scientific theory of structures was rationally introduced only in the nineteenth century.

There was, obviously, another kind of theory, not scientific but certainly effective, based on the geometrical rules of proportions, resulting from trials and errors, and critical observation of the masonry building process.

The effect of settlements

The most apparent consequence of the essentially unilateral behaviour of masonry is the likely appearance of widespread crack patterns, due to settlements or other disturbances of the environment.

As it is observed in [13]"…One could say that, in absence of any settlements or relative movements of the boundary, that is in absence of fractures, the structure is silent. When a fracture pattern appears, the structure speaks and tells us a part of its equilibrium story. If an arch is not fractured, the presence of the thrust is a purely speculative fact; but if cracks open up and three hinges form at the key and at the springings, we have a plastic hint of the force pattern..".

For example, the arch in Fig. 1.10, subjected to its own weight, is in equilibrium, since it is possible to find a thrust line (dashed line in Fig. 1.10a) entirely contained within the arch. If the presence of a horizontal settlement determines a mechanism in which three

hinges are formed (Fig. 1.10c), one of them at the extrados top and the other two at a certain height at the intrados, next to the abutments, then the thrust line must pass through these three hinges (Fig. 1.10b).

Therefore, the settlement determines in the arch a mechanism which selects, among the possible infinitely many thrust lines, the actual thrust line. The arch becomes a statically determined structure, the thrust line is uniquely determined, and it is possible to know the real forces which ensure the equilibrium of the structure.

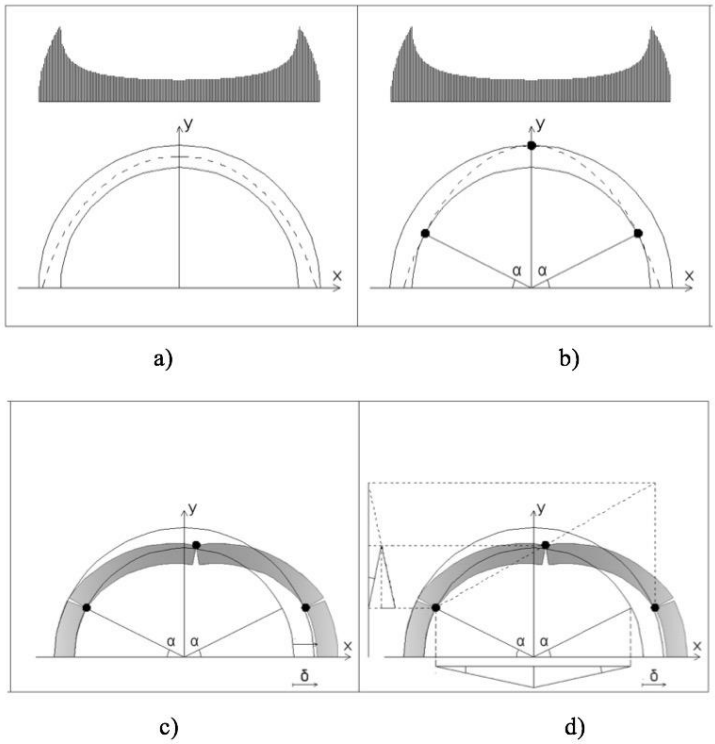

Fig. 1.10: Equilibrium of a masonry arch:
(a), (b) Line of thrust;
(c), (d) Collapse mechanism for a masonry arch due to settlements

An energy criterion

By considering the positions of the hinges at the intrados as unknowns, the total energy of the system can be minimized with respect to these positions. The optimal position of these hinges, obtained through minimization of the potential energy $\wp$, is shown in Fig. 1.10d. Such position coincides with the points at which the thrust line, passing through the extrados top hinge, is tangent to the intrados line (see Fig. 1.10b)

The displacement is compatible with the given settlements, the internal forces are compressive, in equilibrium with the given load, and reconcilable with the displacements. Then this is a simple example of solution of a mixed boundary value problem, for a structure made of Heyman's material.

1.3 Some historical notes

Geometrical rules

It should certainly be highlighted that the medieval builders developed a deep understanding of masonry behaviour, although they did not know anything about mathematics, elastic theory and strength of materials. However, this non-scientific approach is difficult to accept, without prejudice, by modern architects and engineers, who instead feel more confident with an approach based on the concept of strength.

Vitruvius recognizes in Ezekiel's chapters the 'great measure', namely rod, used by the ancient builders in the absence of standard units, and also gives, in his *ordinatio*, proportions for the construction. In the 'dark age', his book was copied again and again for use in monastic schools and in the masonic lodges and the rules of proportion became the heart of the Gothic buildings. They were geometrical rules, found to be effective for buildings whose materials worked at low stresses [14].

Galileo

Galileo, in his *Discorsi* (1638), writes about the strength of materials and brilliantly points out that all these rules, which were mainly proportional, were wrong from the point of view of the strength, because of the square/cube law (that is the weight of any structure rises with the cube of the linear dimensions and the section of the members with the square). So, stresses grow linearly with the size of the structure. Although this condition is true and relevant for the modern structure, which are working very near the limit stresses, it is irrelevant for all the structures in which the stresses are very low, like masonry structures, for which Galileo's law does not apply [3].

Hooke

Hooke showed how arches worked, in a physical sense, through experiments on model arches, and he protected his intuitive understandings into anagrams, published in 1675, even if he could not provide the corresponding mathematical analysis. The solution of his anagram that is *'as hangs the flexible line, so but inverted will stand the rigid arch'*, was published only after his death. However, Hooke knew that by solving the problem of the catenary shape problem, he would at the same time found the corresponding arch shape able to carry the same loads in compression.

Gregory

The mathematical analysis of the catenary problem is given by Gregory in 1697, who states that if any thrust line can be found lying within the masonry, then the arch will stand. Gregory's approach was followed by Poleni, in his study of St. Peter's dome (Fig. 1.11), and by La Hire (Fig. 1.12), who invented the force polygon and the corresponding funicular polygon for the arch and realized that a necessary condition to ensure the arch stability was the presence of friction between the voussoir interfaces, to prevent sliding.

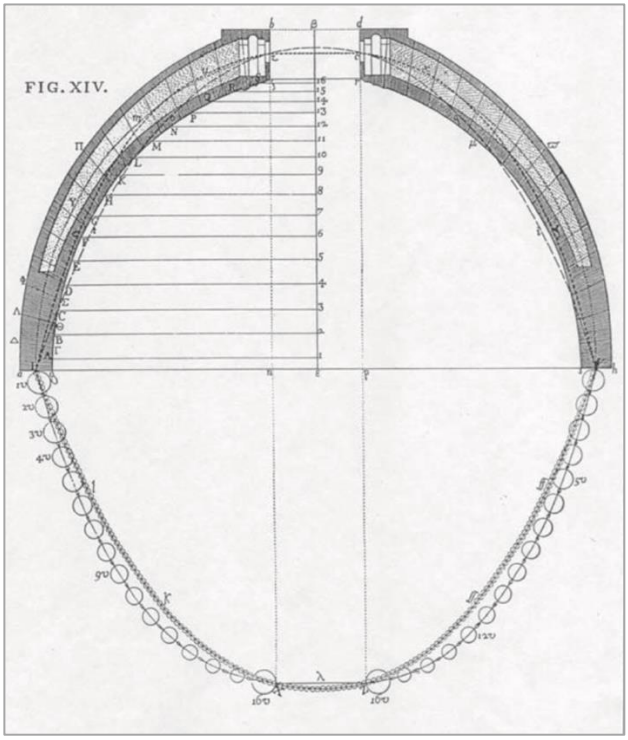

Fig. 1.11: St. Peter's dome: Poleni's hanging model constructed to check the stability of St. Peter's dome (Poleni, 1748) [15], [16]

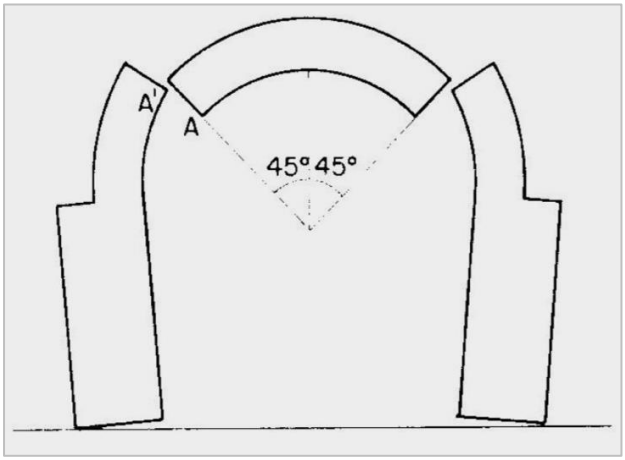

Fig. 1.12:Wedge theory, De La Hire

La Hire

La Hire (in his books of 1695 and 1712) aimed to determine the value of the arch thrust, so that the abutments could be designed and then he concluded that the arch would break at a section, somewhere between the springings and the keystone, in which a 'hinge' is developed. The concept of 'hinge', through which the forces within the arch pass, unlocks the statics of the arch, since the forces and the corresponding stress may be found and then the stability of the whole structure can be obtained.

Couplet

Two remarkable memoirs on arch thrust were written by Couplet in 1729 and 1730. In the first work, Couplet referred to La Hire's analysis of frictionless case and evaluated the forces imposed by an arch on its centering during construction; in the second work, by making precise assumptions about material properties, he realized that voussoirs were bound together without sliding thanks to friction whilst no resistance to separation was offered. In his works, he assumed that ambient stresses are so low that crushing strength is of little importance.

Couplet's statements are summarized in the three key assumptions about masonry material, that is masonry has no tensile strength, it has an infinite compressive strength and sliding failure cannot occur.

Two ways of approaching any structural problem are demonstrated in Couplet's works, namely a static approach, in which the equilibrium is applied and the thrust line is considered, and a kinematic approach, in which a pattern of hinges determine a mechanism of the structure. Couplet then arrived to a sort of 'safe theorem', by stating that an arch will not collapse if the chord of half the extrados does not cut the intrados, but lies within the thickness of the arch; he also attempted to determine the least thickness of a semi-circular arch, which could carry only its own weight, finding the ratio t/R equal to 0.101, being t the thickness of the arch and R its radius, and placing at 45° the hinges positions. Some two hundred years later, Heyman will determine the correct position of the hinges (which is 31° from the springings) and the correct ratio t/R (which is 0.106), even if these different results do not have a substantial effect on the analysis.

Finally, Couplet, by following La Hire's approach, determined the value of the abutment thrust for a generic arch, and then he found that the thrust at the crown act horizontally and could consequently evaluate the magnitude of the abutment thrust, through which the piers' dimensions could be evaluated.

Danyzy

Couplet's contribution was crucial for a correct and complete solution to the problem of arch design, in 1732 an experimental confirmation of his approach was given by Danyzy (see for example Fig. 1.13 in which Danyzy indicates the use of arch and buttress plaster models to investigate collapse mechanisms due to support displacements), and by 1740 this theory could be applied more generally to the analysis of masonry.

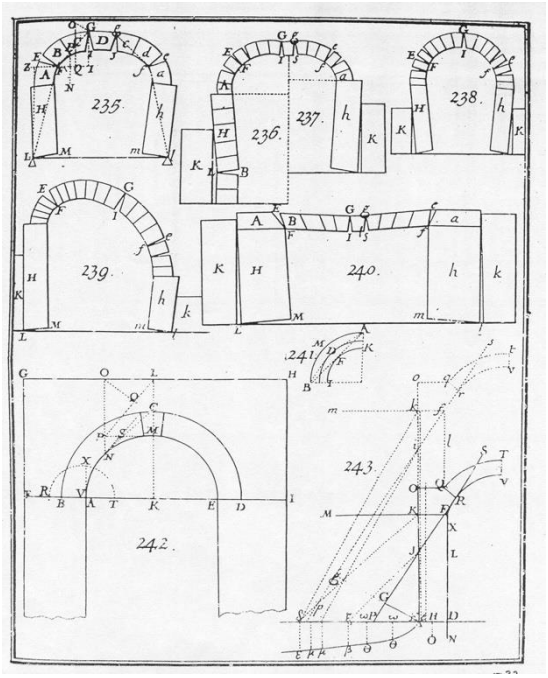

Fig. 1.13: First experiments on the collapse of arches with small gypsum block models, Frézier (1739) [14]

Other contributions to the old theory

In 1743, Poleni gave his contribution in a report on St. Peter's dome, where meridional cracks had opened up; thanks to the previous discoveries by La Hire, Couplet, Hooke and Gregory, he determined, through equilibrium considerations, experimentally the thrust line and, he et al., also suggested the installation of extra ties in order to contain the horizontal thrust.

Coulomb

A big contribution to the major problems of civil engineering, that is the strength of beams and columns and the thrust of soil and arches, was given by Coulomb in 1773. Coulomb's solutions were obtained by combining equilibrium equations with a knowledge of material properties. In particular, Coulomb's solutions for arches are only marginally referred to the strength of the material (masonry), being rather a search of stability through the equilibrium, coupled by principles of maximum and minimum. Thus, he did not examine the strength of the arch, but rather its working state, that is the numerical value of the thrust.

The theory of masonry arches was rigorously completed by Coulomb, who, assuming that slip among stones was prevented by friction, stated that in practice failure always occur when a sufficient number of hinges between voussoirs are developed. Coulomb also defined the minimum and maximum thrust values, within which the arch can be considered stable. His work was assimilated slowly into the technical education of

French engineers, as Navier; a definitive exposition of arch theory was given in 1845 by Villarceau, who developed a 'safe' inverse design method, presented in the form of tables, by imposing that the centre line of the arch must coincide with one of the infinite possible thrust lines for the given loads.

Navier

Claude-Louis Navier (1785-1836) can be considered the father of the modern theory of elasticity. Navier's design philosophy involves the postulation of an elastic law of deformation and the assumption of certain boundary conditions that arise in the solution of the problem. It was, of course, Navier's linear-elastic philosophy that became paramount and was virtually unquestioned for a century and a half as the correct approach to structural design. The *middle third rule* for the arches, which states that the arch is safe if the line of thrust passes within a certain fraction of the thickness, say 1/3, arises since Navier, within the theory of elasticity applied to a beam, finds that the stress profile is linear; in this case, the section is wholly compressed if the centers of pressure are within the middle third of the section.

Castigliano

In 1879, Castigliano applied his energy theorem to masonry bridges, by assuming elastic properties of the stone and mortar, and he obtained solutions for which the bridge did not crack if the thrust line falls within the middle-third of the cross section. However, in the case of masonry, the theory of elasticity is of little help, as well as the middle third rule; the right condition, as Heyman emphasizes, is that the thrust line lies within the geometry of the arch.

The new theory

Pippard et al. (1936, 1938) showed that, referring to steel voussoirs arch, slightest imperfections of fit were able to transform an hyperstatic arch into a statically determinated three-pin arch; Pippard also attempted to interpret his results by applying principles of minimum elastic energy.

Only by the twentieth century, when the plastic theorems are introduced, the 'equilibrium' approach of Poleni, Coulomb and Villarceau is justified in order to be applied to the study of masonry construction.

The necessary assumptions for the application of plastic theory to masonry structures are the same assumptions made by Couplet: masonry has no tensile strength, masonry has an infinite compressive strength and sliding does not occur; these assumptions are used by Kooharian, in 1953, to prove that the analysis of masonry structures could be done in the framework of plasticity, and that the Theorems of Limit Analysis could be employed [17].

Referring to a hinge opened in a voussoir construction, he considered the yield surface of plastic theory, by assuming that the axial load N was transmitted at the hinge and then by evaluating the corresponding effective moment. Since nominal stresses are likely to be less than the acceptable value of 10 per cent of the crushing strength, suggested by Villarceau in the nineteenth-century, the portion of yield surface is usually very restricted.

The 'safe' theorem of plasticity states that if all stress resultants are equilibrated with the loads and lie within the yield surface, then the construction is safe, and cannot collapse. The power of this theorem lies in the fact that if it is possible to find any one safe state, then the structure is safe. Referring to an arch, this means that if it is possible to find, among the infinite thrust lines, one equilibrating the applied loads and located within the arch profile, then the arch will not collapse under those loads and it is stable.

In general, when we approach masonry constructions, subject to low mean stresses, we can apply design rules ensuring that the shape of the structure conforms to the shape required by statics; these rules are purely geometric.

1.4 Organization of work

This PhD thesis is structured into five chapters.

In *Chapter 1* an overview of masonry structures is given; then, the essential aspects that characterize the behaviour of masonry materials, which were the design criteria since antiquity, are described. Finally, some historical notes about design criteria are exposed, that led to the modern Heyman unilateral model, recognized as a valuable tool for describing the behaviour of a broad class of masonry structures.

In *Chapter 2* the characteristic features of unilateral material are set out in detail, also recalling the main experimental evidence regarding fracture modes and failure mechanism affecting the masonry structures. In addition, the three basic assumptions of Heyman's model are analysed and the essential aspects of simplified uniaxial models, namely model zero, one and two, are exposed, referring both to the case 2D and 3D. A mention is also made for refined models. Finally, some observations and experimental data are reported, related to the mechanical behaviour of masonry.

In *Chapter 3* the equations governing the problem of NRNT material (Normal Rigid No-Tension material) are reported, stating the reasons for which it is possible to study the equilibrium of masonry structures with the tools offered by Limit Analysis. Starting from the definition of the boundary value problem, singular stress and strain fields can be used for unilateral material, such as line Dirac deltas. The equilibrium problem and the kinematical problem are described, making reference to statically admissible stress fields and to kinematically admissible displacement fields, and also defining the compatibility of loads and distortions.

Finally, the theorems of Limit Analysis are set out, these being closely connected with the compatibility of loads and, consequently, with the equilibrium problem.

The kinematic problem is solved by employing an energy approach. In particular, for unilateral materials, under Heyman's assumptions, it is possible to solve the kinematic problem by minimizing the only potential energy associated with the loads.

In *Chapter 4* a simple model, based essentially on Heyman's hypotheses, is applied to study the equilibrium of masonry structures made of monolithic pieces, in particular

cantilevered stairs, or, more precisely, spiral stairs, composed of monolithic steps, with an open well are analysed.

As observed by Heyman, the basic structural action for a cantilevered stair of small flight (quarter or half landing) is twist of individual treads, leading to shear stresses in the masonry; such stresses are low for short stairs, but become more and more harmful than direct compression for long flights. In a recent work by Angelillo, based on a continuous approximation of the stair structure, it is shown as the torsional Heyman's mechanism can be combined with a Ring-Like regime, giving rise to large compressive forces and to moderate torsional torques, whose intensity reaches a plateau for long flights. A practical confirmation of the complementarity of Heyman and Ring-Like stress regimes is here obtained, for the case study of the triple helical stair of San Domingos de Bonaval, by employing a discrete model. In order to generate statically admissible sets of internal forces, likely sets of given settlements of the constraints are considered and the corresponding piecewise rigid displacements are found by minimizing the potential energy. The moving part of the structure is statically determined, then the dual static problem is dealt with by solving the equilibrium of the entire structure and of the individual steps. The whole calculation procedure is carried out with the programming language Matlab.

In *Chapter 5* the final considerations about the analysis procedure are given, highlighting the potential for its application in order to analyse also the equilibrium of other kinds of structures, modelled as an assembly of rigid blocks.

Chapter 2

UNILATERAL MODELS FOR MASONRY

Prologue. The main aspect of masonry materials is their physiological weakness under tensile loading, which may produce a sense of fear and lack of confidence in modern engineers, especially when diffuse crack patterns emerge at masonry surfaces. Actually, despite masonry material being rather weak under tensile stresses, when masonry structures present a well-proportioned geometry and load distribution, they work essentially in a compression regime, showing only local and limited sliding on internal surfaces and exhibiting a remarkable stability [3].

Besides their correct proportions and the absence of overall sliding, it is precisely their weakness in tension which enables them to accommodate all the possible, and likely, small changes of boundary conditions (such as those produced by ground settlements or small disarrangements of the stones) with displacement fields which are essentially piecewise rigid and require barely any energy cost.

The price to pay is the appearance of widespread fracture patterns, which, at first sight, may look as if dangerous, but most of times are irrelevant and may be forgotten, even for centuries, by closing the cracks structurally (e.g. with the *scuci-cuci* patching method) and covering them with plaster.

The way in which they accommodate these unavoidable disturbances, with very small elastic deformations, scant irreversible deformations and only slight changes of the geometry, does not compromise the equilibrium of the structure and confers to masonry structures a peculiar stability.

This stability is mainly guaranteed by the shape when the average stress level is low, as observed by Heyman [2]. Geometrical rules of proportion were, in fact, fundamental in ancient structural design, (as an example for Gothic buildings) and, when correctly applied, lead to stable masonry structures (see [18], [19]). The survival through the centuries of ancient masonry buildings has been possible thanks to their low stress levels and their shape. In most of the old masonry constructions there is a difference of one or two orders of magnitude between the working stresses and crushing strength. Heyman

defines 'correct geometry' the shape of the structure which guarantees that the structural forces may somehow be accommodated satisfactorily. Then, in structures whose materials work at low stresses, the effectiveness of the geometrical rules is recognized and their stability is governed by the shape [14].

These concepts were clear to old master masons, whose intuitive understanding of forces and resulting stresses has been consolidated, by trial and error and by recording past experiences, into rules of construction, which have been handed down orally and shared secretly in masonic lodges. The modern class of Architects and Engineers, whose design approach is strongly based on the strength of materials and the calculation of stresses, can hardly accept a design criterion based on shape performances.

A way to overcome this difficulty is to review these ancient and medieval concepts with a modern twist, by adopting the unilateral model, introduced for the first time by Jacques Heyman, in his famous article "The Stone Skeleton" [8]. The three fundamental assumptions of this model, when translated into a continuum model, imply a normality law for stress and strain, then the analysis of masonry structures can be conducted within the frame of Limit Analysis, by applying the static and kinematic theorems on the basis of admissible stress and strain fields (see [13]).

2.1 Unilateral material

Heyman refers to masonry buildings as a collection of dry stones, some squared and well fitted, some left unworked, and placed one on another to form a stable structure; mortar, when it is present, has the function to fill the interstices and does not add strength to the construction. Furthermore, the compaction under gravity of the masonry elements, which implies a general state of compressive stress and negligible tensions, guarantees the stability of the entire masonry construction. Heyman also points out that a low background of compressive stress is essential for the stability of the masonry structure, since it allows the development of friction forces, which lock the stones against to slip and allow the structure to maintain a certain overall shape; this low background stress can be as low as one-tenth of the compressive strength of the material, then crushing failure is rarely an issue [2].

The fundamental element for these structures is represented by geometrical rules of proportion, which have been behind the structural design since antiquity, and are therefore those which guarantee the stability of masonry structures; ancient and medieval designers, although aware of masonry collapses, apparently did not pose any questions about the safety factor or the collapse loads. Heyman cites the studies of Wilars and other manuscripts, which have "uncovered some of the mysteries of the masons' lodges…such reconstructed rules of building are entirely numerical, and deal with the practical determination of $\sqrt{2}$, the relative proportion that one part of a building should bear to another, the automatic determination of elevations from plans, and so on…" [8].

A modern way to approach the analysis of masonry structures by applying these medieval concepts is to adopt a unilateral model, introduced for the first time by Jacques Heyman. The model is set in his famous article 'The Stone Skeleton' (1966), where some extremely raw, but at the same time effectively, fundamental assumptions are made:

i. masonry has no tensile strength;
ii. stresses are so low that masonry has effectively an unlimited compressive strength;
iii. sliding failure does not occur.

With these three simplifying hypothesis, Heyman obtains a material infinitely strong in compression, which cannot accept tensile stresses and does not admit slip.

The first assumption is quite conservative, since individual masonry blocks may be strong in tension, but mortar, if any, is extremely weak in tension; then, an attempt to impose tensile forces would pull the work apart [2]. With the first hypothesis, we assume that the material is unilateral, that is it is incapable of withstanding the slightest tensile load and can also detach, with a zero energy mode, along any internal surface, namely a fracture line; in mathematical terms, for a masonry continuum, this means that the stress tensor T is negative semidefinite, that is it belongs to the cone of negative semidefinite symmetric tensors ($T \in Sym^{-}$ that is $T \cdot v \leq 0, \forall v$), since only compressive stresses are allowed.

The second assumption is made considering the low average values of compressive stresses, compared to the compressive strength of the material in traditional masonry structures; however, as Heyman points out, stress concentrations are possible and may lead locally to splitting or surface spalling. Such distress is usually a local phenomenon and does not normally lead to overall failure of the building; however, this statement must be questioned in relation to the behaviour of apparently solid walls, which may actually consist of two skins containing a rubble fill [2].

With the third assumption sliding along a fracture line is not possible. As noted by Heyman, even if the slippage of individual stones occurs, masonry structures generally maintain their shape remarkably well, especially when a very small compressive pre-stress is applied, in order to avoid the slip and the general loss of cohesion [2]. In mathematical terms, for a masonry continuum, this hypothesis means that the total fracture deformation E_{anel} satisfies a normality law with respect to the cone Sym^{-} of negative semidefinite symmetric tensors, then the tension does not work for the inelastic deformation and the latter is positive semidefinite ($E_{anel} \in Sym^{+}$).

The no-sliding assumption is equivalent to assume infinite friction (see [13]), and friction and sliding are the basic mechanism in block-block, and block-mortar-block interactions. The main strength of the simplified unilateral model of Heyman, which assumes that sliding is prevented and that friction is infinite, is that, even by neglecting these two important phenomena, which are still the most difficult challenges of modern Mechanics, it is still able to provide a good prediction on masonry behaviour.

One of the primary goals for the realization of masonry structures is to avoid the sliding phenomenon between the stones, this is achieved by placing the stone blocks according to a particular construction pattern: on the horizontal planes, where compressive forces are developed by virtue of the vertical loads, the slip phenomenon is hindered by the friction forces, while on the vertical planes, where compressive forces are low, the phenomenon is limited by interlocking between the blocks.

As said, Heyman's assumptions translate, for unilateral continua, into a normality assumption. Such a rule allows to employ the two theorems of Limit Analysis, the static and the kinematic ones. In the years that followed, these tools have been used by many authors (see for example [20], [21], [22]). With these powerful tools, it is possible to describe the behaviour of large masonry structures [2], while remaining their analysis extremely simple, specifically by applying the static and kinematic theorems on the basis of concentrated admissible stress and strain fields, as shown by Lucchesi in the case of the problem of the equilibrium of masonry-like, no-tension material in 2d, and by De Faveri in the case of reinforcement problems [13].

As observed by Angelillo, in the context of masonry structures, only adopting the unilateral assumption we can correctly appreciate and interpret the fracture patterns, which are physiological in masonry and, rather than being the result of an overload, are most often due to small variations of the boundary conditions, as those due to foundation settlements or geometrical changes of the environment [23].

Geometry and loads are in strong relation with the specific fracture pattern which nucleates and evolves into the structure. In [13], Angelillo observes that in absence of any settlements or relative movements of the boundaries, that is in absence of fractures, the presence of the thrust in a masonry arch is a purely speculative fact. But if fractures appear, in the form of a specific crack pattern, the corresponding force pattern can be derived. By discretizing a unilateral masonry structure into rigid blocks, a minimal energy criterion can be employed, in order to select the mechanism of the structure, that is the field of piecewise rigid displacements responding to given eigenstrains and boundary displacements [13].

2.2 Masonry behaviour

In the book [23], Angelillo describes two kind of approaches, through which the modelling of masonry structures is possible, namely simple and refined models. Simple models are based on the No-Tension assumption and can be applied to a large class of masonry buildings; refined models are more sophisticated, since they take into account aspects like softening and brittleness in the stress-strain laws, then they can be applied to specific types of masonry, for which the material properties and the geometrical constructive characteristics are known in detail.

The fundamentals of masonry behaviour are represented by some common experimental facts, which characterize the behaviour of many kinds of masonry material, as:

Local failure modes

Three different modes are recognized. The first one, most frequent and usually irrelevant, is associated to the brittleness of the material and manifests itself with detachment fractures that separate neatly two parts of seemingly intact material (Fig. 2.1); the second is due to high compressive loads with shear and is a kind of mixed mode in which fractures of detachment alternate to lines of sliding (Fig. 2.2); the third is due to the crushing of the material under essentially pure compression and consists of finer detachment fractures, close together and separated by damaged material (Fig. 2.3) and

is the most dangerous, since failure under compression is usually sudden; the latter two modes occur when the load is critical or close to the collapse value.

Fig. 2.1: Detachment fractures

Fig. 2.2: Detachment and sliding fractures

Fig. 2.3: Crushing due to compression

Structural failure mechanisms

Three different modes are described, through which a masonry structure, or a part of it, may collapse. The first one is represented by crushing due to compression (Fig. 2.3); the second, that is the most frequent under seismic loads, is out of plane rocking (Fig. 2.4); the third is in-plane shear, which determines local failure modes of the masonry units in their own plane (Fig. 2.5) such as those shown in Fig. 2.2.

Fig. 2.4: Out-of-plane rocking [24]

Fig. 2.5: In-plane failure

Experimental tests results

Given the high variance, both in terms of strength and stiffness, the qualitative experimental graph shown in Fig. 2.6 can be seen as the uniaxial stress-displacement plot of a high idealized masonry material. The main feature of masonry material is that the tensile strength σ_t is much lower than the compressive strength σ_c; the ratio σ_t/σ_c is usually lower than 0.1 and can be as low as 0.01 or even, locally, vanishingly small.

Masonry behaves essentially as an elastic material in compression up to 80-90% of the strength, even if the stress-strain plot is non-linear due to the early micro-cracking of the material, and, in the post-critical phase, to a sort of plastic behaviour characterized by irreversible deformations (Fig. 2.6).

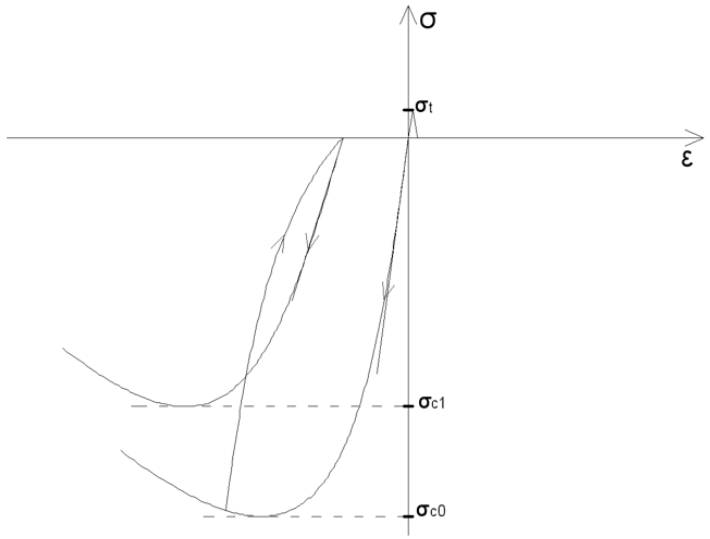

Fig. 2.6: Typical uniaxial behaviour

2.3 Simplified uniaxial models

In order to describe the mechanical behaviour of an idealized masonry-like material, three simplified models can be adopted: 1) Model zero (RNT), 2) Model one (ENT) and 3) Model two (ML), where the notations "*zero*", "*one*" and "*two*" are referred to the number of parameters required in each model to describe the behaviour of the material.

In *model zero (RNT)*, where RNT means Rigid No-Tension material, a first approximation of the mechanical behaviour of masonry material is given, through a raw stress-strain diagram (Fig. 2.7a) where the material is indefinitely strong and stiff in compression and it is incapable of sustaining any tensile stress. This is essentially the model proposed by Heyman (see [2], [8]). The model is named *zero* since there are no material parameters. Both strength and stiffness are considered infinite in compression and are neglected in tension, then these two parameters must not be defined in the model. In fact, since in this model it is assumed that the material is rigid in compression and can elongate freely, if the bar exhibits a positive deformation, it can be interpreted as a measure of fracture into the material, either smeared or concentrated. Even if the material has a limited repertoire of admissible stresses and strains and exhibits fractures, its uniaxial behaviour in elongation is elastic [23]. Indeed, there is a univocal relation between stress and strain: if the bar elongates the stress is zero, then, even if deformations occurs, the material does not accumulate any kind of energy.

In *model one (ENT*), where ENT means Elastic No-Tension material, there is only one defined parameter, represented by the stiffness in compression, namely the elastic modulus *E* (Fig. 2.7b). In this model, the compressive strength is assumed infinite, whilst strength and stiffness are completely neglected in tension. Moreover, the strain can be positive or negative; in particular, a positive strain represents the fracture part of deformation, while negative strain the elastic part. The ENT material has a global elastic behaviour, that is strain determines stress for any value of strain [23].

In *model two (ML)*, where ML means Masonry-Like material, besides a defined stiffness in compression, there is also a limitation in terms of strength σ_c in compression (Fig. 2.7c). Then, this model is useful in order to describe failure modes and mechanisms described above (see Fig. 2.2, Fig. 2.3, Fig. 2.5). As can be noted in Fig. 2.7c, the material exhibits a perfectly plastic behaviour in compression with an incremental constitutive response, the actual stress state is path dependent, that is it is determined by the whole strain history. Moreover, the anelastic deformation is composed by a reversible fracture part and in an irreversible crushing part; hence, the material is perfectly plastic, due to different behaviour in tension (elastic fracture) and compression (incremental plasticity), then the plastic deformations cannot be cancelled by reversing the strain [23]. In this model, the elastic modulus *E* and the strength σ_c in compression are defined, while strength and stiffness in tension are neglected.

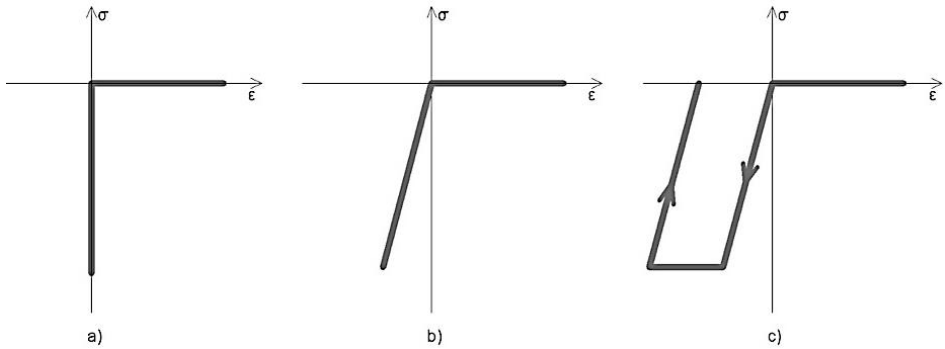

Fig. 2.7: Simplified models: a) model zero; b) model one; c) model two

2.4 Three-dimensional Simplified Models

For real applications, these three simplified models must be extended to the three-dimensional space. The No-Tension assumption translates to the condition that the stress tensor belongs to the cone of negative semidefinite symmetric tensors ($\mathbf{T} \in Sym^{-}$). The introduction of a convenient rule for the latent part of the deformation is necessary, that is the strain sustaining the unilateral constraint on the stress; this rule considers that no sliding along the fracture line occurs, that is the total fracture strain satisfies a normality law with respect to the cone of negative semidefinite symmetric tensors, namely $(\mathbf{T} - \mathbf{T}^{*}) \geq 0,\ \forall\, \mathbf{T}^{*} \in Sym^{-}$. Such normality law, which is equivalent to $\mathbf{T} \cdot \mathbf{E}_a = 0\ \ \&\ (\mathbf{E}_a \in Sym^{+})$, allows for the application of the static and kinematic theorems of Limit Analysis.

The linear elastic assumption in compression in model *one*, can be generalized in case we refer to an isotropic material, by introducing a convenient Poisson ratio, usually set for masonry between 0.1 and 0.2. By combining the normality law with the linear elastic assumption in compression, the global response of model one is elastic, as well as hyper-elastic, that is path independent.

The isotropy restriction also simplifies the model *two*, where, besides the definition of the compressive strength σ_c , the shape of the limit compressive surface must be given.

Even if the RNT model is rather raw, it is the only one appropriate for old masonry constructions, as acknowledged by many masonry experts (among which Heyman (1955), Huerta (2006) and Como (2010)), since the elastic models are incapable to define correctly the initial state of the structure, due to the uncertainties about boundary conditions and on the previous construction history [23].

As recognized by Angelillo [23], the elastic assumption in models *one* and *two* provides that the given settlements are accommodated by means of a small displacement mechanism, that is a kind of rigid body relative displacement of some parts of structure; then, the stress produced during the nucleation and growth of the fracture, necessary to activate the mechanism, are almost completely released, and the final state can be considered an essentially stress free reference state.

By adopting the simplified models, we obviously neglect many aspects of real masonry mechanical properties, such as damage since the early stages of loading, which determine a stiffness reduction and a non-linear trend in the stress-strain plot; the brittle behaviour in tension, because of which energy is expended to open a crack; the fact that sliding is ruled by friction (then the anelastic strains and strain rates are not purely normal); the fact that ductility, when present, is rather limited, and finally that the elastic and anelastic responses are anisotropic; furthermore, in the anelastic compressive behaviour, after an initial hardening phase, a subsequent phase of softening is observed; under extreme conditions, there is also a sort of viscoelastic behaviour, since the cyclic response is hysteretic and the stress-strain plot depends on the rates; when large displacements occur, geometric non-linearities must be taken into account.

Some of these more sophisticated aspects of masonry behaviour are described in §2.6.

2.5 Elastic solutions versus Limit Analysis

Once we accept the unilateral hypothesis as the basic assumption to capture masonry behaviour, still we have the option to consider deformability in compression, that is to adopt model *zero* or models *one* and *two*.

It should be noted that by applying the rigid unilateral model, we give up the idea of searching the actual stress state of the structure, and we limit our interest to the structural safety assessment with the tools offered by the Limit Analysis.

Indeed, the lack of information about the construction history, the presence of stone rearrangements and of unknown settlements in real structures, makes the Elastic Analysis the wrong tool to study the equilibrium of the structure correctly, since, for overdetermined structures, the elastic solution is extraordinary sensitive to very small variations of these unknown conditions. In other words, the '*actual*' state of the structure

could be determined knowing exactly all the conditions that affect the solution, considering the detailed material properties and taking into account the compatibility of deformations; but, as noted by Heyman [2], "the 'actual' state can indeed be determined, but only by taking account of the material properties (which may not be well-defined for an assembly of say stones and mortar), and by making some assumptions about compatibility of deformation – for example, the boundary conditions at the abutments of the arch. Even then, it must be recognized that the 'actual' state of the structure is ephemeral; it could in theory be determined if all the conditions affecting the solution were known exactly, but a sever gale, a slight earth tremor, a change in water table will produce a small change in the way the structure rests on its foundations, and this will produce an entirely different equilibrium state for the structure".

For this reason, the Elastic Analysis should be replaced by Limit Analysis, which is based on a fundamental premise: if we take two seemingly identical structures, which in fact have small imperfections, different from each other, so they are in different initial states, and they are slowly loaded up to reach the collapse condition, we will find that their collapse loads, and thus their ultimate strength values, are identical. Then, we arrive to the conclusion that small initial imperfections do not affect the ultimate strength of the structures [2].

Hence, we give up the search of the '*actual*' state of the structure, which is ephemeral, while we focus on the way in which this can collapse. Obviously it is not expected that the structure really collapses, a calculation is made, in which one imagines that the loads are increased by a certain factor; then, by applying the Static Theorem of Limit Analysis in the context of masonry structures, it must happen that a balanced stress field can be found that is compressive, which means that the stresses at every cross-section of the structure are less by some margin than the yield stress of the material, then the real structure is subject to working loads 'lower' than the ultimate ones, and will not collapse. In fact, as noted by Heyman, "the power of this safe theorem is that the equilibrium state examined by the designer need not be the *actual* state …if the designer can find a way in which the structure behaves satisfactorily, then the structure itself certainly can" [2].

2.6 Refined models

Masonry is a heterogeneous assemblage of units and joints, being the units represented by bricks, adobes, blocks, irregular stones and others, while mortar can be made of clay, bitumen, lime/cement, glue or other (see Lourenço and Milani in [23]). Thus, considering the enormous number of possible combinations given by the geometry, the nature of units and mortar and the arrangement of units, the first basic aspect to be clarified should consist in what we consider as masonry material. Of course, the analysis of regular masonry structures, with a regular arrangement of units and, consequently, a periodic repetition of the microstructure, provides important information in that sense.

Experimental tests are rather difficult. The first difficulty is represented by the fact that the 'microscale' of the material is large, compared to the actual structural size. Furthermore, the behaviour of masonry depends, besides on the composition of units and joints, also on the arrangement and the treatment of units, which can be polished, sawn or artificially made with rough. Besides, the innumerable variations of masonry, the large

scatter of in situ material and the impossibility of reproducing it all in a specimen, forced the experimental research in the last decades to concentrate on brick block masonry.

Different representations are possible (see for example [25], [26], [27]), depending on the level of accuracy and the simplicity desired: (a) micro-modelling, where the geometry of units and joints is directly considered and the constitutive laws are obtained experimentally; (b) macro-modelling, where units and joints are smeared out in the continuum and the constitutive laws are obtained experimentally; (c) homogenization, where the micro-structure is handled mathematically in terms of geometry and material data to obtain a smeared continuum model; (d) structural component models, where constitutive laws of structural elements are directly provided in terms of internal forces, such as shear force or bending moment (and related generalized displacements), instead of stresses and strains [23], seeFig. 2.8:

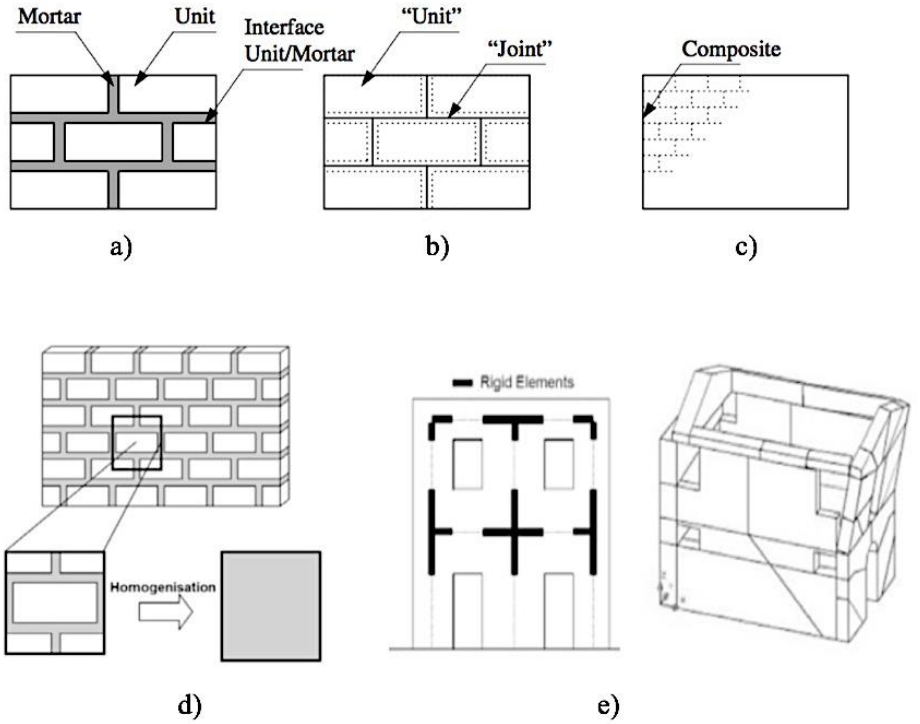

Fig. 2.8: Modelling approaches for masonry:
a) representation of regular running bond masonry; b) micro-modelling; c) macro-modelling; d) homogenization; e) illustrative structural component models, with beam elements or macro-blocks [23]

2.7 Mechanical behaviour, observations and numerical data

A basic aspect in the mechanical behaviour of masonry is softening, which, if it is not abrupt, that is it consists in a gradual decrease of the mechanical resistance under a

continuous increase of the deformation applied, provides to the material a sort of ductility.

In (Fig. 2.9) the experimental behaviour of masonry under tensile and compressive actions is depicted, where f_t is the tensile strength, f_c is the compressive strength, G_f is the tensile fracture energy and G_c is the compressive fracture energy. Softening is one of the main features of material which fail due to a process of progressive internal crack growth, like brick, mortar, stone or concrete.

This phenomenon had been well identified for tensile failure, as well as it had been observed for shear failure, in which also an associated degradation of cohesion occurs; furthermore, for compressive failure, the behaviour is governed both by local and continuum fracturing processes. Referring to the experimental results, the shape of the non-linear response is also considered a parameter controlling the structural response, even if for engineering applications, this seems less relevant than the other parameters [23].

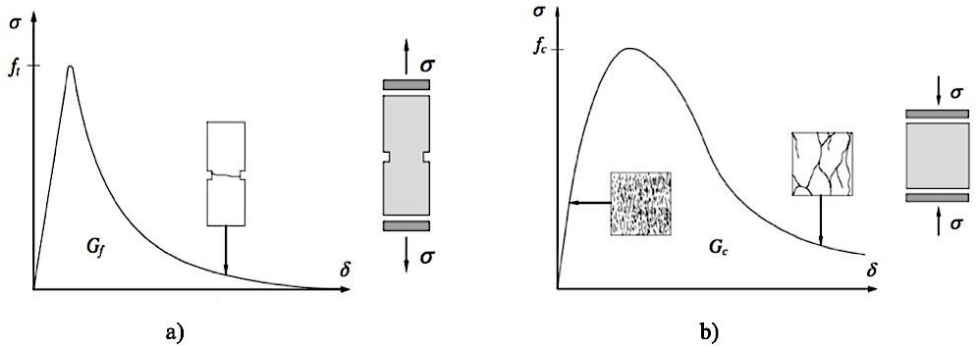

Fig. 2.9: Softening and definition of fracture energy: a) tension; b) compression

Experimental tests show how the properties of masonry strongly depend on its constituents ones, as well as the interface between mortar and units controls the joints behaviour [23]. It is also noteworthy that the bond between unit and mortar is often the weakest link in masonry assemblages and that the non-linear response of the joints, which is controlled by the unit-mortar interface, is one of the main features of masonry behaviour. In particular, the unit-mortar interface is affected by two different phenomena, namely the tensile and the shear failure, described by Lourenço et al. as Mode I and Mode II.

The parameters needed for the tensile mode (Mode I) are the bond tensile strength f_t and the bond fracture energy G_f. The factors that affect the bond between unit and mortar are highly dependent on the units, on the mortar and on the workmanship. The Eurocode 6 provides indications about the characteristic value of the bond tensile strength. The shear response (Mode II) of masonry joints is affected by the ability of the experimental tests to generate a uniform stress state in the joints, since the equilibrium constraints determines non-uniform normal and shear stresses in the joints. As noted in [23], in order to obtain the post-peak characteristics, the stress normal to the bed joint should be

maintained constant during testing. Experimental results provide an exponential shear softening diagram with a residual dry friction level.

The main structural masonry property is represented by the compressive strength of masonry orthogonal to the bed joints and it is widely recognized that the precursor of masonry failure is due to the different elastic properties of unit and mortar. There are different formulas, which predict the compressive strength of masonry as a function of its components mechanical properties (Eurocode 6, OPCM 3431, PIET-70), even if they are affected by the direction of compressive load, the quality of mortar, the type of stone, the masonry bond and the masonry types.

With reference to the Italian Code for Constructions (DM 14.1.2008), the values of strength in compression f_c and shear f_t of different types of coarse masonry with poor mortar are reported below (Tab. 2.1).

Then, with reference to Model Code 90 (CEB-FIP, 1993), the expressions of G_c and G_f, namely the compressive and tensile fracture energy are given:

$$G_{f,c} = 15 + 0.43f_c - 0.0036f_c^2 \,, \tag{2.1}$$

$$G_f = 0.04f_t^{0.7} \,, \tag{2.2}$$

with f_c and f_t expressed in N/mm^2 and $G_{f,c}$ in N/mm. As can be observed in Tab. 2.1, the values of tensile fracture energy are negligible, compared to the compressive ones.

Masonry Type	f_c		f_t		$G_{f,c}$		G_f		$G_{f,c}$ / G_f	
	[N/mm^2]		[N/mm^2]		[N/mm]		[N/mm]		[-]	
Disarranged masonry of cobbles/boulders	1,00	1,80	0,01	0,02	15,43	15,76	0,0016	0,0022	9687,34	7123,22
Masonry of roughhewed stones	2,00	3,00	0,02	0,03	15,85	16,26	0,0024	0,0031	6725,46	5301,74
Masonry of cut stones	2,60	3,80	0,03	0,04	16,09	16,58	0,0033	0,0040	4915,69	4167,12
Masonry of soft stones	1,40	2,40	0,01	0,02	15,59	16,01	0,0020	0,0027	7738,10	5981,53
Masonry of squared stone blocks	6,00	8,00	0,05	0,06	17,45	18,21	0,0046	0,0056	3823,81	3262,38
Brickwork of solid blocks and lime mortar	2,40	4,00	0,03	0,05	16,01	16,66	0,0034	0,0046	4659,94	3595,40
Brickwork of semisolid blocks and cem. mortar	5,00	8,00	0,12	0,16	17,06	18,21	0,0091	0,0111	1881,45	1641,94
Brickworks of air bricks (45%)	4,00	6,00	0,15	0,20	16,66	17,45	0,0106	0,0130	1571,86	1345,94
Brickworks of air bricks (<45%)	3,00	4,00	0,05	0,07	16,26	16,66	0,0049	0,0059	3309,16	2822,53
Masonry of concrete air-blocks (45-65%)	3,00	4,40	0,09	0,12	16,26	16,82	0,0074	0,0091	2192,94	1855,23
Masonry of concrete air-blocks (45-65%)	1,50	2,00	0,05	0,06	15,64	15,85	0,0047	0,0057	3299,17	2758,88

Tab. 2.1: Reference mechanical strength and stiffness of different types of coarse masonry with poor mortar. Compressive and tensile strength f_c and f_t, compressive and tensile fracture energy G_c and G_f

Chapter 3

NORMAL RIGID NO-TENSION (NRNT) MODEL

Prologue. In this chapter, we adopt the simplest possible unilateral model for masonry, namely the Normal Rigid No-Tension model.

The fundamental assumptions for the NRNT model, are the no-tension assumption and the normality law of the total strain (coinciding with the anelastic strain) to the cone of admissible stress states. Thanks to the rule of normality, the theorems of Limit Analysis can be applied, in order to assess the ultimate capacity of masonry buildings, described through a unilateral model.

When adopting the No-Tension assumption, the systematic use of singular stress and strain fields can be a powerful tool in the analysis of the structural model. Singular strains are commonly used in perfect plasticity, while the use of singular stress fields, although introduced for the first time in a mathematically unconscious way by Méry [28](1840), has been rigorously formulated by Lucchesi, Silhavi and Zani, only in 2005 [29].

3.1 The Rigid No-Tension material

The masonry structure is identified with the set $\Omega = \Omega \cup \partial\Omega_D$, i.e. it is considered closed on $\partial\Omega_D$ and opened on the rest of the boundary, $\partial\Omega_D$ being the constrained part of the boundary. The body is composed of Rigid No-Tension material, that is the stress **T** is negative semidefinite:

$$\mathbf{T} \in Sym^{-}, \tag{3.1}$$

the effective strain $\mathbf{E}^{*}=\mathbf{E}(\mathbf{u}) - \underline{\mathbf{E}}$, is positive semidefinite:

$$\mathbf{E}^* \in Sym^+, \tag{3.2}$$

Sym^- , Sym^+ being the convex cones of negative semidefinite and positive semidefinite symmetric tensors and $\underline{\mathbf{E}}$ being the given eigenstrains, and the stress **T** does no work for the corresponding effective strain E^*:

$$\mathbf{T} \cdot \mathbf{E}^* = 0\,. \tag{3.3}$$

The effective strain $\mathbf{E}^*$ is the latent strain, that is a positive definite tensor field, which does no work for the corresponding stress, and represents detachment fractures (see [30]). $\mathbf{E}^*$ is a sort of "reaction" deformation associated to the constraint on stress (3.1). In order to avoid trivial incompatible loads ($\underline{\mathbf{s}}$, **b**), it is assumed that the tractions $\underline{\mathbf{s}}$ satisfy the condition:

$$\underline{\mathbf{s}} \cdot \boldsymbol{n} < 0 \quad , \quad \text{or} \quad \underline{\mathbf{s}} = \mathbf{0} \quad , \quad \forall \mathbf{x} \in \partial\Omega_N \ . \tag{3.4}$$

In the plane case (n=2), conditions (3.1) and (3.2) can be written as follows:

$$tr\mathbf{T} \leq 0 \quad , \quad det\mathbf{T} \geq 0 \ , \tag{3.5}$$

$$tr\mathbf{E}^* \geq 0 \quad , \quad det\mathbf{E}^* \geq 0 \ . \tag{3.6}$$

3.1.1 The boundary value problem

We consider the typical boundary value problem (BVP) for a continuum 2d body Ω, whose boundary $\partial\Omega$ is partly loaded and partly constrained. Then, we consider the equilibrium equations and the boundary conditions for the stress field, as well as the normality law for the inelastic strain, which arises when a detachment occurs.

It is assumed that the body $\Omega \in \mathbb{R}^n$ (here n=2), loaded by the given tractions $\underline{\mathbf{s}}$ on the part $\partial\Omega_N$ of the boundary, and subject to given displacement $\underline{\mathbf{u}}$ on the complementary, constrained part of the boundary $\partial\Omega_D$, is in equilibrium under the action of such given surface displacements and tractions, besides body loads **b** and distortions $\underline{\mathbf{E}}$, and undergoes displacements **u** and local deformations so small that the infinitesimal strain $\mathbf{E}(\mathbf{u})$ is a proper strain measure.

The data of the problem are collectively denoted as d = ($\underline{\mathbf{u}}$, $\underline{\mathbf{E}}$; $\underline{\mathbf{s}}$, **b**). When eigenstrains are considered, under the small strain assumption, the total strain $\mathbf{E}(\mathbf{u})$ is decomposed additively as follows: $\mathbf{E}(\mathbf{u})=\mathbf{E}^* + \underline{\mathbf{E}}$, being $\mathbf{E}^*$ the *effective* strain of the material.

The boundary value problem can be formulated as follows:

"Find a displacement field $\boldsymbol{u}$ *and the allied strain* $\boldsymbol{E}$*, and a stress field* $\boldsymbol{T}$ *such that*

$$\mathbf{E}^* + \underline{\mathbf{E}} = \frac{1}{2}(\nabla \mathbf{u} + \nabla \mathbf{u}^T) \ , \qquad \mathbf{E}^* \in Sym^+ \ , \ \mathbf{u} = \underline{\mathbf{u}} \ on \ \partial\Omega_D \ , \tag{3.7}$$

$$div\mathbf{T} + \mathbf{b} = 0 \ , \ \mathbf{T} \in Sym^- \ , \ \mathbf{T}\boldsymbol{n} = \underline{\mathbf{s}} \ on \ \partial\Omega_N \ , \tag{3.8}$$

$$\mathbf{T} \cdot \mathbf{E}^* = 0 \ ", \tag{3.9}$$

$\boldsymbol{n}$ being the unit outward normal to $\partial\Omega$.

We introduce the sets of kinematically admissible displacements K, and of statically admissible stresses H, defined as follows:

$$K = \left\{ \mathbf{u} \in S \text{ s.t. } \mathbf{E}^* = \mathbf{E}(\mathbf{u}) - \underline{\mathbf{E}} \ , \mathbf{E}^* \in Sym^+ , \ \mathbf{u} = \underline{\mathbf{u}} \ on \ \partial\Omega_D \right\}, \tag{3.10}$$

$$H = \left\{ \mathbf{T} \in S' \text{ s.t. } div\mathbf{T} + \mathbf{b} = 0 \ , \ \mathbf{T} \in Sym^- \ , \ \mathbf{T}\boldsymbol{n} = \underline{\mathbf{s}} \ on \ \partial\Omega_N \right\}, \tag{3.11}$$

S, S' being two suitable function spaces. As observed in [23], a sensible choice for these spaces is $S \equiv SBV$ and $S' \equiv SBM$, that is the spaces of Special Bounded Variation and of Special Bounded Measures. A solution of the bvp for masonry-like structures is a triplet $(\mathbf{u}, \mathbf{E}^*(\mathbf{u}), \mathbf{T})$ such that $\mathbf{u} \in K$, $\mathbf{T} \in H$, and $\mathbf{T} \cdot \mathbf{E}^*(\mathbf{u}) = 0$.

3.1.2 Singular stress fields

If the differential equations of equilibrium are considered in a *strong sense*, the stress field **T** must be differentiable and its divergence must be continuous. On adopting a variational formulation, if the material is linear elastic, the minimal request for **T** is to be square summable, that is:

$$\sqrt{\int_\Omega \mathbf{T} \cdot \mathbf{T} da} < \infty. \tag{3.12}$$

For some rigid perfectly plastic materials (such as rigid unilateral materials), less regular and even singular stresses may be admitted. The minimal request for such materials is that **T** be summable:

$$\int_\Omega \sqrt{\mathbf{T} \cdot \mathbf{T}} da < \infty \, . \tag{3.13}$$

If one admits stress fields that are only summable, the set of competing functions enlarges to bounded measures, that is to summable distributions $\widetilde{\mathbf{T}}$:

$$\int_{\Omega} |\widetilde{\mathbf{T}}| < \infty, \tag{3.14}$$

which, in general, can be decomposed into the sum of two parts:

$$\widetilde{\mathbf{T}} = \widetilde{\mathbf{T}}_{\mathbf{r}} + \widetilde{\mathbf{T}}_{\mathbf{s}}\,, \tag{3.15}$$

where $\widetilde{\mathbf{T}}_{\boldsymbol{r}}$ is absolutely continuous with respect to the area measure (that is $\widetilde{\mathbf{T}}_{\boldsymbol{r}}$ is a density per unit area) and $\widetilde{\mathbf{T}}_{\boldsymbol{s}}$ is the singular part.

If the stress field is summable (and also if it is square summable), it is not differentiable in a strong sense, and the equilibrium equations have to be reformulated in variational form, e.g. through the Virtual Work equation:

$$\int_{\Omega} \mathbf{T} \cdot \mathbf{E}(\delta\mathbf{u}) da = \int_{\partial\Omega_N} \underline{\mathbf{s}} \cdot \delta\mathbf{u} ds + \int_{\Omega} \mathbf{b} \cdot \delta\mathbf{u}\, da \;,\; \forall \delta\mathbf{u} \in K^0, \tag{3.16}$$

where K^0 is the set of statically admissible stress field, whose expression is:

$$H^{\circ} = \{\mathbf{T}^{\circ} \in S(\Omega) s.t. div\mathbf{T}^{\circ} = \mathbf{0}\,, \mathbf{T}^{\circ}\boldsymbol{n} = \mathbf{0}\; on\; \partial\Omega_N, \mathbf{T}^{\circ} \in Sym^{-}\}, \tag{3.17}$$

Singular stresses require also special modifications of the boundary conditions; the trace of the stress **T** on the loaded part of the boundary is not given by $\mathbf{T}\boldsymbol{n}$ if **T** is singular.

As reported in [30], when we consider the boundary conditions related to the stress tensor **T**, the emerging stress vector $\mathbf{s}(\mathbf{T})$ on the loaded part $\partial\Omega_N$, that is its trace at the boundary, is not expressed in a Cauchy form $\mathbf{s}(\mathbf{T}) = \mathbf{T}\boldsymbol{n}$, unless **T** is regular. If **T** is a line Dirac delta of the form $\mathbf{T} = \mathrm{P}\,\delta(\Gamma)\,\mathbf{t} \otimes \mathbf{t}$, and the line of thrust Γ crosses the boundary at a point $\mathrm{X} \in \Gamma$ at an angle, that is $\mathbf{t} \cdot \boldsymbol{n} \neq 0$, then $\mathbf{s}(\mathbf{T}) = \mathrm{P}\,\delta(\mathrm{X})\,\mathbf{t}$. The special case in which the line of thrust Γ is tangent to the boundary $\partial\Omega_{\mathrm{N}}$, deserves a special attention. In such a case, even if any stress vector $\mathbf{s}(\mathbf{T})$ emerges at the boundary due to the singular stress, the boundary condition $\mathbf{T}\boldsymbol{n} = \underline{\mathbf{s}}$ must be modified, since singular stress concentrated on Γ can balance, wholly or in part, the given tractions $\underline{\mathbf{s}}$. Therefore, the sign of the normal component of the tractions, given along the boundary, is not locally restricted, and, if the boundary is locally concave, purely tangential tractions and even tensile loads may be applied. In particular, if the interface is straight, equilibrium and material restrictions can be enforced if and only if $\underline{\mathbf{s}} \cdot \boldsymbol{n} \leq 0$, but the quantity $\underline{\mathbf{s}} \cdot \boldsymbol{k}$, where $\boldsymbol{k}$ is the unit tangent vector to the boundary $\partial\Omega$, is still not restricted.

3.1.3 Singular strain fields

Furthermore, we recall that a displacement field $\mathbf{u}$ is said to be compatible if, besides being *regular enough* for the corresponding infinitesimal strain $\mathbf{E}(\mathbf{u})$ to exist, $\mathbf{u}$ satisfies the boundary conditions on the constrained part $\partial\Omega_D$ of the boundary:

$$\mathbf{u} = \underline{\mathbf{u}}, on\ \partial\Omega_D\ . \tag{3.18}$$

For linearly elastic bodies, on adopting a variational formulation, the usual assumption is that $\mathbf{E}$ be square summable, that is:

$$\sqrt{\int_\Omega\ \mathbf{E}\cdot\mathbf{E}da} < \infty\ , \tag{3.19}$$

for some rigid, perfectly plastic (or rigid unilateral) materials, it is sufficient to assume that $\mathbf{E}$ be summable:

$$\int_\Omega\ \sqrt{\mathbf{E}\cdot\mathbf{E}}da < \infty\ . \tag{3.20}$$

As before, the set of competing functions enlarges to bounded measures, that is to summable distributions $\tilde{\mathbf{E}}$; then the displacement $\mathbf{u}$ can admit finite discontinuities, i.e. $\mathbf{u}$ can be a function with bounded variation. If $\mathbf{E}$ were the whole gradient of $\mathbf{u}$, the summability of $\mathbf{E}$ would entail: $\mathbf{u} \in BV(\Omega)$, exactly. Since $\mathbf{E}$ is only the symmetric part of $\nabla\mathbf{u}$, $\mathbf{u}$ must belong to a larger space: $BD(\Omega)$. The strain corresponding to $\mathbf{u}$ is again a bounded measure:

$$\int_\Omega\ |\tilde{\mathbf{E}}| < \infty\ . \tag{3.21}$$

which, in general, can be decomposed into the sum of two parts:

$$\tilde{\mathbf{E}} = \tilde{\mathbf{E}}_\mathrm{r} + \tilde{\mathbf{E}}_\mathrm{s}\ . \tag{3.22}$$

where $\tilde{\mathbf{E}}_\mathrm{r}$ is absolutely continuous with respect to the area measure (that is $\tilde{\mathbf{E}}_\mathrm{r}$ is a density per unit area) and $\tilde{\mathbf{E}}_\mathrm{s}$ is the singular part. $\tilde{\mathbf{E}}_\mathrm{s}$ has support on the union of a set of linear 1d measure (the jump set of $\mathbf{u}$) and a set of fractional measures.

If $\mathbf{u} \in BD(\Omega)$, that is $\mathbf{u}$ can be discontinuous, the boundary condition $\mathbf{u} = \underline{\mathbf{u}}$ on $\partial\Omega_D$ makes no sense. A way to keep alive the boundary condition of Dirichelet type is to identify the masonry body with the set $\Omega \cup \partial\Omega_D$, rather than with the domain Ω (usually an open set), and to assume that $\mathbf{u}$ must comply with the constraint $\mathbf{u} = \underline{\mathbf{u}}$ on the *skin* $\partial\Omega_D$, admitting possible singularities of the strain at the constrained boundary. Then, from here on, we identify the masonry body with the set $\Omega \cup \partial\Omega_D$.

Given the displacement field $\mathbf{u}$ of $\mathbf{x}$, by taking the gradient of $\mathbf{u}$, in a classical sense if $\mathbf{u}$ is regular, and in a generalized sense if $\mathbf{u}$ is singular, the strain $\mathbf{E}(\mathbf{u})$ is derived. Vice versa, if $\mathbf{E}$ of $\mathbf{x}$ is given, the possibility of integrating the components $E_{\alpha\beta}$ to get (possibly discontinuous) components u_α of $\mathbf{u}$, is submitted to the necessary compatibility conditions (also sufficient if Ω is simply connected):

$$E_{11,22} + E_{22,11} - 2E_{12,12} = 0\,, \tag{3.23}$$

where a comma followed by an index, say α, means differentiation with respect to x_α. Only admitting discontinuous displacements this condition can be interpreted in a generalized sense and applied (with some care), also to discontinuous, and even singular, strains.

The class of functions that can be used with Heyman's materials is rather large, since it includes both continuous and discontinuous and even singular fields. In particular, singular strain fields are associated to piecewise linear discontinuous displacements, whilst singular stress fields can be interpreted as the internal forces arising in 1d structures located inside the 2d structure. In the present work, we refer to a specific set of functions contained in this large class, namely the set of piecewise rigid displacements.

3.1.4 Stress and strain as line Dirac deltas

When we adopt unilateral models for masonry materials, it makes sense to admit singular stresses and strains, that is stress fields $\mathbf{T}$ and strain fields $\mathbf{E}$ that can be concentrated on lines, named line *Dirac deltas*. These distributions are not functions in a strict mathematical sense, since they assign finite values to all points $\mathbf{x} \in \Omega$, except to those belonging to a set of lines of $\Omega \cup \partial\Omega_D$, to which infinite values are associated. Anyway, these infinite values must be such that these stresses or strains be summable, that is:

$$\int_\Omega |\mathbf{T}| < \infty \;, \int_\Omega |\mathbf{E}| < \infty\,, \tag{3.24}$$

or, in other words, $\mathbf{T}$ and $\mathbf{E}$ must be bounded measures. We call $M(\Omega)$ the set of bounded measures on $\Omega \cup \partial\Omega_D$. Line Dirac deltas are special bounded measures [23].

Hence, we restrict to consider stress and strain fields as being special bounded measures, namely Dirac deltas with support on a finite number of regular arcs.

Regarding the *strain*, special displacement fields of bounded variation can be considered. In particular, restricting to discontinuous displacement fields $\mathbf{u}$ having finite discontinuities on a finite number of regular arcs Γ, the strain $\mathbf{E}(\mathbf{u})$ is composed by a regular part $\mathbf{E}_r$, that is a diffuse deformation over $\Omega - \Gamma$, and a singular part $\mathbf{E}_s$, in the form of Dirac delta, concentrated on Γ.

We can interpret the jump of **u** along Γ as a fracture, since Γ is the crack surface that separates the body Ω into two parts (see Fig. 3.1) and the jump of **u** represents the relative translation of the two parts.

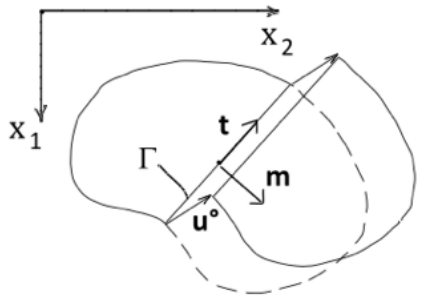

*Fig. 3.1: Discontinuous displacement along a straight line Γ: unit tangent **t** and normal **m** to Γ [23]*

On such line, the jump of **u** can be expressed as follows:

$$[\![\mathbf{u}]\!] = \mathbf{u}^{+} - \mathbf{u}^{-}, \tag{3.25}$$

where **t** and **m** are the unit tangent and normal to Γ and $\mathbf{u}^{+}$is the displacement on the side of Γ where **m** points. The jump of **u** can be decomposed into normal and tangential components:

$$\Delta v = [\![\mathbf{u}]\!] \cdot \mathbf{m}\,,\ \Delta w = [\![\mathbf{u}]\!] \cdot \mathbf{t}\,. \tag{3.26}$$

Moreover, on any crack the unilateral restriction about the non-compenetrability of matter requires that condition $\Delta v \geq 0$ must hold. The strain **E** corresponding to a piecewise rigid displacement field **u** is zero everywhere on $\Omega - \Gamma$ and is singular on Γ:

$$\mathbf{E}(\mathbf{u}) = \delta(\Gamma)\left(\Delta v \mathbf{m}\otimes\mathbf{m} + \frac{1}{2}\Delta w \mathbf{t}\otimes\mathbf{m} + \frac{1}{2}\Delta w \mathbf{m}\otimes\mathbf{t}\right), \tag{3.27}$$

where $\delta(\Gamma)$ is the line Dirac delta with support on Γ, **m** is the unit normal to Γ, **t** is the unit tangent to Γ, and Δv is the amplitude of the fracture.

Regarding the *stress*, if the stress field **T** is non-singular (say $\mathbf{T} \in L^2(\Omega)$), on a possible discontinuity line Γ, for equilibrium, the stress emerging on Γ must be continuous. Then, at any regular point of Γ, denoting with **m** the unit normal to Γ, the stress **T** must satisfy the following condition:

$$(\mathbf{T}^+ - \mathbf{T}^-)\mathbf{m} = \mathbf{0}\,, \tag{3.28}$$

where $\mathbf{T}^+$ is the stress on the side Γ where $\mathbf{m}$ points. Then, if $\mathbf{T} \in L^2(\Omega)$, the possible jumps of $\mathbf{T}$ must be restricted to the part of $\mathbf{T}$ not-emerging on Γ. If $\mathbf{T}$ is singular, say a Dirac delta on Γ, also the part of $\mathbf{T}$ emerging on Γ can be discontinuous.
The unbalanced emerging stress:

$$\mathbf{q} = (\mathbf{T}^+ - \mathbf{T}^-)\mathbf{m}\,, \tag{3.29}$$

in equilibrium, must be balanced by the stress concentrated on Γ (see Fig. 3.2).

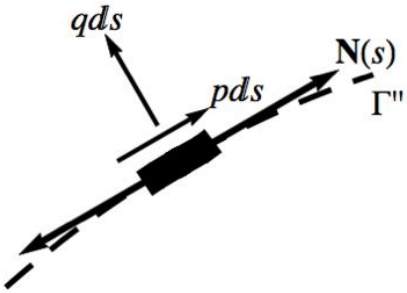

Fig. 3.2: Stress singularity: forces acting on the curve Γ [23]

Referring for notations to Fig. 3.2, the representation of the singular part $\mathbf{T}_s$ of $\mathbf{T}$ on Γ, is:

$$\mathbf{T}_s = N(s)\delta(\Gamma)\mathbf{t}\otimes\mathbf{t}\,, \tag{3.30}$$

where $N(s)$ is the intensity of the axial load, $\delta(\Gamma)$ is the line Dirac delta with support on Γ, and $\mathbf{t}$ is the unit tangent to Γ; therefore, q must be zero if Γ is straight. If the material is No-Tension, the unilateral assumption on stress implies the condition:

$$N(s) \leq 0\,, \tag{3.31}$$

that means that only compressive axial forces are admitted along the interface Γ.

3.1.5 Airy's stress function formulation

In absence of body forces (**b**=**0**), the equilibrium equations admit the following solution in terms of a scalar function *F*:

$$T_{11} = F_{,22} \quad , \quad T_{22} = F_{,11} \quad , \quad T_{12} = -F_{,12} \, . \tag{3.32}$$

This is the general solution of the equilibrium equations, if the loads are *self-balanced* on any closed boundary delimiting Ω (see [31]). The boundary condition $\mathbf{T}\,\mathbf{n} = \underline{\mathbf{s}}$ on $\partial\Omega_N$, must be reformulated in terms of *F*. Denoting **x**(s) the parametrization of $\partial\Omega_N$ with the arc length, the boundary conditions on *F* are:

$$F(s) = m(s) \quad , \quad \frac{dF}{dv} = n(s) \qquad on\ \partial\Omega_N \, , \tag{3.33}$$

in which dF/dv is the normal derivative of *F* at the boundary (that is the slope of *F* in the direction of **n**) and $m(s), n(s)$ are the moment of contact and the axial force of contact produced by the tractions $\underline{\mathbf{s}}(s)$, on a beam structure having the same shape of $\partial\Omega$, and cut at the point $s = 0$.

Regular and singular equilibrated stress fields can be derived by stress functions meeting the prescribed boundary condition on *F* and dF/dv. The projection of a fold of *F* on Ω is called folding line and is denoted with Γ. On a fold of *F*, the second derivative of *F*, with respect to the normal **m** to the folding line Γ, is a Dirac delta with support on Γ. Therefore, along Γ the Hessian **H**(*F*) of the stress function *F* is a dyad of the form:

$$\mathbf{H}(F) = \Delta_m F \delta(\Gamma) \mathbf{m} \otimes \mathbf{m} \, , \tag{3.34}$$

where $\Delta_m F$ is the jump of slope of *F* in the direction of the normal **m** to Γ. Recalling the Airy's relation, the corresponding singular part of the stress is:

$$\mathbf{T}_s = N \delta(\Gamma) \mathbf{t} \otimes \mathbf{t} \, , \tag{3.35}$$

where the axial contact force *N* is given by:

$$N = \Delta_m F \, . \tag{3.36}$$

3.1.6 The equilibrium problem: statically admissible stress fields

A stress field **T** is said *statically admissible* for a NRNT body, when it is in equilibrium with the body force **b** and the tractions $\underline{\mathbf{s}}$ on $\partial\Omega_N$, that is it is an equilibrated stress field, and also satisfies the unilateral condition (2.3), or equivalently condition (2.7) in a plane case. Then, the set of statically admissible stress fields *H* is:

$$H = \left\{ \mathbf{T} \in S(\Omega) \;\; s.t. \; div\mathbf{T} + \mathbf{b} = \mathbf{0}, \mathbf{T}\boldsymbol{n} = \underline{\mathbf{s}} \; on \; \partial\Omega_N, \mathbf{T} \in Sym^{-} \right\} , \tag{3.37}$$

where $S(\Omega)$ is a function space of convenient regularity, which, for RNT materials, can be assumed as the set of bounded measures $S(\Omega) = \mathrm{M}(\Omega)$. The set of functions which compete for equilibrium for NRNT materials is so large that the search of statically admissible stress fields becomes easier.

The equilibrium is imposed in a variational form, in order to reformulate the differential equations for non-smooth **T**, this can be done by using the Virtual Work Principle. Thus, we introduce the set of virtual displacements:

$$K^0 = \{\delta\mathbf{u} \in S^*(\Omega) \;\; s.t. \, \delta\mathbf{u} = \mathbf{0} \; on \; \delta\Omega_D\}\,, \tag{3.38}$$

the stress field **T** is in equilibrium with the force system ($\underline{\mathbf{s}}, \mathbf{b}$) if and only if:

$$\int_{\partial\Omega_N} \underline{\mathbf{s}} \cdot \delta\mathbf{u} + \int_{\Omega} \mathbf{b} \cdot \delta\mathbf{u} = \int_{\Omega} \mathbf{T} \cdot \mathbf{E}\,(\delta\mathbf{u}) \;\; , \forall \delta\mathbf{u} \in \delta\mathrm{K}\,. \tag{3.39}$$

$S^*(\Omega)$ is a function space of convenient regularity and, if $\mathbf{T} \in M(\Omega)$, condition $S^*(\Omega) = C^1(\Omega)$ occurs, which ensures the possibility of computing the internal virtual work.

Referring to any statically admissible stress field **T**, the domain $\Omega = \Omega \cup \partial\Omega_D$ can be partitioned as follows:

$$\Omega_1 = \{\mathbf{x} \in \Omega \, s.t. \, tr\mathbf{T} \leq 0 \,, det\mathbf{T} \geq 0\}\,, \tag{3.40}$$

$$\Omega_2 = \{\mathbf{x} \in \Omega \, s.t. \, tr\mathbf{T} \leq 0 \,, det\mathbf{T} = 0\}\,, \tag{3.41}$$

$$\Omega_3 = \{\mathbf{x} \in \Omega \, s.t. \, \mathbf{T} = 0\}\,. \tag{3.42}$$

Hence, by representing the stress field **T** through the following spectral decomposition:

$$\mathbf{T} = \sigma_1 \mathbf{k}_1 \otimes \mathbf{k}_1 + \sigma_2 \mathbf{k}_2 \otimes \mathbf{k}_2\,, \tag{3.43}$$

the set Ω_1 contains biaxial compressive stresses ($\sigma_1 < 0, \sigma_2 < 0$), the set Ω_2 contains uniaxial compression stresses ($\mathbf{T} = \sigma\, \mathbf{k} \otimes \mathbf{k}\,, \sigma < 0$) and the set Ω_3 is inert. The form and the regularity of these regions depend on the smoothness of **T** and, even in the case in which these regions degenerate, by admitting bounded measures (that is Dirac deltas with support on a finite number of regular arcs), the domain $\Omega = \Omega \cup \partial\Omega_D$ can be still partitioned in this way.

In absence of body forces, we can express a statically admissible stress field, referring to a scalar function F, named Airy's function, then the unilateral condition for the stress field **T**, in the plane case, can be rewritten as follows:

$$tr\mathbf{T} = F_{,11} + F_{,22} \leq 0 \ , \quad \det \mathbf{T} = F_{,11}F_{,22} - F_{,12}^2 \geq 0 \ , \tag{3.44}$$

Then, since the Hessian **H**(*F*) of *F* is negative semidefinite, the stress function *F* must be concave, thus in absence of body forces the equilibrium problem for a No-Tension material translates into the search of a concave function F, whose slope and value are specified on the part $\partial\Omega_N$ of the boundary.

3.1.7 The kinematical problem: kinematically admissible displacement fields

When a displacement field **u** satisfies the boundary conditions $\mathbf{u} = \underline{\mathbf{u}}$ on the constrained part $\partial\Omega_D$ of the boundary, such that the effective strain $\mathbf{E}^* = (\mathbf{E}(\mathbf{u}) - \underline{\mathbf{E}})$ is positive semidefinite, it is defined *kinematically admissible* for a NRNT body, and it is denoted *K*:

$$K = \left\{\mathbf{u} \in T(\Omega) \ \ s.t. \mathbf{u} = \underline{\mathbf{u}} \ on \ \partial\Omega_D, \ \ \mathbf{E}^* = (\mathbf{E}(\mathbf{u}) - \underline{\mathbf{E}}) \in Sym^+\right\}, \tag{3.45}$$

where $T(\Omega)$ is a function space of convenient regularity and $\Omega = \Omega \cup \partial\Omega_D$.

Since for a Normal Rigid No-Tension material we can consider discontinuous displacements, it can be assumed that the function space $T(\Omega)$ is represented by the set of functions of bounded variation, that is, for example, functions **u** admitting finite discontinuities, which consist in finite jumps on a finite number of regular arcs.

Since the derivative of **u** does not exist in a classical sense, and the trace of **u** on $\partial\Omega_D$ is not well defined, we reformulate the relation between **E** and **u** in a weak form, by imposing the compatibility in a variational form, namely by using the Complementary Virtual Work Principle. Hence, we introduce the set of virtual stress field:

$$H^0 = \{\delta\mathbf{T} \in T^*(\Omega) \ \ s.t. div\delta\mathbf{T} = \mathbf{0} \ , \delta\mathbf{T}\boldsymbol{n} = \mathbf{0} \ on \ \partial\Omega_N\} \ , \tag{3.46}$$

the displacement field **u** is compatible with the kinematical data $(\underline{\mathbf{u}}, \underline{\mathbf{E}})$ if and only if:

$$\int_{\partial\Omega_D} (\delta\mathbf{T}\mathbf{n}) \cdot \underline{\mathbf{u}} - \int_{\Omega} \delta\mathbf{T} \cdot \underline{\mathbf{E}} = \int_{\Omega} \delta\mathbf{T} \cdot \underline{\mathbf{E}}\,(\mathbf{u}), \forall \delta\mathbf{T} \in \delta H\,, \tag{3.47}$$

where $T^*(\Omega)$ is a function space of convenient regularity. If we consider, as in the case of linear elasticity, that $\mathbf{u} \in H^1(\Omega)$, then condition $T^*(\Omega) = L^2(\Omega)$ guarantees that the internal virtual work is finite. If $\mathbf{u} \in \mathrm{BV}(\Omega)$, the possibility of computing the internal virtual work is ensured by condition $T^*(\Omega) = C^\circ(\Omega)$.

3.1.8 Compatibility and incompatibility of loads and distortions

The loads $(\underline{\mathbf{s}}, \mathbf{b})$ and the distortions $(\underline{\mathbf{u}}, \underline{\mathbf{E}})$ represent the data of a general BVP for a NRNT body. For NRNT materials, the equilibrium problem and the kinematical problem, that is the search of admissible stress and displacement fields for given data, are uncoupled, except when we refer to the condition which implies that the masonry material do not dissipate energy, that is $\mathbf{T} \cdot \mathbf{E} = \mathbf{0}$.

$$\boldsymbol{\ell}\left(\underline{\mathbf{s}}, \mathbf{b}\right) \;\; loads$$
$$\boldsymbol{\ell}^*\left(\underline{\mathbf{u}}, \mathbf{E}\right) \;\; distortions$$

When we refer to a NRNT material, the existence of statically admissible stress fields for given loads and kinematically admissible displacement fields for given distortion is submitted to particular conditions, named compatibility conditions of the data. Hence, we define compatible loads, the data $(\underline{\mathbf{s}}, \mathbf{b})$ for which the set of statically admissible stress field H is not empty, as well as compatible distortions, the data $(\underline{\mathbf{u}}, \underline{\mathbf{E}})$ such that the set of kinematical admissible displacement field K is not empty:

$$\ell \; is \; compatible \;\Leftrightarrow \{H \neq \emptyset\}\,, \tag{3.48}$$

$$\ell^* \; is \; compatible \Leftrightarrow \{K \neq \emptyset\}\,. \tag{3.49}$$

Hence, we can check the compatibility of loads and distortions by constructing a statically admissible stress field and a kinematically admissible displacement field. However, the compatibility of ℓ and ℓ^* is necessary but not sufficient to prove the existence of a solution to the BVP for a NRNT material, since also the material restriction about the absence of internal dissipation must be satisfied.

There is also an indirect way to verify the incompatibility of loads and distortions, which implies to consider the sets:

$$H^\circ = \{\mathbf{T}^\circ \in S(\Omega)\ s.t.\ div\mathbf{T}^\circ = \mathbf{0}\ ,\ \ \mathbf{T}^\circ \boldsymbol{n} = \mathbf{0}\ on\ \partial\Omega_N, \mathbf{T}^\circ \in Sym^-\} \tag{3.50}$$

$$K^\circ = \{\mathbf{u}^\circ \in T(\Omega)\ s.t.\ \mathbf{u}^\circ = \mathbf{0}\ \ on\ \partial\Omega_D\ ,\ \ \mathbf{E}(\mathbf{u}^\circ) \in Sym^+\}\,, \tag{3.51}$$

which can reduce to the corresponding null stress and strain fields sets $H^{\circ\circ}$ and $K^{\circ\circ}$, depending on the geometry of the boundary, of the loads and of the constraints.
The incompatibility of loads can be assessed as follows:

$$\ell\ is\ compatible\ \Leftarrow \{\exists \mathbf{u}^\circ \in K^\circ\ \ s.t.\ \langle \ell, \mathbf{u}^\circ\rangle > 0\}\,, \tag{3.52}$$

$$\ell^* is\ compatible\ \Leftarrow \{\exists \mathbf{T}^\circ \in H^\circ\ \ s.t.\ \langle \ell^*, \mathbf{T}^\circ\rangle > 0\}\,. \tag{3.53}$$

The incompatibility of loads implies the absence of equilibrium and the possibility of indefinite acceleration for the structure; the incompatibility of distortions implies the absence of zero energy modes through which the kinematical data can be accommodated.

3.2 The Equilibrium problem: Limit Analysis

As we have seen, the boundary value problem for masonry-like (NRNT) materials can be split in two problems, that is the kinematical problem and the equilibrium problem. The first consists in the search of a kinematically admissible displacement field, that is a displacement field belonging to the set K, the latter consists in the search of a statically admissible stress fields, that is a stress field belonging to the set H.

Considering the equilibrium problem, for a structure made of NRNT material (that is a structure occupying the domain Ω, subject to the action of body loads **b**, constrained on the part $\partial\Omega_D$ of the boundary and loaded by given tractions $\underline{\mathbf{s}}$ on the remaining part $\partial\Omega_N$), we observe that the material restrictions defining NRNT materials are sufficient for the theorems of Limit Analysis to be valid.

The theorems of Limit Analysis are strictly connected to the compatibility of load data ($\underline{\mathbf{s}}, \mathbf{b}$) (see § 3.1.8), as it will be seen below. In what follows we give a short account of the theory on which the theorems of Limit Analysis are constructed.

3.2.1 Theorems of Limit Analysis

We refer to perfectly-plastic materials, characterized by an associate plastic potential, according to the normality law and the stability postulate by Drucker: such materials are briefly defined as *normal materials* or *stable materials*.

In Appendix B, the basic ingredients of kinematics, balance laws and material restrictions characterizing perfectly plastic materials are given in detail. Who is already familiar with the Plasticity theory can skip Appendix B, and read directly what follows.
When we consider an elastic-plastic material, stresses cannot grow indefinitely, since they cannot exceed the yielding limits; for this reason, the body loads **b** and the tractions $\underline{\mathbf{s}}$ cannot be indefinitely amplified.

We now introduce some definitions.

We define *plastic collapse* a state for which the structure, in whole or in part, suffers an unbounded acceleration driven by the given loads $(\underline{\mathbf{s}}, \mathbf{b})$. The fact that the loads drive the acceleration is attested by a positive value of the kinetic energy of the system.

We observe that during collapse both the strains and the displacements grow indefinitely either over the whole structure or in a part of it. The part of the displacement field, which indefinitely grows at collapse (and the allied strains) defines a *collapse mechanism*.

The stress field $\boldsymbol{\sigma}^a$ is called *statically admissible stress field*, if it satisfies the equilibrium equations (3.54) and the boundary equations (3.55):

$$\frac{\partial \sigma_{ij}^a}{\partial x_i} + b_i = 0 \ , \qquad x \in V \ , \tag{3.54}$$

$$\sigma_{ij}^a n_j = s_i \ , \qquad x \in \partial V \ , \tag{3.55}$$

as well as the feasibility condition:

$$f(\boldsymbol{\sigma}^a) \leq 0 \ , \tag{3.56}$$

being n the outward normal to V, whose boundary is ∂V.

We call *admissible loads* the load system $(\underline{\mathbf{s}}, \mathbf{b})$ which is in equilibrium with the admissible stress field $\boldsymbol{\sigma}^a$. The set $(\underline{\mathbf{s}}, \mathbf{b}, \boldsymbol{\sigma}^a)$ is said to be equilibrated. The collapse load system $(\underline{\mathbf{s}}, \mathbf{b})$ and the stress $\boldsymbol{\sigma}$ at collapse, represent the *admissible load-tension system* $(\underline{\mathbf{s}}, \mathbf{b}, \boldsymbol{\sigma})$ determined under the collapse of the structure.

The stress field $\boldsymbol{\sigma}^s$ is called *statically safe stress field* or *safe stress field*, if it satisfies the equilibrium equations (3.54) and the boundary equations (3.55), and also the compatibility condition:

$$f(\boldsymbol{\sigma}^s) < 0 \ , \tag{3.57}$$

and the load system $\left(\mathbf{b}^s, \underline{\mathbf{s}}^s\right)$, which is in equilibrium with this safe stress field, is said *safe load system.*

We consider the *displacement rate field* $\dot{\mathbf{u}}_\mathbf{0}$, which satisfies the kinematic conditions on the constrained boundary of the domain *V*:

$$\dot{\mathbf{u}}_\mathbf{0} = \underline{\dot{\mathbf{u}}}_\mathbf{0} \ , \qquad \mathbf{x} \in \partial V_D \ , \tag{3.58}$$

The corresponding infinitesimal *strains rate field*, which satisfies the kinematic conditions with $\dot{\mathbf{u}}_\mathbf{0}$ are expressed as follows:

$$\dot{\varepsilon}_{0ij} = \frac{1}{2}\left(\frac{\partial \dot{u}_{0i}}{\partial x_j} + \frac{\partial \dot{u}_{0j}}{\partial x_i}\right) , \qquad \mathrm{x} \in \partial V \ . \tag{3.59}$$

The set $(\dot{\mathbf{u}}_\mathbf{0}, \dot{\varepsilon}_0)$ is said *kinematically admissible strain-displacement field*, or briefly *admissible kinematism*.

3.2.2 Static Theorem of Plastic Collapse

Part I. If a load program is assigned, the existence of a statically safe stress field $\boldsymbol{\sigma}^s$, for each instant of the load program, is a sufficient condition so that the plastic collapse will not occur.

Part II. The structure cannot sustain an external load system if there is not even an admissible stress distribution $\boldsymbol{\sigma}^a$. In such a case, indeed, the equilibrium is not possible unless we violate the yielding limit. Hence collapse will occur.

The Theorems of Limit Analysis can be enunciated through a very intuitive and discursive way, as follows:

I. The structure does not collapse under an assigned load condition, if there exist at least one statically admissible stress field which is in equilibrium with the external load.

II. The structure does collapse under an assigned load condition, if there exist at least one kinematically admissible mechanism such that the power dissipated inside the material is lower than the power produced by the external loads.

3.2.3 Limit Analysis for NRNT Materials

The *Static Theorem* states that the load data $\{\underline{\mathbf{s}}, \mathbf{b}\}$ do not produce collapse, if there exists at least one balanced stress field of pure compression and balancing the load data $\{\underline{\mathbf{s}}, \mathbf{b}\}$.

The *Kinematical Theorem* states that the given loads produce collapse, if there exists at least one kinematically admissible displacement field $\mathbf{u}$, for which the load data $\{\underline{\mathbf{s}}, \mathbf{b}\}$ perform positive work. Such a displacement field, that is a no-sliding, no-shortening deformation, satisfying homogeneous boundary conditions on the constrained part of the boundary, represents a possible collapse mechanism. In this case, the structure is not in equilibrium and will accelerate.

3.3 The kinematical problem: an energy criterion

With the NRNT model, the problem of equilibrium, that is the search of a statically admissible stress field, and the kinematical problem, that is the search of a kinematically admissible displacement field, are essentially uncoupled, then they can be treated separately.

The only equation which couples them is the condition that the internal work density must be zero; then we say that the solution of the equilibrium problem is reconcilable with the solution of the kinematical problem, if the stress corresponding to the former does, point by point, zero work for the strain corresponding to the latter. Actually, the kinematical problem is not completely independent of the equilibrium one. When a mechanism due to settlements or distortions is activated in a part of the structure, that part becomes statically determined and the reactive forces in that part can be obtained from the equilibrium equations. This behaviour is illustrated with a simple example in § 1.2.

Although the kinematical data $\{\underline{\mathbf{u}}, \underline{\mathbf{E}}\}$ are not at all secondary for masonry analysis, for which fractures and cracks are associated to compatible mechanism provoked by such a kind of actions, they do not appear into the theorems of Limit Analysis, then they are irrelevant for the assessment of structural safeness. By assuming, indeed, that the unilateral material is rigid in compression, cannot withstand any tensions and is non-dissipative, the reference equilibrium geometry is not affected by the kinematical data; this is also a consequence of the small displacement assumption.

Then, whether settlements are considered or not, under the action of given loads the structural geometry in stable. This condition is particularly advantageous, since most of the time the kinematical data are not known in detail, as the external forces. However, in real problems, the effect of these data is associated to a specific crack pattern, which implies a compatible mechanism that can be deduced through an inverse analysis.

Moreover, among all the infinite possible kinematically admissible displacement fields, the special mechanism activated by the kinematical data $\{\underline{\mathbf{u}}, \underline{\mathbf{E}}\}$, also depends on the load data $\{\underline{\mathbf{s}}, \mathbf{b}\}$.

3.3.1 The kinematical problem

Regarding the kinematical problem, if the kinematical data cannot be adjusted through a compatible mechanism, that is a no-shortening, no-sliding displacement complying with the boundary constraints, the structure must deform, we say that the problem does not admit a solution. Then we can recall the existence and non-existence theorems.

Compatibility theorem. The kinematical data $\{\underline{\mathbf{u}}, \underline{\mathbf{E}}\}$ are compatible if there exists at least one displacement field $\mathbf{u}$ which is kinematically admissible, complying with the NRNT restrictions and satisfying the given boundary conditions.

Incompatibility theorem. The given kinematical data $\{\underline{\mathbf{u}}, \underline{\mathbf{E}}\}$ are not compatible if there exists a statically admissible stress field, whose eigenstress are all negative, which performs positive work for these data.

Remark 2. It can be observed that the kinematical and the equilibrium problems can be incompatible, in the sense that both the sets K, H can be empty. In particular, the compatibility of the equilibrium problem is the key issue of the two theorems of Limit Analysis, which deal with the possibility of collapse of the structure.

3.3.2 The energy criterion

In the case study here analysed, it is assumed that the kinematical and the equilibrium problems are both compatible, that is the sets K, H are not void and that collapse is not possible. A trivial case of compatibility of the kinematical problem and equilibrium problem occurs when the displacement data and the load data are zero respectively.

When trying to solve the kinematical problem, the problem arises of selecting, among the possibly many kinematically admissible displacement fields, responding to the given kinematical data (settlements and distortions), the ones that guarantee also the equilibrium of the loads imposed on the structure. For elastic, and even for some elastic-brittle materials, these states, that we can call solutions of the boundary value problem, can be found by searching for the minimum of some, suitably defined, form of energy. For elastic-brittle materials this energy is the sum of the potential energy of the loads, of the elastic energy and of the interface energy necessary to activate a crack on an internal surface (see [32], [33], [34]). For elastic materials, it is the sum of the potential energy of the loads and of the elastic energy. For Heyman's materials, it is just the potential energy of the loads.

Then we may search a displacement field which is the solution of the kinematical boundary value problem, by minimizing the potential energy $\wp$ of the loads over a convenient function set, namely the set of piecewise rigid displacements. Such minimum problem is formulated as follows:

"*Find a displacement field* $\boldsymbol{u}^\circ \in K$*, such that:*

$$\wp(\boldsymbol{u}^\circ) = \min_{\boldsymbol{u} \in K} \wp(\boldsymbol{u}) \ ," \tag{3.60}$$

where:

$$\wp(\mathbf{u}) = -\int_{\partial\Omega_N} \underline{\mathbf{s}} \cdot \mathbf{u}\, ds - \int_{\Omega} \mathbf{b} \cdot \mathbf{u}\, da\,, \tag{3.61}$$

is the potential energy of the given loads.

The numerical approximation of the solution of the kinematical problem is the object of some papers (see [35], [36], [37], [38]). A trivial example of the application of the energy criterion to a simple structure composed of rigid blocks, is shown in §1.2.

The proof of the existence of the minimizer $\mathbf{u}^\circ$ of $\wp(\mathbf{u})$ for $\mathbf{u} \in K$, is a complex mathematical question, as observed in [37]. On assuming that the kinematic problem is compatible (that is $K \neq \emptyset$), what we can easily show is that:

a. If the load is compatible (that is $H \neq \emptyset$) the linear functional $\wp(u)$ is bounded from below.
b. If the triplet $(\mathbf{u}^\circ, \mathbf{E}(\mathbf{u}^\circ), \mathbf{T}^\circ)$ is a solution of the bvp, it corresponds to a weak minimum of the functional $\wp(\mathbf{u})$.

Proofs.

a. If the load is compatible, then there exists a stress field $\mathbf{T} \in H$, through which the functional $\wp(\mathbf{u})$ defined on K, for any $\mathbf{u} \in K$, can be rewritten as follows:

$$\begin{aligned} \wp(\boldsymbol{u}) = \quad & -\textstyle\int_{\partial\Omega_N} \underline{\mathbf{s}} \cdot \mathbf{u}\, ds - \int_{\Omega} \mathbf{b} \cdot \mathbf{u}\, da \;= \\ & = \textstyle\int_{\partial\Omega_D} \mathbf{s}(\mathbf{T}) \cdot \underline{\mathbf{u}}\, ds - \int_{\Omega} \mathbf{T} \cdot \mathbf{E}(\mathbf{u}) da\,, \end{aligned} \tag{3.62}$$

$\mathbf{s}(\mathbf{T})$ being the trace of $\mathbf{T}$ at the boundary. Assuming that the displacement data are sufficiently regular (say continuous), being $\mathbf{s}(\mathbf{T})$ a bounded measure, the integral $\int_{\partial\Omega_D} \boldsymbol{s}(\mathbf{T}) \cdot \underline{\mathbf{u}}\, ds$ is finite; then, since $\mathbf{T} \in Sym^-$ and $\mathbf{E} \in Sym^+$, the volume integral is non-negative, and $\wp(\mathbf{u})$ is bounded from below.

b. If $(\mathbf{u}^\circ, \mathbf{E}(\mathbf{u}^\circ), \mathbf{T}^\circ)$ is a solution of the bvp, then, for any $\mathbf{u} \in K$, we can write:

$$\begin{aligned} \wp(\mathbf{u}) - \wp(\mathbf{u}^\circ) = & -\textstyle\int_{\partial\Omega_N} \underline{\mathbf{s}} \cdot (\mathbf{u} - \mathbf{u}^\circ) ds - \int_{\Omega} \mathbf{b} \cdot (\mathbf{u} - \mathbf{u}^\circ) da \;= \\ & = -\textstyle\int_{\Omega} \mathbf{T}^\circ \cdot \big(\mathbf{E}(\mathbf{u}) - \mathbf{E}(\mathbf{u}^\circ)\big)\, da\,. \end{aligned} \tag{3.63}$$

The result $\wp(\mathbf{u}) - \wp(\mathbf{u}^\circ) \geq 0\ ,\ \forall \mathbf{u} \in K$, follows form normality (see [39]).

The physical interpretation of the above result is the following. Since the displacement field solving the b.v.p corresponds to a state of weak minimum for the energy, then it is

a neutrally stable equilibrium state, in the sense that the transition to a different state requires a non-negative supply of energy.

Based on the minimum principle, if the *equilibrium problem* is compatible and the *kinematical problem* is homogeneous, $\mathbf{u} = \mathbf{0}$ is a minimum solution. Indeed, in such a case:

$$\wp(\mathbf{u}) = -\int_{\partial\Omega_N} \underline{\mathbf{s}} \cdot \mathbf{u}\, ds - \int_{\Omega} \mathbf{b} \cdot \mathbf{u}\, da = -\int_{\Omega} \mathbf{T} \cdot \mathbf{E}(\mathbf{u}) da\,, \tag{3.64}$$

$\mathbf{T}$ being any element of H. Since the right-hand side of (3.61) is non-negative, $\wp(\mathbf{0}) = 0$ is the minimum of $\wp$ and $\mathbf{u} = \mathbf{0}$ is a minimizer of the potential energy. Notice that, in this case, any $\mathbf{T} \in H$ is a possible solution in terms of stress, since $\mathbf{T} \cdot \mathbf{E}(\mathbf{0}) = 0$ for any $\mathbf{T}$.

An approximate solution of the minimum problem can be obtained, by restricting the search of the minimum in the restricted class of piecewise rigid displacements. In this case, the infinite dimensional space is discretized by considering a finite partition of the domain Ω into a number M of rigid pieces Ω_i with $i = 1, \dots, M$ such that the sum of the relative perimeters $P(\Omega_i)$ is a finite quantity. The boundary $\partial\Omega_i$ of these rigid pieces Ω_i is composed in n segments Γ, whose extremities are denoted with 0 and 1 and whose length is ℓ. The segments Γ, called *interfaces*, consist of the common boundaries between both two inner adjacent elements and an inner element and the constrained boundary. Hence, we refer to the minimum problem where the displacement variable $\mathbf{u}$ belongs to a partitioned set, that is $\mathbf{u} \in K^M_{part}$:

$$\wp(\hat{\mathbf{u}}) = \min_{\boldsymbol{u} \in K^M_{part}} \wp(\mathbf{u})\,. \tag{3.65}$$

In this case, we represent the generic piecewise rigid displacement through the vector $\boldsymbol{U}$ of $6M$ components, represented by the $6M$ rigid body parameters of translations and rotations of the elements, for which the assumption about positive semidefinite strain must hold. When we refer to piecewise rigid displacement, which are the most frequent and evident manifestation of masonry deformation in real masonry constructions, the strain is concentrated along the interfaces Γ, and on each interface, we consider the unilateral conditions and the absence of sliding among blocks. The associated stress vector must satisfy the negative semidefinite condition, that is it must be a compressive stress field.

As pointed out in [40], "…the piecewise rigid displacements, are not at all simple displacement fields for a continuum, and are usually ruled out in the standard numerical codes for fluids and solids which are employed to handle the complex boundary value problems of continuum mechanics. The main difficulty with discontinuous displacements, besides the managing of the singularity of strain for deformable materials, is the fact that the location of the support of the singularity (that is of the jump

set of the displacement) is not known in advance…". This latter issue is discussed with the aid of some simple examples in the forthcoming paper [36].

The situation becomes simpler if the interfaces between rigid parts can be fixed in advance, as is actually the case for masonry structures composed by monolithic blocks. In such a case, we may search the piecewise rigid displacement field by minimizing the potential energy $\wp$ of the loads applied to a known structure, formed by "M" given rigid blocks in unilateral contact without sliding with the soil and among each other. We can consider, as primal variable, the vector $\widehat{\mathbf{u}}$ of the rigid body parameters ($6M$ in space problems) of the structure; the functional $\wp$ is linear in $\widehat{\mathbf{u}}$, then the minimization of $\wp$ reduces to the minimization of a linear functional under linear unilateral and bilateral constraints. Such a problem is an easy problem of convex analysis that can be solved with Linear Programming (see [40], [41], [42]).

Chapter 4

APPLICATIONS TO STRUCTURES MADE OF RIGID BLOCKS

Prologue. The main mechanical aspect of masonry structures is their essentially unilateral behaviour. Such structures may actually fracture everywhere at their inside, forming rigid blocks in relative displacement among each other. Such piecewise rigid-body displacements in masonry are physiological, and rather than the result of over-loading, are most likely the direct product of small changes of the displacement type boundary conditions.

It can be observed as, while for a standard over-determined structure, subject to bilateral constraints, the effect of small settlements and eigenstrains has a high probability of determining a substantial change of the internal forces, a structure subject to unilateral constraints, even if heavily over-constrained, is more prone to compensate the effect of large settlements without any increase of the internal forces, through the mobilization of zero energy modes.

Furthermore, for a standard structure the existence of an equilibrium solution can be ensured only by virtue of its geometry and constraints and, if zero energy modes are admitted, the possibility of maintaining the equilibrium solution is severely restricted. Instead, for unilateral structures the equilibrium solution depends only on the loads and the coexistence of equilibrium solutions and of zero energy dissipation mechanisms, such as piecewise rigid displacements, is usually the rule.

When a mechanism due to settlements or distortions is activated in a part of the structure, that part becomes statically determined and the reactive forces in that part can be obtained from the equilibrium equations.

Here a simple model, based essentially on Heyman's hypotheses, is applied to study the equilibrium of masonry structures made of monolithic pieces, in particular cantilevered stairs, or, more precisely, spiral stairs, composed of monolithic steps, with an open well

are analysed. The modelling of masonry structures made of monolithic blocks, through distinct element methods, has become popular in recent years (see [43], [44]).The case of cantilevered stairs is analysed with a discrete element approach by Rigò and Bagi in the forthcoming paper [45].

As observed by Heyman in his paper [46], the basic structural action for a cantilevered stair of small flight (quarter or half landing) is twist of individual treads, leading to shear stresses in the masonry; such stresses are low for short stairs, but become more and more harmful than direct compression for long flights. In a recent work by Angelillo [47], based on a continuous approximation of the stair structure, it is shown as the torsional Heyman's mechanism can be combined with a Ring-Like regime, giving rise to large compressive forces and to moderate torsional torques, whose intensity reaches a plateau for long flights.

In the present work, we obtain a practical confirmation of the complementarity of Heyman and Ring-Like stress regimes, for the case study of the triple helical stair of San Domingos de Bonaval, by employing a discrete model. In order to generate statically admissible sets of internal forces, likely sets of given settlements of the constraints are considered and the corresponding piecewise rigid displacements are found by minimizing the potential energy. The moving part of the structure is statically determined, then the dual static problem is dealt with by solving the equilibrium of the entire structure and of the individual steps. The whole calculation procedure is carried out with the programming language Matlab.

4.1 Case study

The present work concerns the study of the equilibrium and of the effect of settlements in structures made of monolithic blocks; in particular, as an illustration of the method, we consider the case study of the triple helical stair of the convent of San Domingos de Bonaval, built by the Galician Baroque architect Domingo de Andrade, in the XVII century. The convent of San Domingos de Bonaval, founded by St. Dominic de Guzman in 1219, is located in the countryside of San Domingos, in the Bonaval district of Santiago de Compostela.

This triple helical staircase consists of three separate interwoven coils, that lead to different storeys; only one of them reaches the upper viewpoint. Each step of the stair, made of a whole stone piece of granite, is built into the outer cylindrical wall for a depth of 0.3 m (see Fig. 4.1). The steps are not in contact among each other but at their inner end, where they form a rib and the railing is present (Fig. 4.1d).

Fig. 4.1: Convent of San Domingos de Bonaval:
a), b), c) View of the triple helical stair; d) Detail of the steps

For what concerns the application of the unilateral model to vaults, the existing more recent literature is rather vast; apart from the production of the school of Salerno, originated by the paper on the Lumped Stress Method [48], and applied to vaults in the papers by Fraternali et al. [49], Angelillo & Fortunato [5], Fraternali [50], and recently by Angelillo et al. in [51], we recall the pioneering work by O'Dwyer [52], and the works by Block [53], Block et al. [54], Vouga et al. [55], De Goes et al. [56], Block and Lachauer [57], Miki et al. [58] and Marmo and Rosati [59].

The equilibrium of helical stairs with an open well is formulated and applied to some case studies in [47], [60], [61].

The equilibrium of the staircase shown in Fig. 4.1 is studied by Angelillo in [47], by applying Heyman's model for masonry material (rigid no-tension), and considering that each step behaves as a beam, supported and built in torsionally at the outer wall, and simply supported at the inner rib, a structural element which can transmit only contact compressive forces.

4.1.1 Heyman's solution

As observed by Heyman [46], the basic structural action for a cantilevered stair for small flight (quarter or half landing), is represented by twist of individual steps, which leads to shear stresses in the masonry; such stresses are low for short stairs, but become more harmful than direct compression for long flights.

Heyman considers that each step is supported by the step below on the free edge and it is inserted into the wall on the other edge, hence he models each step as a simply supported beam (Fig. 4.2). Considering that in the centroid of each step it is applied the load P, he obtains the reactive forces at the edges, equal to P/2. Proceeding from the top to the bottom, the equilibrium on the second step is given by the forces applied in the four edges of the step, then each step is subject to a torque: $\mathrm{M_t} = \frac{1}{2}\mathrm{Pb}$.

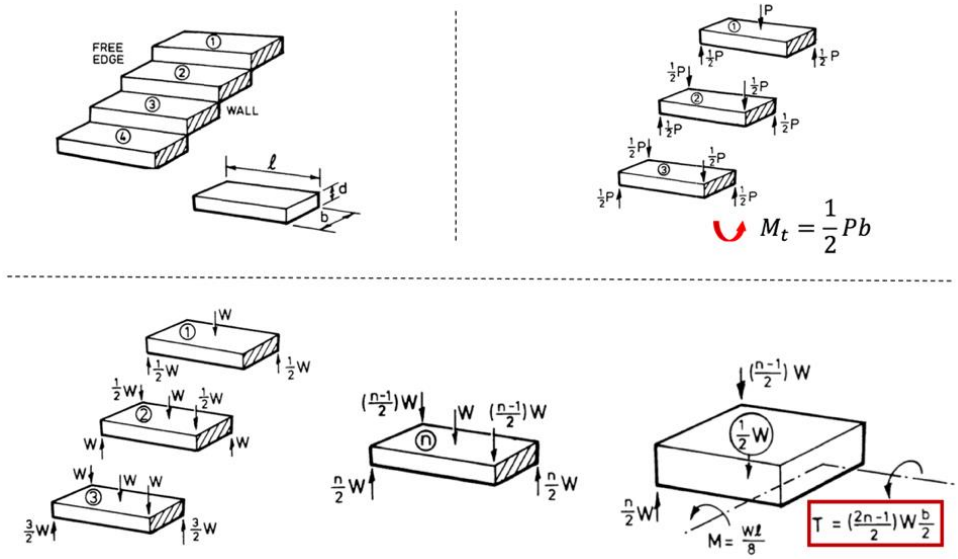

Fig. 4.2: "The mechanics of masonry stairs", J.Heyman [46]

The forces acting on the step 2 are given by the forces on the step 1 and that of the step 2, and so on. Thus, on the generic step, denoting with *n*=1 the step at the top of the stair, and with *W* the self-weight of the step, we have the following stress values:

$$\mathrm{M_t} = \left(\frac{2n-1}{2}\right)\mathrm{W}\frac{\mathrm{b}}{2}\ , \qquad \mathrm{M_f} = \frac{\mathrm{Wl}}{8}\ . \tag{4.1}$$

As can be seen, the bending moment is the same of that of a simply supported beam, while the torque linearly increases from the top to the bottom of the stair. It is evident that this kind of model is valid only for stairs of modest heights, otherwise we could have torque values too high for the steps near the ground, which would lead to their break.

4.1.2 Continuum (Ring-Like) equilibrium solution

In a recent work by Angelillo [47], based on an approximation of the stair structure with a 2d curved continuum, it is shown as the torsional mechanism, described by Heyman, can be combined with a Ring-Like regime, which determines large compressive forces and to moderate torsional torques, whose intensity reaches a plateau for long flights.

In [47] the stair is considered as a helical surface, composed by radial segments AB (representing the steps) and by a helical arch (representing the rib), on which the steps transmit part of the load. The outer edge of the step is inserted into the wall, where a bending and torsional support is considered, while the inner edge of the step is simply supported on top of the step below, this contact is modelled as a unilateral contact. On assuming that the stair is a membrane, the stresses concentrate on a surface (as a fan of uniaxial stresses) and on a line, namely the internal rib (Fig. 4.3).

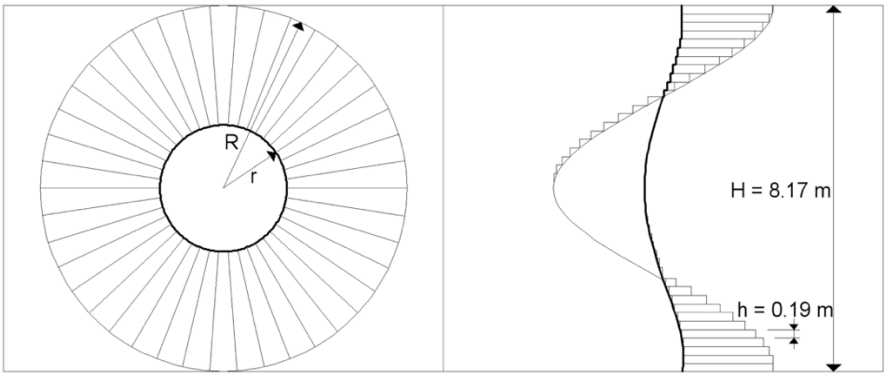

Fig. 4.3: Unilateral 2d and 1d curved structures where compressive stresses and stress resultants are concentrated

According to *Heyman's behaviour*, the steps transmit to the line structure Γ, to which the end points A of the steps are attached, a force, per unit length of Γ, directed vertically: $\underline{q} = q\underline{\hat{k}}$, and a resisting moment, per unit length of Γ, directed radially: $\underline{m} = m\underline{\hat{n}}$. A vertical load q=q(A) is applied to the spiral arch, whilst a moment equal and opposite to the distributed moment, due to the step load offset and acting on Γ, can be transmitted by the steps to the wall, through torsional internal contact moments. Indeed, the structure Γ has no bending resistance and can transmit only contact forces R such that $\underline{R} \cdot \underline{t} \leq 0$, since the material is unilateral.

From the equilibrium, we obtain the internal generalized stresses, that is the shear V(s), the bending moment $M_f(s)$ and the torsional moment $M_t(s)$ per unit length in the membrane:

$$V(s) = -qs\,,$$
$$M_f(s) = -\frac{qs}{\sqrt{1+p^2}}\,,$$

$$M_t(s) = qsr\delta\,,$$

where q is the constant load, r is the internal radius, δ is the angle of the step, and p is the slope of the spiral.

As described in § 4.1.1, Heyman assumes that the loads Q(A) are transferred from the upper steps to the lower steps through vertical forces applied at the contact points between them. The forces transmitted to the step *i* by the upper step *i-1* and by the lower step *i+1* are vertical forces balanced with the vertical load due to the step *i* and form a torque, representing a torsional moment acting on the step. The torque value increases on proceeding from the upper steps to the lower steps and produces, inside the step, shear stresses (that is tensile stresses) that remain low if the torque is not too high.

Then, the Heyman's solution is valid for stairs of moderate flight, otherwise there would be too high torque values, and, consequently, undesired tensile stresses.

It is evident that another solution is necessary. For this reason, in [47], with the continuum solution, the combination of Heyman's results with that of the Ring-Like behaviour is considered (Fig. 4.4).

Fig. 4.4: Coupling of Heyman's and Ring-Like behaviours [47]

Considering the *Ring-Like behaviour*, there is an axial contact force $\underline{R} = N\hat{\underline{t}}$ tangent to the spiral arch Γ. Moreover, the steps, besides the vertical load $\underline{q} = q^1\hat{\underline{k}}$ acting on Γ and defined per unit length of Γ, transfer to the spiral arch Γ, at each point of Γ, a distributed compressive force r (defined per unit of length of Γ) contained inside the steps and belonging to the plane $(\hat{\underline{n}}, \hat{\underline{k}})$, that is $\underline{r} = -r_k\hat{\underline{k}} + r_n\hat{\underline{n}}$.

From the equilibrium, we obtain a constant axial force N, which is tangent to the spiral arch Γ. We also have radial forces inside each step, whose slope is equal to: $\omega = \frac{h}{R-r}$. The components of these radial forces, contained in the steps, are:

$$r_k = q^1 \quad , \quad r_n = \frac{r_k}{\tan\omega} = \frac{q^1}{\tan\omega} \,, \tag{4.2}$$

Then, the axial force is:

$$N = -\frac{q^1 r^0}{\tan\omega}\,. \tag{4.3}$$

This solution is valid for stairs constrained at both ends, or equivalently, to stairs whose ends are subject to convenient compressive axial forces.

Therefore, one is forced to use the Heyman's equilibrium solution in a first sector springing from the top of amplitude α^0, and the Ring-Like solution in the remaining part of the stair. The minimal amplitude α^0 of the sector, in which the Heyman's solution can be adopted, is determined by the condition that the force transmitted from the first sector (free at the upper end) to the second sector must be a normal force tangent to the spiral arch Γ.

In order to transform the vertical force, transmitted by the first sector in correspondence of the amplitude α^0, in a force tangent to Γ, the horizontal force P is considered. This horizontal force is transmitted to the outer wall Γ_0, as a compressive force (Fig. 4.5).

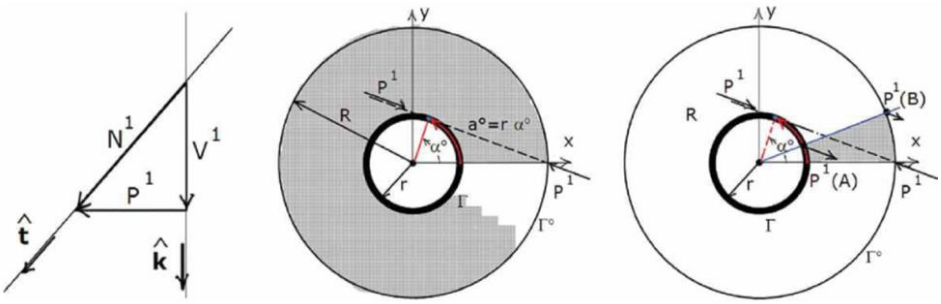

Fig. 4.5: Transmission of forces within the stair:
a) Equilibrium of forces at the end of the first sector; b) Minimal amplitude of the first sector; c) Equilibrium of horizontal forces due to the compressive force P^1 on a sector of amplitude α^0 proceeding from the top [47]

With this combined solution, limited shear and tensile stresses into the steps and also limited compressive stresses into the central rib are obtained, whatever be the flight of the helical stair.

The main result of the analysis presented in [47] is that the regime of torsion that is present in the upper, free part of the stair, can be gradually substituted by the Ring-Like stress regime which stabilizes and becomes essentially independent of the length of the stair.

One of the scopes of the present work is to provide a practical confirmation of the analytical solution presented in [47], by employing a discrete model of the stair, formed by *M* rigid pieces, which are the steps of the stair. The solution of this complex multi-body model, in terms of displacements and internal forces, represents a nice example of the application of the energy criterion, and confirms the general validity of the proposed approach for the analysis of discrete structures, whose pieces are in unilateral contact, without sliding, among each other.

4.1.3 Geometrical and mechanical data

The helical stair is characterized by a height of a complete landing $H = 8.17$ m, by an outer radius $R = 2.70$ m and an inner radius $r = 1.00$ m; each landing contains 42 steps, the rise of each step is $h = 0.19$ m, the step angle is $\delta = 0.1496$ rad, the width of the step at the inner and outer boundaries are respectively $\ell_r = 0.1496$ m and $\ell_R = 0.4039$ m, and the length of the built in end is 0.30 m (Fig. 4.6 and Fig. 4.7).

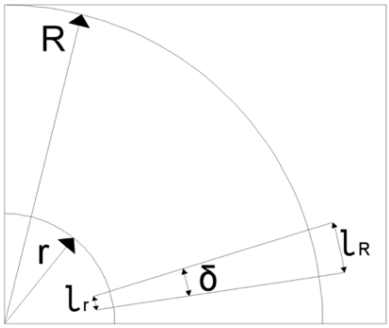

Fig. 4.6: Basic geometry of the stair

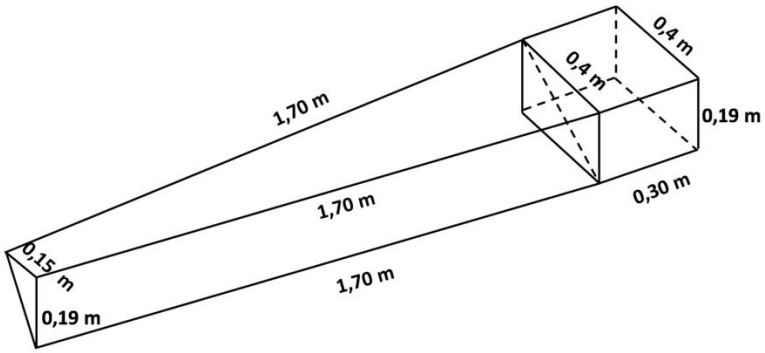

Fig. 4.7: Dimensions of the step

The steps we consider are made of monolithic stones. In particular, in the case study, the material of the stone is granite. We recall here the main mechanical properties of Galician granite (see [47]):

- $\sigma_c \approx 170\ MPa$ compressive strength;
- $\sigma_t \approx 16\ MPa$ tensile strength;
- $\tau^\circ \approx 25\ MPa$ shear strength;
- $E \approx 24\ GPa$ Young's modulus;
- $\rho \approx 2700\ kg/m^3$ density;

4.1.4 Reference systems

Different reference systems (Fig. 4.8) are introduced, in order to facilitate the writing of the constraint conditions. In particular, we consider three different reference systems, as described below:

1. *G: Global System*, whose origin is in the centre of the helix at ground level and whose z-axis is coincident with the axis of the helix and is directed upward; this system is used for describing the global geometry of the stair (Fig. 4.8a).
2. *S: Local System*, chosen in such a way that its origin is in the middle point of the upper outer edge of the step, the first axis is directed radially and represents the axis of symmetry for the step, as seen from above; the y-axis is directed along the upper outer edge; finally, the third axis is vertical and directed upwards (Fig. 4.8b).
3. *K: Local System*, whose origin is in the point N, the x-axis is directed radially, the z-axis parallel to the z-axis of the global system (Fig. 4.8c).

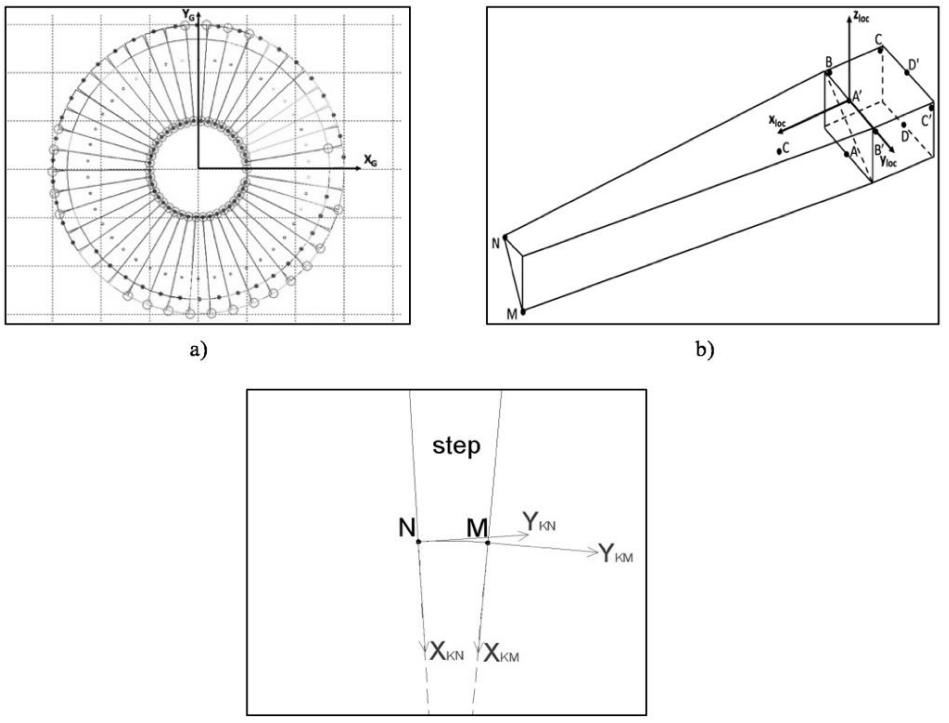

Fig. 4.8: Reference Systems: a) Global System G, b) S-Local System S, c) Local System K

4.1.5 Three-dimensional Modelling

The first aspect is the definition of the stair's geometry in the program, this is done referring to the *Global* reference system. Hence, the helical equation is built starting from R (outer radius) and H (height of a complete landing of the helix); knowing the dimensions of the step, a couple of points is located on the helical equation, by using the $(\frac{2\pi}{n})$ angle, in order to identify the width of the step (plan view); finally, the correspondent upper points are determined, by adding the rise value of the step to the previous points (Fig. 4.9).

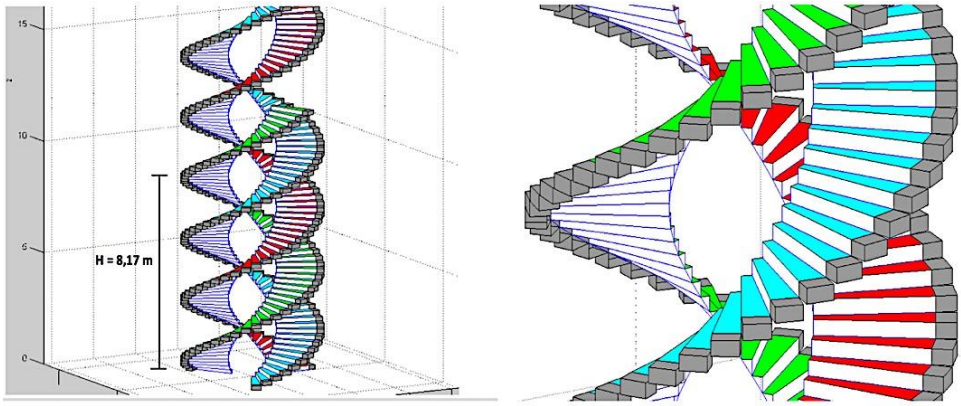

Fig. 4.9: 3D views of the triple helical stairs

Consequently, the nodes that belong to the visible part of the step and also to the socket part are built; each step is modelled with 15 nodes. Since we consider that the steps behave as rigid blocks, we also identify the relative centroids, where their own weight can be applied (Fig. 4.10).

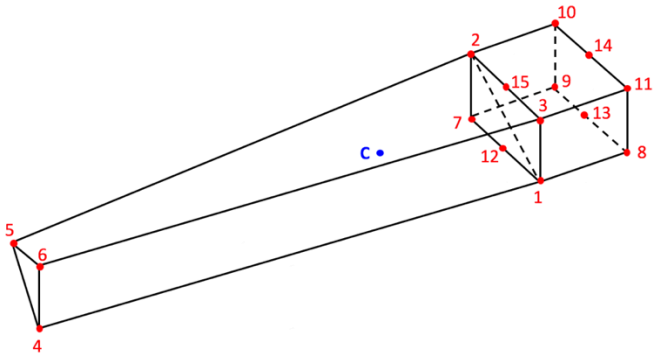

Fig. 4.10: Discretization of the step

Once defined the geometry of the stair, we need to model the movement of the steps in order to allow them to move accordingly to our assumptions.

In order to do it, we define the displacement variables for the steps; since we assume that the structure is composed by rigid blocks, that is each step behaves as a rigid monolithic block, it is possible to evaluate how each step moves by referring to the displacements and rotations of the relative centroids; then we define the primal variables of our analysis, that is the *Lagrangian parameters* of the mechanical system, namely the six rigid body displacements (the three translations U, V, W and the three rotations φ_1, φ_2, φ_3) which describe the infinitesimal translation and rotation, referred to the centroids of each step, expressed in the *Global* reference system.

Given the fact that those movements are just theoretical, and, in any case, they will be limited to few decimetres at maximum, we can assume the small displacement and small angles hypothesis; this allows us define the displacement rule for the generic node P of the step with a linear equation in reference to the roto-translation of its centroid:

$$\Delta P = \begin{bmatrix} u_1(P) \\ u_2(P) \\ u_3(P) \end{bmatrix} = u(G) + \phi(G) \cdot [x(P) - x(C)] = \\ = \begin{bmatrix} U \\ V \\ W \end{bmatrix} + \begin{bmatrix} 0 & -\varphi_3 & \varphi_2 \\ \varphi_3 & 0 & -\varphi_1 \\ -\varphi_2 & \varphi_1 & 0 \end{bmatrix} * [x(P) - x(C)] , \tag{4.4}$$

where P is the node label, G is the centroid, $u(G)$ is the translation vector of the centroid and $\phi(G)$ is the skew matrix of infinitesimal rotation about the centroid, $x(P)$ and $x(G)$ are the coordinates of nodes P and G. Finally, we introduce the vector of rigid body displacement of the whole structure as:

$$\hat{u} = \{u_{1,1}, u_{2,1}, u_{3,1}, \varphi_{1,1}, \varphi_{2,1}, \varphi_{3,1}, \dots, u_{1,n}, u_{2,n}, u_{3,n}, \varphi_{1,n}, \varphi_{2,n}, \varphi_{3,n}\} . \tag{4.5}$$

Moreover, we need to express these displacements in all reference systems introduced. Being the *Global* system the canonical basis, for any valid basis B, the displacement rule for the generic node P can be written with the following rule:

$$\Delta P_{loc} = B^{-1}(P + \Delta P) - B^{-1}P . \tag{4.6}$$

The important fact is that the displacement ΔP_{loc} is still a function of the displacement variables, U, V, W, φ_1, φ_2, φ_3, referred to the *Global* system. This approach allows us to compare displacements of nodes belonging to different steps.

4.1.6 Constraints

For simplicity, the contact among blocks is condensed into 15 contact nodes for each step. Depending on the node to which we refer, we can consider that the displacement is

prevented in both directions or just in one of them. In the first case a bilateral constraint is necessary, which is expressed by equality, while in the latter case, a unilateral constraint can be employed, expressed by inequality.

The generic constraint is defined as follows:

$$\begin{aligned} &U_i(P) = a && \leftrightarrow \ \textit{bilateral constraint} \\ &U_i(P) \leq a \\ &U_i(P) \geq a && \leftrightarrow \ \textit{unilateral constraint} \end{aligned} \tag{4.7}$$

where i is the index of one of the three axes, P is the generic node to which the constraint condition is applied, $U_i(P)$ represents the displacement of node P on the direction i, and a is the constant term.

The constraint conditions can be defined in the more convenient local or global reference system (*G*, *S*, *K*). At the constrained boundary, these constraint conditions take into account the effect of possible settlements.

The constraint conditions, summarized in Fig. 4.11, are grouped as follows:

a. For each step (*i*) we consider the absolute constraint conditions:
   - *Equalities*, expressed in the *S-Local System*, representing the bilateral constraints for nodes in brackets:

$$eq1. \quad U_1(D/A) = 0\,, \tag{4.8}$$

$$eq2. \quad U_2(D/A) = 0\,, \tag{4.9}$$

     These equalities are written both for nodes D and A, as two case studies are here analysed, and convey the condition that node D (or A) cannot displace in the horizontal plane, that is it behaves as a bilateral horizontal support.

   - *Inequalities*, expressed in the *S-Local System*, representing the unilateral constraints for nodes in brackets:

$$ineq1. \quad U_3(A) \geq -c_1 \qquad \text{(settlement)}, \tag{4.10}$$

$$ineq2. \quad U_3(D) \geq 0\,, \tag{4.11}$$

$$ineq3. \quad U_3(D') \leq c_3 \qquad \text{(settlement)}, \tag{4.12}$$

$ineq4.\quad U_3(B) \geq -\varepsilon_1$ (tolerance), (4.13)

$ineq5.\quad U_3(C) \geq -\varepsilon_1$ (tolerance), (4.14)

$ineq6.\quad U_3(B') \leq \varepsilon_1$ (tolerance), (4.15)

$ineq7.\quad U_3(C') \leq \varepsilon_1$ (tolerance), (4.16)

$ineq8.\quad U_3(A') \leq c_3$ (settlement). (4.17)

These conditions take into account the fact that the part of the step inserted into the wall presents inevitably a backlash, therefore, we considered free movements for each node in specific directions to account for this clearance. In particular, node A can move freely along the positive direction 3 and can drop to the quantity c_1; node D can move freely along the positive direction 3 starting from its local reference position; node D' can move freely along the negative direction 3 and can rise up to the quantity c_3; nodes B, C, B', C' can move freely along the locally inward direction 2 and move laterally up to the quantity ε_1; node A' can move freely along the negative direction 3 and can rise up to the quantity c_3.

b. For the ground step, we consider the absolute constraint condition expressed by an *inequality*, in the *S-Local System*, representing the settlement of the unilateral constraint for node in brackets:

$ineq9.\quad U_3(M) \geq -c_2$ (settlement). (4.18)

This inequality conveys the assumption that at the base of the helical stair it is likely that a vertical settlement shows up; therefore, node M can drop of the quantity c_2. The order of magnitude of c_2 is chosen in such a way that the small displacement hypothesis applies.

c. For all other steps, we also consider the relative constraint condition, expressed by *inequalities* written in the *K-Local System*, representing the unilateral constraints for nodes in brackets:

$ineq9.\quad U_1(M_i) - U_1(N_{i-1}) \leq \varepsilon_2$ (tolerance), (4.19)

$ineq10.\quad U_1(M_i) - U_1(N_{i-1}) \geq -\varepsilon_2$ (tolerance), (4.20)

$ineq11.\quad U_3(M_i) - U_3(N_{i-1}) \geq 0\,.$ (4.21)

These inequalities convey the condition that in the horizontal plane the relative displacement between node M of the step (*i*) and node N of the step (*i-1*) is allowed in a neighbourhood of size ε_2, so small that the small displacement hypothesis is verified, while along the vertical direction this relative displacement must be equal

to zero, so as to realize contact between the two nodes, through which the reactive force can be transmitted.

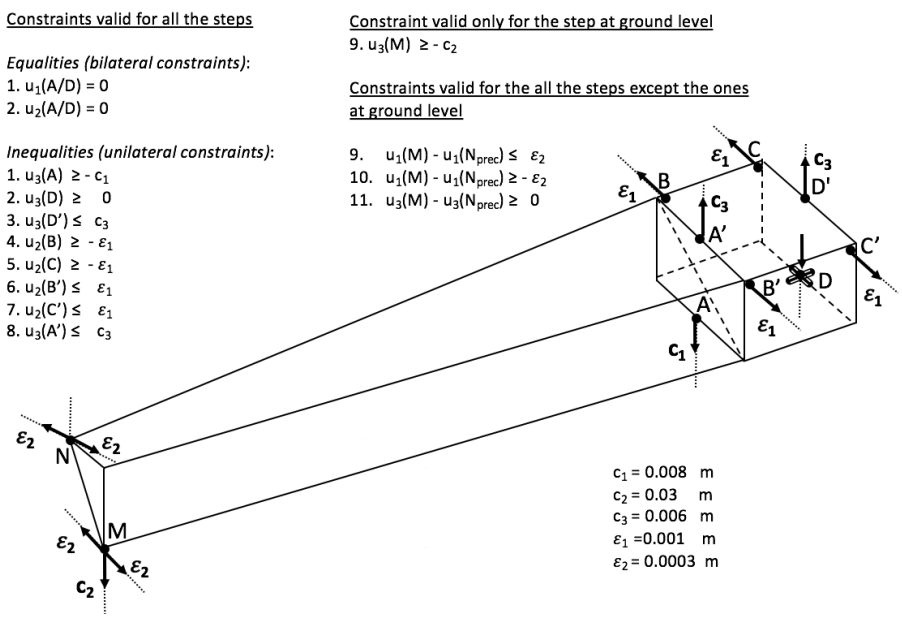

Fig. 4.11: Bilateral and unilateral constraints conditions considered at the nodes of each step

Different sets of settlement and clearance values are considered, according to the small displacement hypothesis; the values of tolerances and settlements adopted in this application are reported in (4.22) - (4.26). Tolerances and settlements have one order of magnitude difference, namely:

$$c_1 = 8 \cdot 10^{-3} \quad [m]$$ (vertical settlement downward at node D of the socket), (4.22)

$$c_2 = 3 \cdot 10^{-2} \quad [m]$$ (vertical settlement downward for the ground step), (4.23)

$$c_3 = 6 \cdot 10^{-3} \quad [m]$$ (vertical settlement upward at node D' of the socket), (4.24)

$$\varepsilon_1 = 1 \cdot 10^{-3} \quad [m]$$ (horizontal tolerance in the socket), (4.25)

$$\varepsilon_2 = 3 \cdot 10^{-4} \quad [m]$$ (tolerance between M_i and N_{i-1} nodes at step to step contact). (4.26)

As previously stated, in order to facilitate the writing of some constraint conditions, such as those related to points M and N, in which we consider the presence of two pendulums in the horizontal plane (inclined at an angle $\delta/2$ relative to the y-axis of the *S-Local System*), the *K-Local System* is used. One of the axes of the *K-Local System* coincides with the axis of the pendulum, along which its reaction is explicated (Fig. 4.8c). Writing the constraint conditions in Matlab, the position of the point to which they relate and the direction of movement prevented are specified. These two vectors are successively used to determine the point of application and the direction of the corresponding reaction vector.

As stated at the beginning of this work, the multi-body structure of the stair is a highly statically indeterminate scheme, in the sense that the number of possible reactions is largely greater than the number of balance equations. When a mechanism is activated by the settlements, the moving part of the structure becomes a one degree of freedom mechanism and becomes statically determined, then it is possible to derive the forces which ensure the equilibrium of the structure through the balance equations. Then, if we can imagine or predict a likely scenario for the settlements, we can obtain a hint of the possible equilibrium regime of the structure. In this particular application, we consider two types of possible settlements, that we call settlements and tolerances, having one order of magnitude difference among each other.

The proper settlements, which we assume present in the form of a vertical displacement of the node at the base of the stair and of vertical settlements of node A and D' at the wall socket, are larger. The tolerances, which simulate a small clearance in the horizontal plane, at the wall socket and at the step to step contact, are smaller.

According to the small displacement hypothesis, we considered different sets of reasonable settlements of the internal and of the external constraints of the stair, that is small relative movements of the steps at the wall and at the central rib. The settlements are imposed both as displacements of the ground step and as backlashes, assigned to the nodes in the socket (the results of the present work are referred to the values described in § 4.1.6). These settlements are likely to occur either during construction or a short time after construction.

4.1.7 Energy

In general, for an elastic-brittle structure, the energy is the sum of three quantities: the potential energy of the loads, the elastic energy and the interface energy necessary to activate a crack on an internal surface. The material considered in the case study responds to the hypothesis of Heyman's model, in the sense that unilateral conditions with no-sliding holds at contact between parts considered as rigid. Consequently, the energy quantity is represented, as said before, by the potential energy $\wp$ associated to the own weight of the steps:

$$\wp = -\sum_{step=1}^{n} m_{step}\, g U_{z,step}\,, \tag{4.27}$$

where ($m_{step}g$) is the weight of each step (≈ 1700 N) and $U_{z,step}$ is the vertical displacement of the centroid of each step. The search of the solution of the boundary value problem, that is the displacement field compatible with the settlements imposed on the structure, is done through the minimization of the potential energy of the loads.

Since in this case we consider rigid block displacement fields, the contribution of the elastic energy is zero. Furthermore, Heyman's material is non-dissipative, in the sense that the stress makes no-work for the corresponding strain. The no-dissipation assumption implies, in particular, that there cannot be stress across a detached fracture line, and, dually, that there cannot be a fracture at a point across a surface if, at that point, there is compressive stress across the interface [23]. Then, the interface energy necessary to activate a crack on an internal surface is zero.

4.1.8 Energy minimization

The minimization problem is set in Matlab. Being Matlab a programming language that operates on matrices, the previous constraint equalities and inequalities are converted into matrix form and then a linear programming problem is solved. The solution of the minimum problem is performed with a linear programming routine, through a function built in Matlab and called 'linprog', whose signature is set in the form:

$$min_x\, f^T x \quad such\ that \begin{cases} A_{ineq}\, x \leq b_{ineq}\,, \\ A_{eq}\, x = b_{eq}, \\ l_b \leq x \leq u_b, \end{cases} \tag{4.28}$$

where:

$$A_{ineq}\, x \leq b_{ineq}\,, \quad \text{constraint conditions written as inequalities} \tag{4.29}$$

$$A_{eq}\, x = b_{eq}\,, \quad \text{constraint conditions written as equalities} \tag{4.30}$$

$$l_b \leq x \leq u_b\,, \quad \text{upper and lower limits of the variable x} \tag{4.31}$$

and the function to be minimized $f^T x$ is represented by the potential energy $\wp$ associated to the loads imposed on the structure.

The 'linprog' function of Matlab recommends in its documentation, for minimization problems, the use of the 'Interior Point' or of the 'Dual-Simplex' algorithms, which are the fastest and use less memory space than the other algorithms. In particular, the Interior Point algorithm is chosen, which is a large-scale algorithm that uses linear algebra rules and that does not require either to store or to operate on the entire matrix that defines the problem. This is possible as it works on sparse matrices and uses sparse linear algebra

calculations, when it is possible, making the calculation procedure particularly performing, both in terms of quality of solution and of execution timing. Medium-scale algorithms work on the entire matrix and use dense linear algebra formulas; then, for large problems, such as the present, full matrices occupy a memory space that requires high computing time.

4.1.9 Saturated conditions

In the case at hand we always have inequalities written with the "≤" condition, since "Linprog" function in Matlab requires the equalities and inequalities conditions written in this form. Considering, for example, the unilateral constraint $x \leq a$ in Fig. 4.12, that admits infinite solutions in the $]-\infty, a]$ interval, we are interested, among all the infinite solutions, to spot the one for which the condition $x = a$ is met, which implies that, in an iterative optimization procedure, the value of the x variable cannot grow any longer.

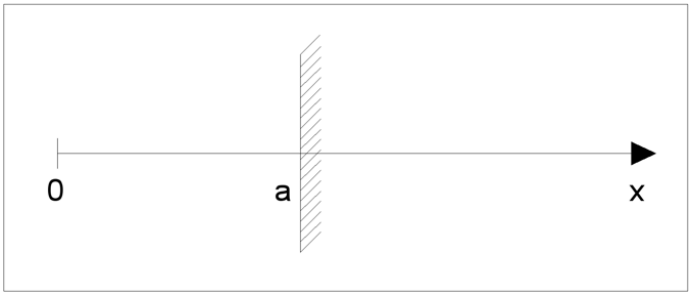

Fig. 4.12: Unilateral condition $x \leq a$

In our case this means that the displacement in a particular direction has reached a limit, physically represented by the wall or by any other type of obstacle, such as the adjacent tread or the limit clearance. We consider this condition particularly interesting, because it shows that a contact has been realized, through which the internal forces can be transmitted. From now we call *saturated inequalities* the inequalities which are satisfied as equalities at the end of the optimization process.

4.1.10 Kinematic Solution and Equilibrium

The kinematical problem, formulated as a minimum problem, is solved by linear programming, and finally is reduced to the following matrix form:

$$C \cdot \hat{u} = q \,, \tag{4.32}$$

where:

- C is the kinematic matrix, whose size is $6n \times 6n$ and n is the number of the steps;
- $\hat{u}$ is the displacements vector (unknown), whose size is $6n \times 1$;
- q is the settlements vector (known), whose size is $6n \times 1$.

Once the solution of the problem, that is the minimizer of the potential energy, is obtained, then the Static matrix S is constructed by means of the transposition of the Kinematic one, recalling the static-kinematic duality, so that $\mathrm{S} = \mathrm{C}^{\mathrm{T}}$. The Static matrix, thus obtained, allows the resolution of the equilibrium problem:

$$S \cdot r + f = 0\,, \tag{4.33}$$

where:

- S is the Static matrix, whose size is $6n \times 6n$;
- r is the reactive force vector (unknown), whose size is $6n \times 1$;
- f is the active force vector (known), whose size is $6n \times 1$.

From the Static problem, defined above, the vector of the unknown reactions is obtained:

$$r = -S^{-1} \cdot f\,. \tag{4.34}$$

Once the forces exerted by the bonds are selected and calculated, it is possible to compute the stress resultant inside the stair, in terms of contact forces, bending moments and torque, using the following vector formulas:

Contact forces

$$r(x) = \sum_{i=1}^{n} f(v_i) + \int_x^l -P(\xi)\widehat{e_3}\, d\xi\,, \tag{4.35}$$

where:

- x is the cross section along the x-axis of the *S-Local System*, from the wall interface till the end of the step, defined between 0 and L;
- v_i are the vertices of the step;
- $f(v_i)$ are the reactive forces on the step;
- $\sum_{i=1}^{n} f(v_i)$ is the sum of all forces at the right of the section x;
- $\int_x^l -P(x')\widehat{e_3}\, dx'$ is the weight of the part of the step at the right of the section x;

Bending moments and torque

$$m(x) = \sum_{i=1}^{n} f(v_i) \times [G_x - v_i] + \int_x^l -P(\xi)\widehat{e_3} \times (x-\xi)\widehat{e_1}d\xi, \tag{4.36}$$

where:

- G_x is the centroid of the cross section x;
- $\widehat{e_1}$ is the unit vector along the symmetrical axis of the step, approximated (with a factor of 10^{-18}) with the direction of the segment $G_l - G_0$;
- $\widehat{e_3}$ is the unit vector along the z-axis of the *Global System*.

4.1.11 Identification of saturated conditions and construction of the C matrix

The resulting solution, called $x_{,sol}$, complies with the equalities and inequalities that characterize the minimization function (4.28). Subsequently, the inequalities transformed into equalities are identified through the solution $x_{,sol}$.

Recalling that A_{ineq} represents the rows of the original matrix A that refers only to inequalities and x_{sol} is the solution of the minimization problem, the first step is the evaluation of a new column vector, named b_{ineq_sol}, defined as follows:

$$b_{ineq\_sol} = A_{ineq} x_{sol}\,, \tag{4.37}$$

once obtained b_{ineq_sol}, the identification of the set of rows *i*, for which holds the following condition, is possible:

$$\left| b_{ineq,i} - b_{ineq\_sol,i} \right| < 10^{-6}\,. \tag{4.38}$$

Once identified these rows, they are selected from A_{ineq} matrix and are used to create a new matrix, called A_{ineq_sat}. Then it is possible to reconstruct the kinematic matrix of the problem, simply by assembling the matrix of coefficients of the saturated inequalities A_{ineq_sat}, just found, with that of the coefficients of the equalities A_{eq}:

$$C = \begin{bmatrix} A_{eq} \\ A_{ineq\_sat} \end{bmatrix}. \tag{4.39}$$

In the same way, the displacement and settlements vectors are obtained:

$$\hat{u} = \begin{bmatrix} x_{sol\_eq} \\ x_{sol\_ineq\_sat} \end{bmatrix} \quad , \quad q = \begin{bmatrix} b_{eq} \\ b_{ineq\_sat} \end{bmatrix}. \tag{4.40}$$

4.1.12 Results

Two cases are analysed, the first in which, for each step, the horizontal bilateral constraint is located in vertex A; the second in which it is located in vertex D. For these two cases, considering as given the same set of settlements, the optimization algorithm provides a minimum solution and the corresponding statically determined structure is identified. Since under the effect of the settlements that we consider, all the steps are mobilized, the whole structure becomes statically determined, then the evaluation of all internal forces is possible through the static-kinematic duality.

Since in the case at hand the three helical flights do not interact with each other, the behaviour of each flight is independent from that of the others, hence the analysis can be carried out just referring to one of them. When the bilateral horizontal constraint is considered in vertex A, the optimization algorithm produces the graphic output depicted in Fig. 4.13:

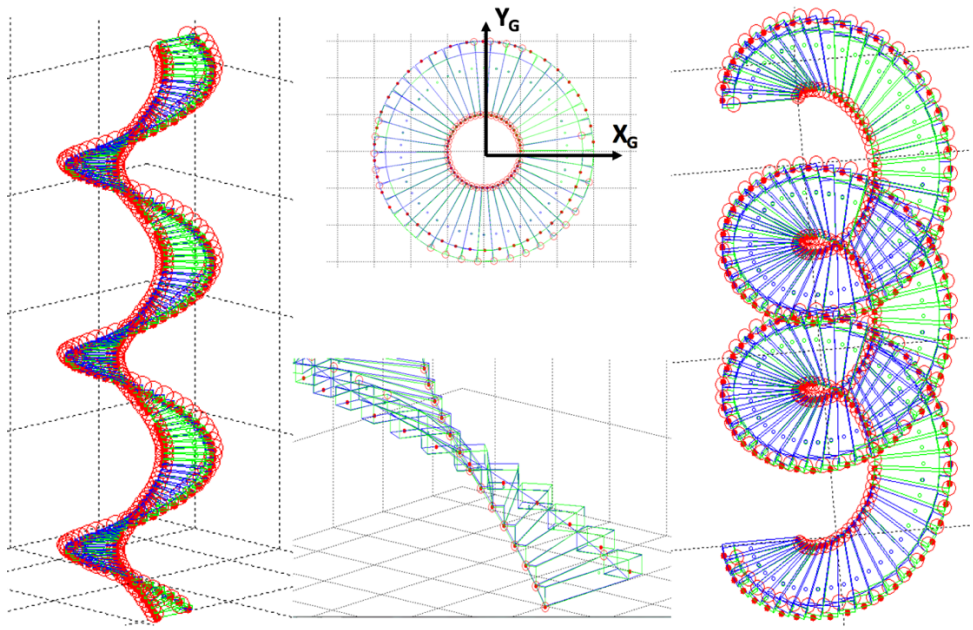

Fig. 4.13: Graphic output of the optimization algorithm

In particular, Fig. 4.13 shows the structure in its initial (blue lines) and final (green lines) displaced condition and the activated unilateral constraints along the horizontal plane (represented by red circles) and along the z-axis (represented by red points), that is the points where the internal forces are acting on the structure, enforcing equilibrium. The concept of activated constraints is particularly interesting and is described in § 4.1.9.

In order to visualize easily and rapidly the saturated inequalities for each tread, that is the internal forces exerted by the unilateral constraints on each tread, the graphic in Fig.

4.14, referred to one of the coils of the stair composed by three complete helix rounds (that is 126 steps), is employed.

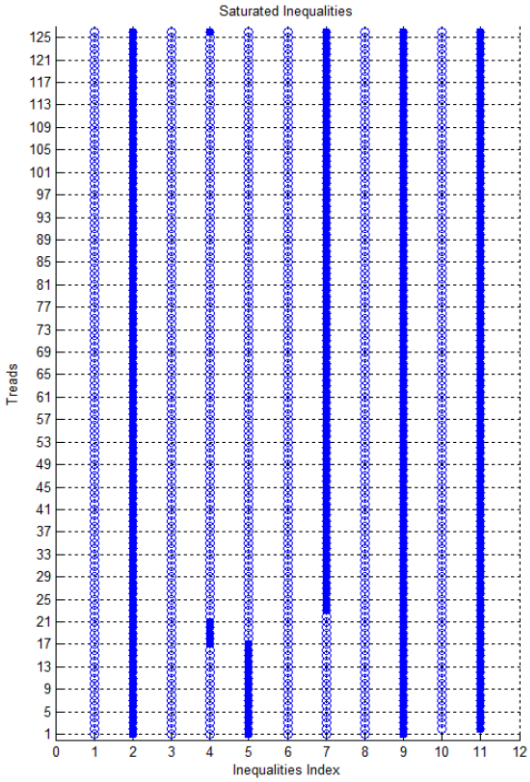

Fig. 4.14: Saturated inequalities for all the 126 treads (horizontal bilateral constraint in node A)

On the x-axis, the numbers from 1 to 11 identify, for each tread, the index related to the unilateral constraint conditions; on the y-axis, the step number, ordered from 1 to 126 (from bottom to top) is reported (for the set of unilateral constraints see § 4.1.6). The filled dots represent the saturated inequalities, while the empty dots represent the non-saturated inequalities. Then, some interesting considerations can be made.

As we can observe, node D (2nd column) always exhibits its maximum possible vertical settlement, that is it remains on the ground, whilst node A (1st column) does not reach the minimum value of vertical displacement (that is settlement c_1). Moreover, node M reaches the given settlement, that is value c_2, for the first tread at the floor level (9th column for the first tread), and for the other 125 treads the contact along the z-axis between node M of tread '*i*' and node N of tread '*i-1*' (11th column for treads from 2 to 126) always occurs. Finally, node M of tread '*i*' and node N of tread '*i-1*', separate from each other in the horizontal plane (9th column for treads from 2 to 126).

The infinitesimal clearance that we admit for nodes M and N in the horizontal plane is imposed so that the unilateral inequalities 9 or 10 can be easily verified as equalities,

making possible to evaluate the emerging internal forces in these nodes (see the red arrows in Fig. 4.15 and Fig. 4.16, representing the activated internal forces).

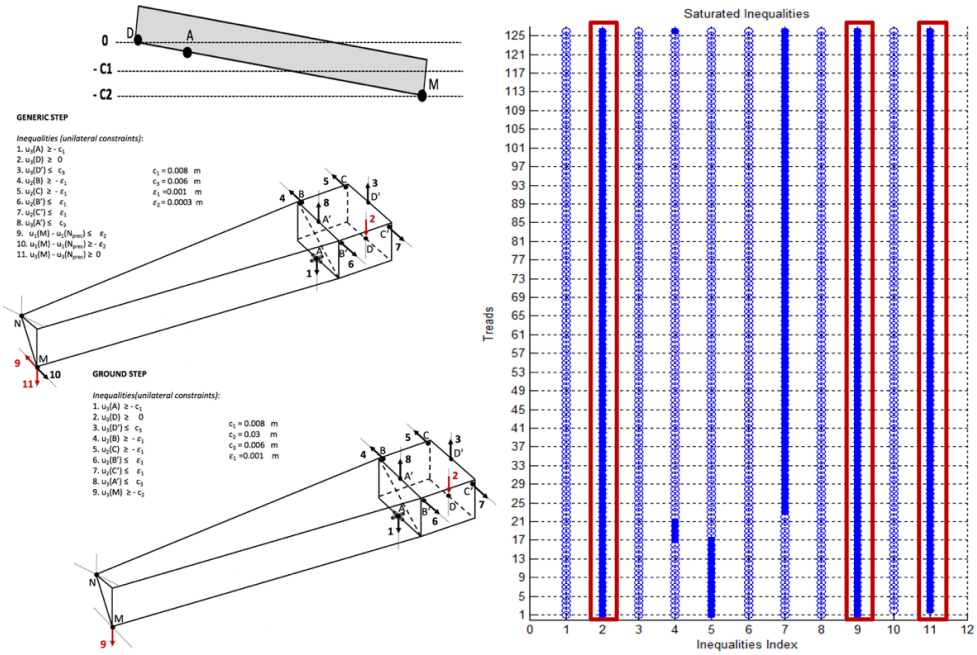

Fig. 4.15: Emerging internal forces in nodes D and M (horizontal bilateral constraint in node A)

In addition, looking at the 4th, 5th and 7th columns, which are referred to the part of the tread that is inserted into the wall socket, we can observe that for the first 17 treads node C touches the wall (5th column); for the treads from 18 to 22, node B touches the wall, whilst, for all the others treads, node C' touches the wall. Thus, for the socket part, the internal forces are applied either in nodes B or C' (Fig. 4.16).

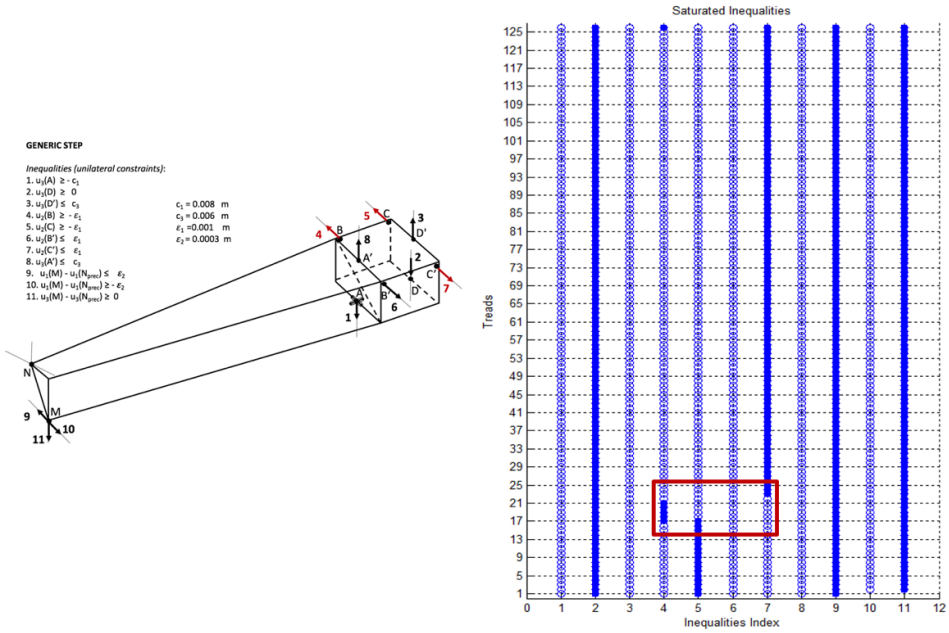

Fig. 4.16: Emerging internal forces in nodes B, C and C' (horizontal bilateral constraint in node A)

This particular behaviour is due to the sudden change of strategy chosen by the optimization algorithm, which looks for the minimum solution by applying an adaptive strategy in terms of displacement and rotation of the centroids of the treads. This can be seen from the rotation trend of the centroids along x-axis in Fig. 4.17 (highlighted part in the box), where a change of direction of the rotation occurs. A similar behaviour is also observed for translations of the centroids (Fig. 4.18).

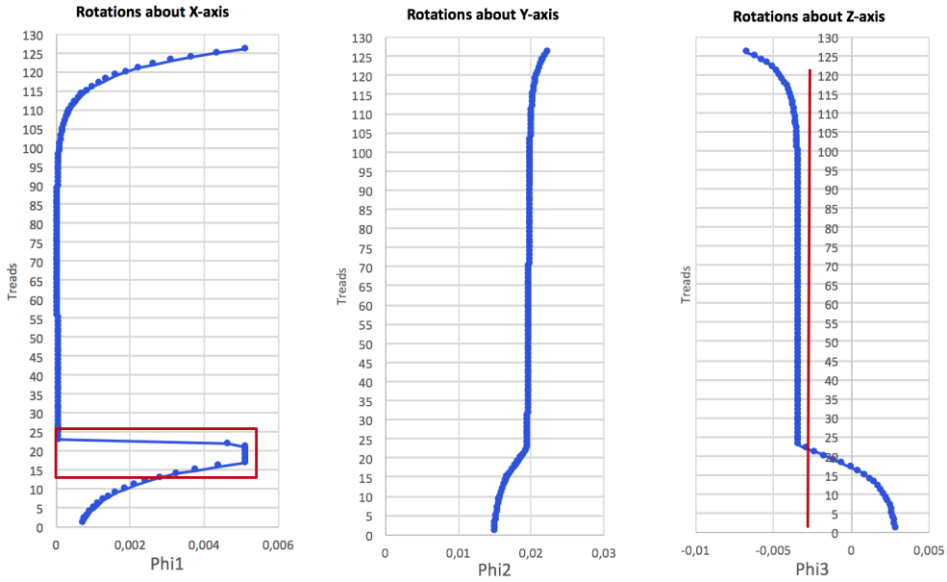

Fig. 4.17: Trend of the angles of rotation about the centroids (horizontal bilateral constraint in node A)

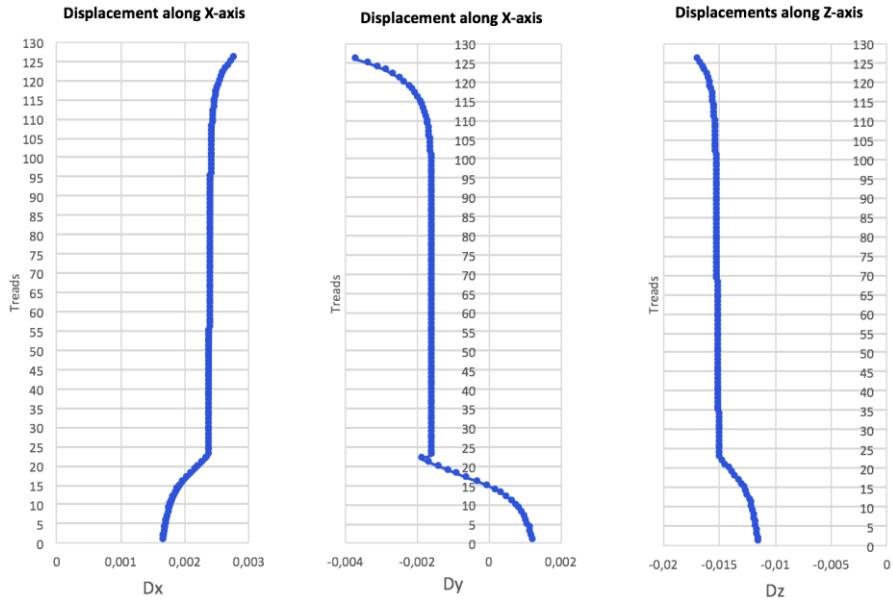

Fig. 4.18: Trend of the displacement of the centroids (horizontal bilateral constraint in node A)

This sudden change is also due to the fact that we have a saturated inequality on the z-axis for node D (2nd column), that is an equality in node D, and also a bilateral constraint in the horizontal plane for node A, defined in the initial constraint condition of this first case. Thus, the algorithm needs to satisfy two bilateral constraints in two different nodes, that is a mathematical condition very restricting. For this reason, a second case is analysed, where the bilateral constraint in the horizontal plane is positioned in node D, so that this sudden change is mitigated.

We remember that these bilateral constraints are defined by the user in the initial setting and represent equalities that are always active, while the activation of the inequalities along the z-axis depends on the solution found by the optimization algorithm.

When the bilateral constraint is considered in node D, the optimization algorithm produces the output shown in Fig. 4.19, in terms of saturated inequalities:

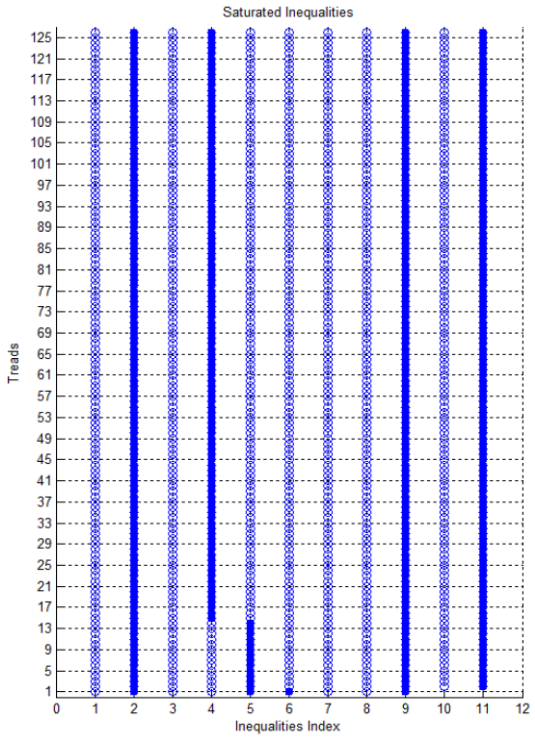

Fig. 4.19: Saturated inequalities for the 126 treads (horizontal bilateral constraint in node D)

As for the previous case, node D always exhibits its maximum possible vertical settlement, that is it remains on the ground, whilst node A does not reach the minimum value of vertical displacement (that is settlement c_1). Moreover, node M reaches the maximum settlement c_2 at the ground, and for the other 125 treads the contact along z-axis between node M of tread '*i*' and node N of the tread '*i-1*' always occurs. Finally, node M of tread '*i*' and node N of the tread '*i-1*' separate from each other in the horizontal plane (Fig. 4.20).

In addition, referring to the part of the tread that is inserted in the wall socket, we can observe that, for the first 14 treads, node C touches the wall, then for all the others treads node B touches the wall (Fig. 4.20).

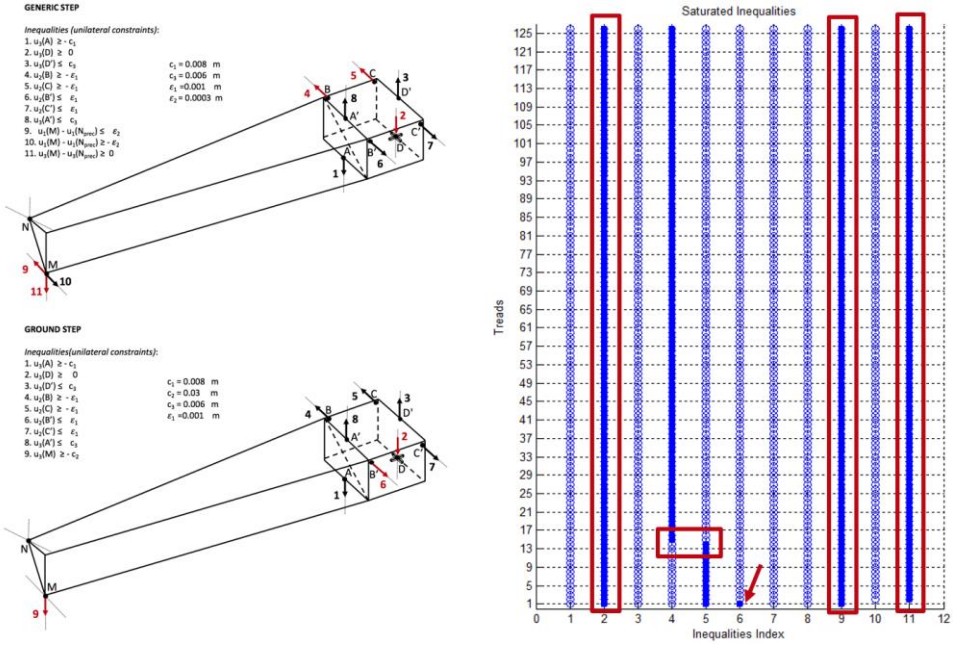

Fig. 4.20: Emerging internal forces in nodes D, M, B, B', C and C' (horizontal bilateral constraint in node D)

This behaviour is due to the fact that the treads rotate in the horizontal plane, that is round the z-axis, first in clockwise and then counter clockwise directions. In this second case, the sudden change of strategy of the optimization algorithm is not so evident, thus the trends of displacement and rotation of the centroids are more uniformly varying, as can be seen in Fig. 4.21 and Fig. 4.22. For this reason, we choose to continue the analysis for this second case.

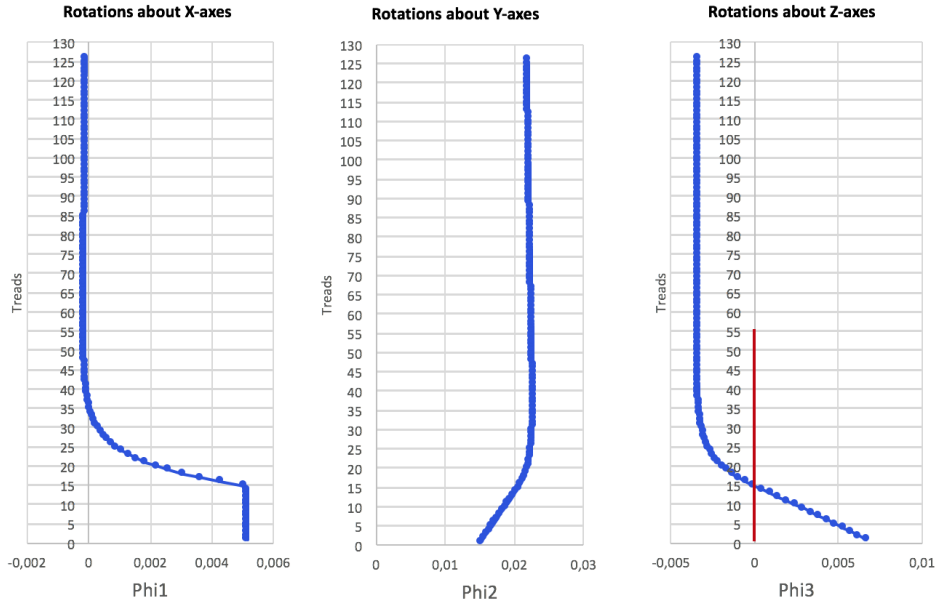

Fig. 4.21: Trend of the angles of rotation about the centroids (horizontal bilateral constraint in node D)

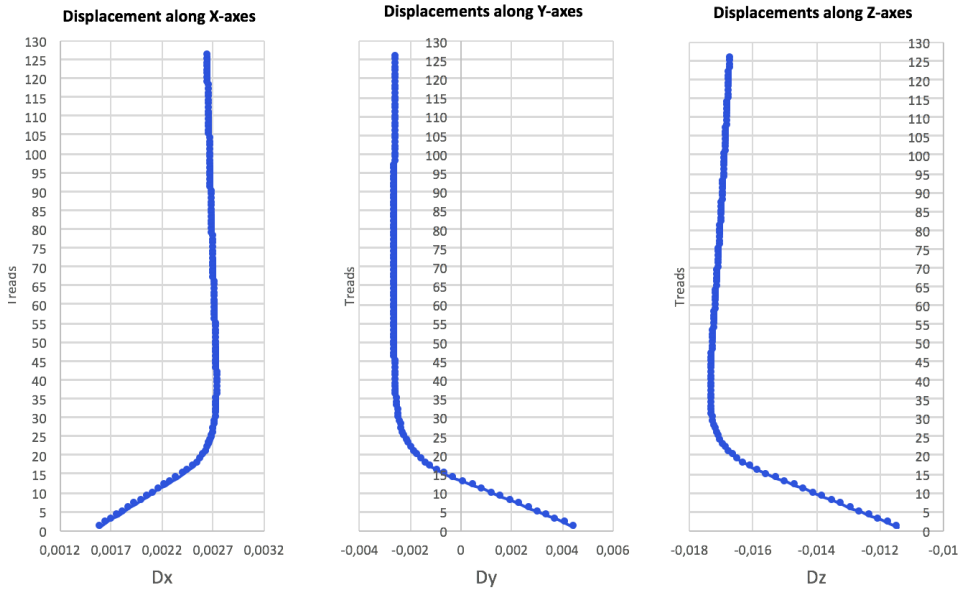

Fig. 4.22: Trend of the displacement of the centroids (horizontal bilateral constraint in node D)

At the end of the optimization process, the kinematical problem solution is obtained, which consists in the translations and rotations values of the centroid of each step. Then,

it is possible to obtain the Static Matrix S, by means of transposition of the Kinematic one, through static-kinematic duality. From the Static problem, the vector of unknown reactive forces is obtained and consequently it is possible to calculate the internal stress resultants.

An example of the representation of reactive forces is given in Fig. 4.23, where the internal forces which guarantee the equilibrium of step 44 are reported. The corresponding bending moment about axis 2 is shown in Fig. 4.24. Considering the internal forces of the entire stair, is also possible to evaluate the global trend of the stress resultants, the most meaningful for us being the axial force and torque, depicted in the graphs of Fig. 4.25.

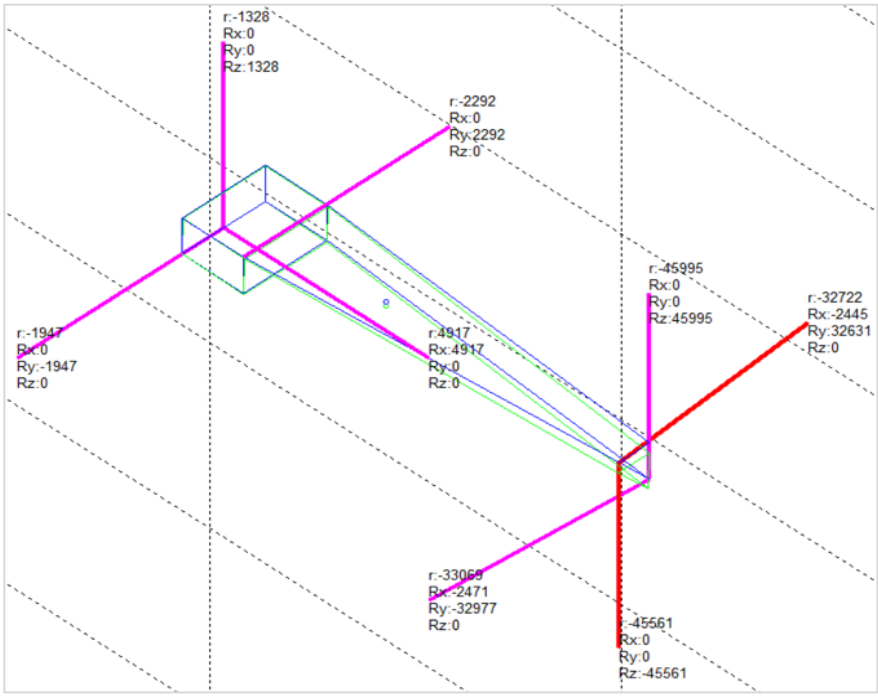

Fig. 4.23: Internal forces (tread 44)

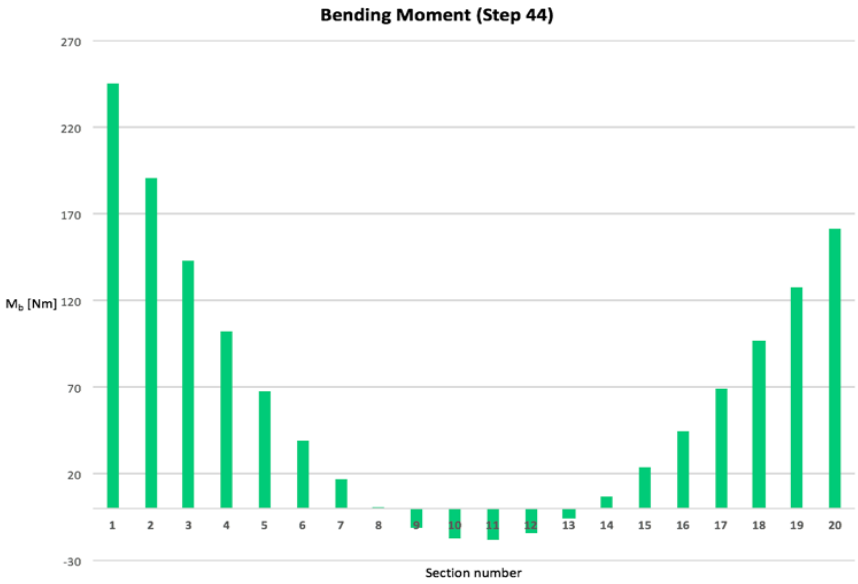

Fig. 4.24: Bending moment about axis 2 (tread 44)

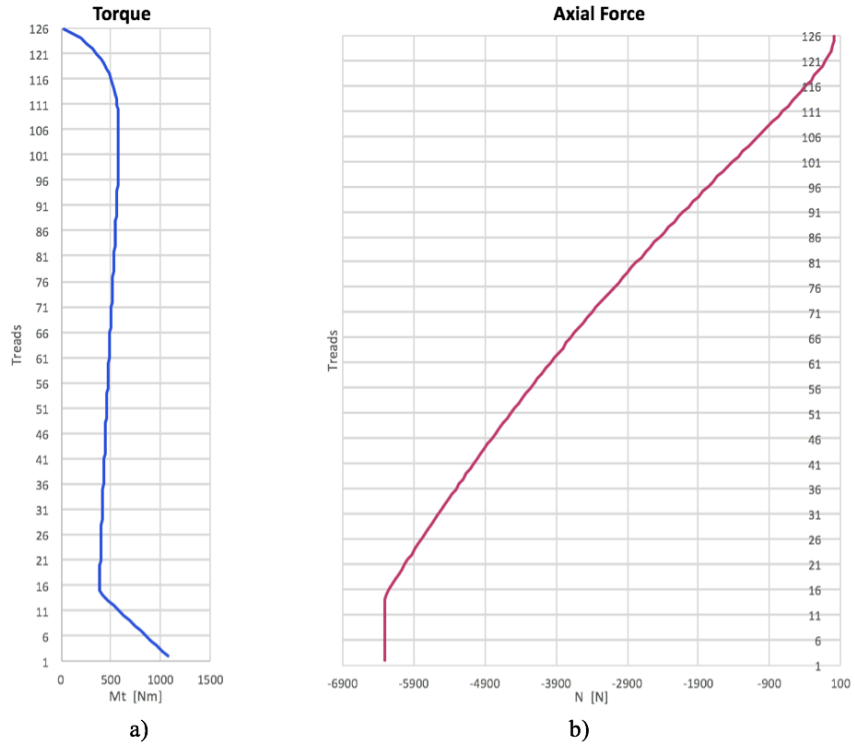

Fig. 4.25: Stress resultants for 3 complete rounds (126 treads).
a) Torque b) Axial force

As can be noted in Fig. 4.25, if we examine the diagrams from the top to the bottom of the stair, we can observe that the axial force gradually increases up to a certain step (the 16th step from the bottom), after which it stabilizes around a constant value, while the torque initially increases with a linear trend up to the first 10 steps, then it stabilizes up to a certain step (the 16th step from the bottom), as happens for the axial force, and then it increases again.

The complementarity between these two stresses can be noted; this gives a practical confirmation of the solution in the continuum obtained by Angelillo in [47]; indeed, we can observe a smooth combination between the Heyman's equilibrium solution, for which the torque is considered as the prevalent stress regime, and the Ring-Like model, which produces the increase of axial forces.

Comparing the Heyman's solution, which considers a linear increase of torque, with the equilibrium solution here obtained, it is possible to recognize Heyman's behaviour for the first steps, and then the gradual substitution of the Ring-Like behaviour as proceeding from top to bottom. (Fig. 4.26).

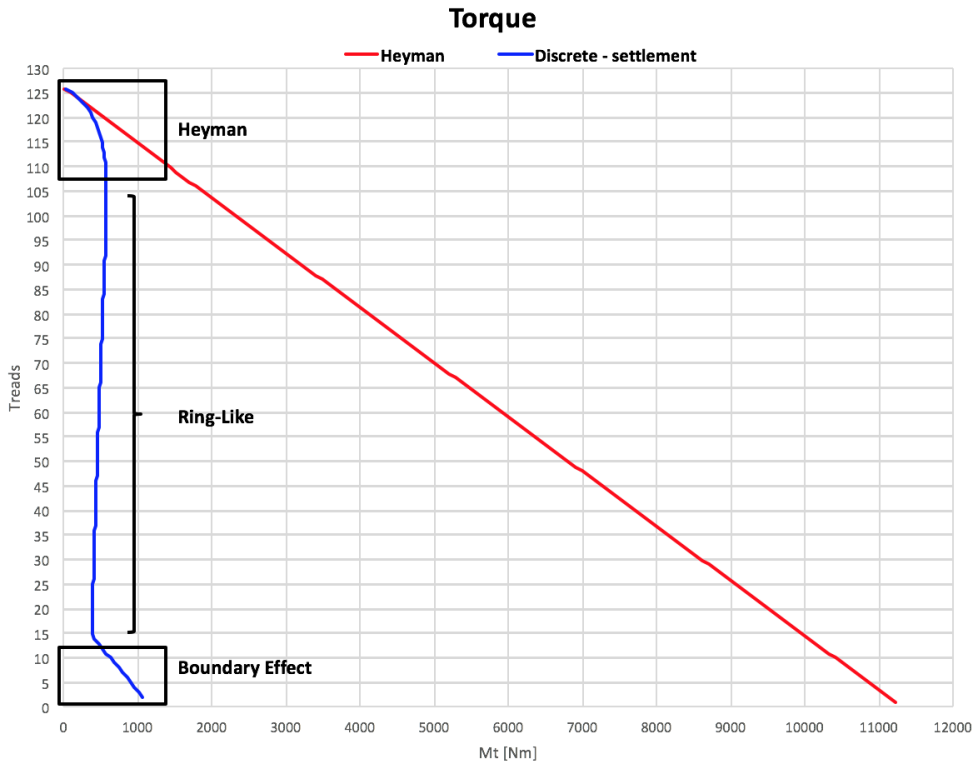

Fig. 4.26: Torque for Heyman and for the discrete with settlement solution

Furthermore, as said, for the steps near the ground level, a sort of boundary effect, deserving further studies, can be also noted.

Moreover, it is noteworthy that the maximum torque and the shear stress values obtained with our solution (M_t=1,2 kNm, τ=5,38 MPa) are far less than that obtained using the Heyman's solution (M_t=11,22 kNm, τ=50,27 MPa), the difference being of one order of magnitude. In the case at hand we can estimate a shear stress value compatible with the shear strength of the material (see § 4.1.3).

For what concerns the bending moment diagram, the non-zero values at the ends are due to the eccentricity between the pressure line and the axis along which the bending moment is evaluated. Besides, the values of the bending moment in the vertical plane of the steps are of the same order of those of a simply supported beam and are very low (σ=0,0016 MPa) with respect to the tensile strength of the material (see § 4.1.3).

4.2 Program user-interface

The results seen above, are taken using the program developed for this work. In this paragraph, the user-interface of the program and all the possible functions are presented.

When the program starts, all the minimization problem is carried out automatically, because the geometrical parameters cannot be modified by the user at this stage. Once the initial results are obtained, a selection screen is displayed to the user (Fig. 4.27), allowing both to deepen certain types of analysis (referring to a single step), and manipulate results in an appropriate manner, through graphical display or export of data in .csv files.

In the control panel are reported the parameters used for the analysis, in particular the number of steps (that is 126 if we consider three complete landing of the helical stair) and the value of assigned settlements. Then, five function buttons are available:

- Saturated inequalities;
- Displacements;
- Rotations;
- Step analysis;
- Stress.

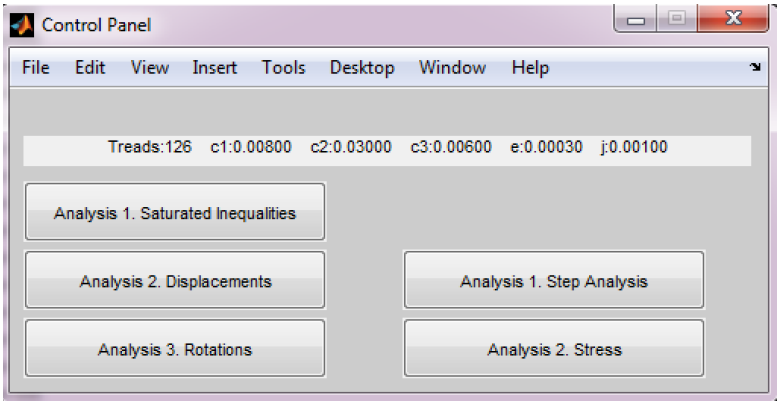

Fig. 4.27: Control Panel of Matlab program

Each of these buttons allows access to one or more of the methods described above. They can be activated in any order, as everyone does independent operations. Now we proceed to analyze in detail what offers each function.

Saturated inequalities

The first function (Fig. 4.28) is used to obtain graphics and 3D models, with graphical representation of the results (settlements, saturated inequality, etc.).

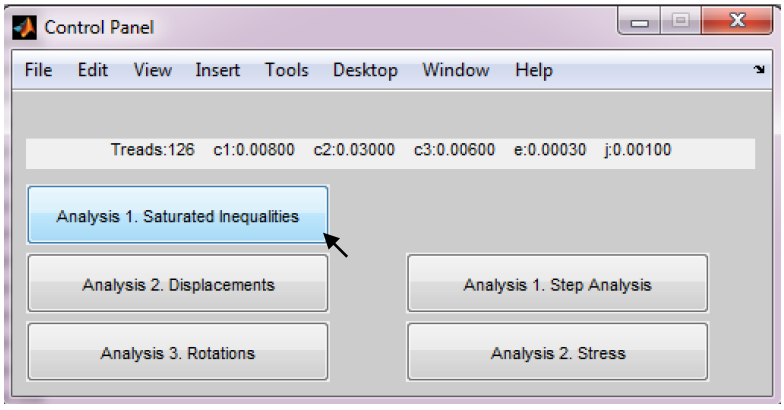

Fig. 4.28: Saturated inequalities command

The graph in Fig. 4.29 represents the saturated inequalities for each step, and uses a convenient representation with full or empty circles in the step-inequality graph. The 3D model (Fig. 4.30) makes clear the spatial points (red) of stair where a contact is realized, by adopting a differentiated representation according to the plan on which a contact is made; in blue is drawn the stair in its original position, in green its translated position.

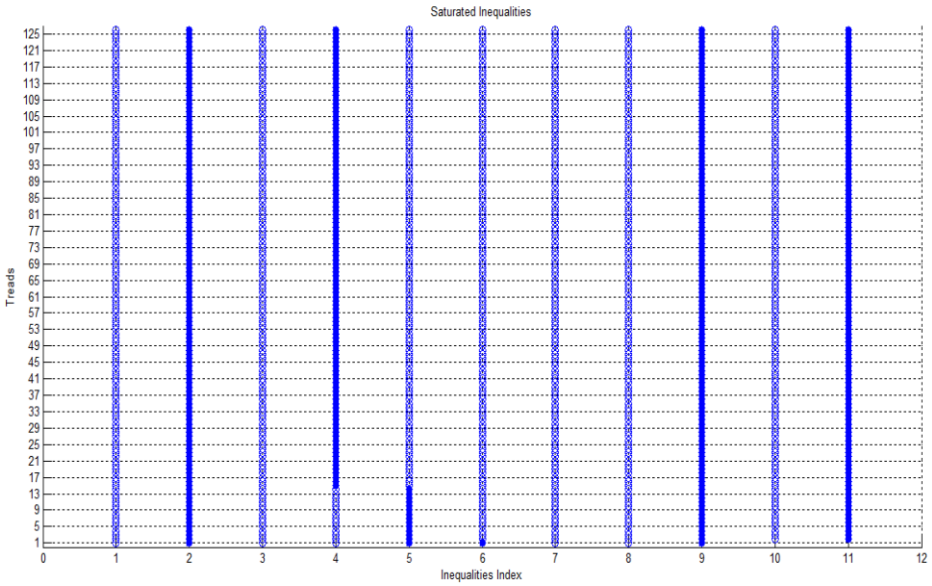

Fig. 4.29: Saturated and non-saturated inequalities

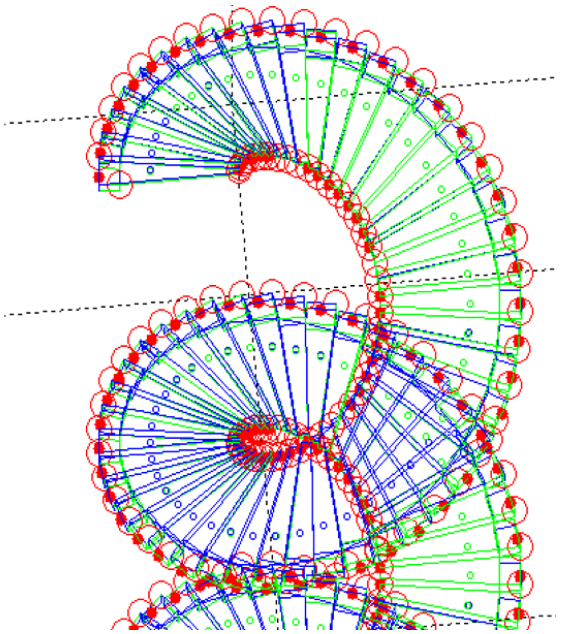

Fig. 4.30: View of the spatial contact points

Displacements and rotations

The second and third function (Fig. 4.31, Fig. 4.32) are useful to analyse the displacements and rotations obtained for all the steps, with reference to the relative centroids.

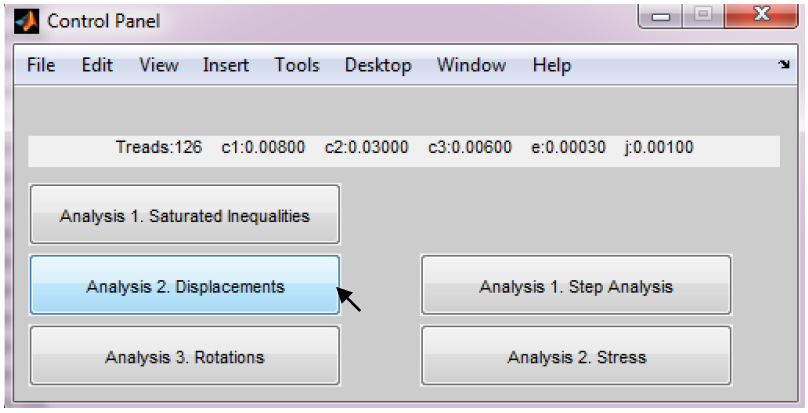

Fig. 4.31: Displacements command

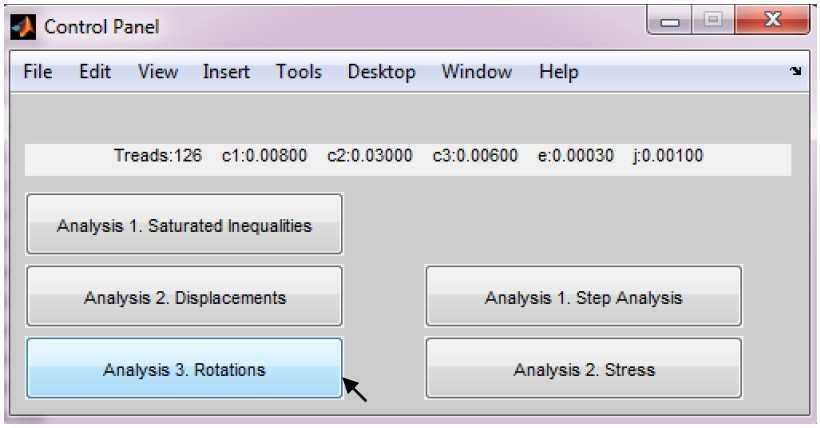

Fig. 4.32: Rotations command

The results are reported in relation to the *S-Local System*, and are made available in two modes: the first is the graph with the trends of the displacements and rotations of the centroids (Fig. 4.33, Fig. 4.34); the second consists in the exportation of .csv data files, which are then imported and analysed with other programs. For example, in this study the graphs were produced, for convenience, using Excel.

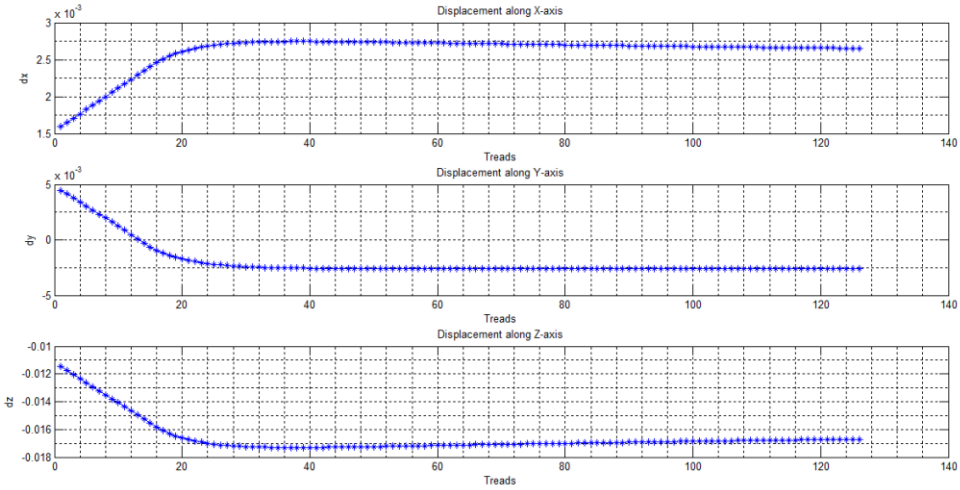

Fig. 4.33: Displacements trend of the centroids

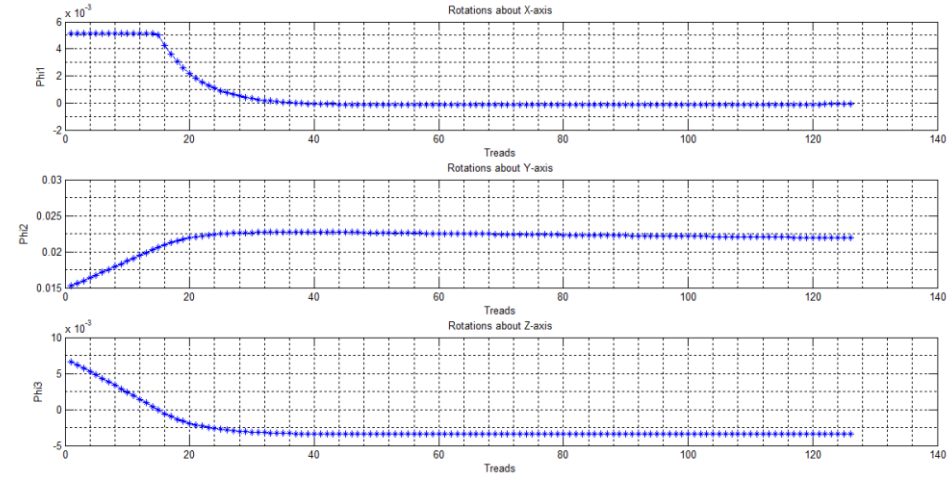

Fig. 4.34: Rotations trend of the centroids

Step analysis

The fourth function (Fig. 4.35) is more complex, since it allows to calculate the reactive forces and also allows to check the balance of the steps.

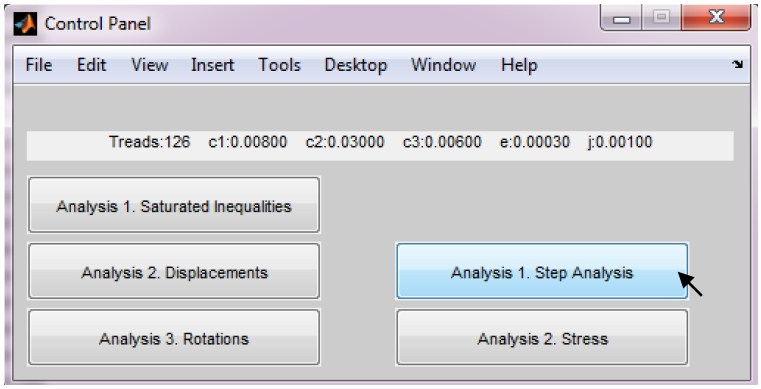

Fig. 4.35: Step analysis command

After testing the balance of all the step of the stair, the user can interact with a dynamic interface (Fig. 4.36), where he can select two main options:

- the reference system to use for the results;
- the step to be analysed.

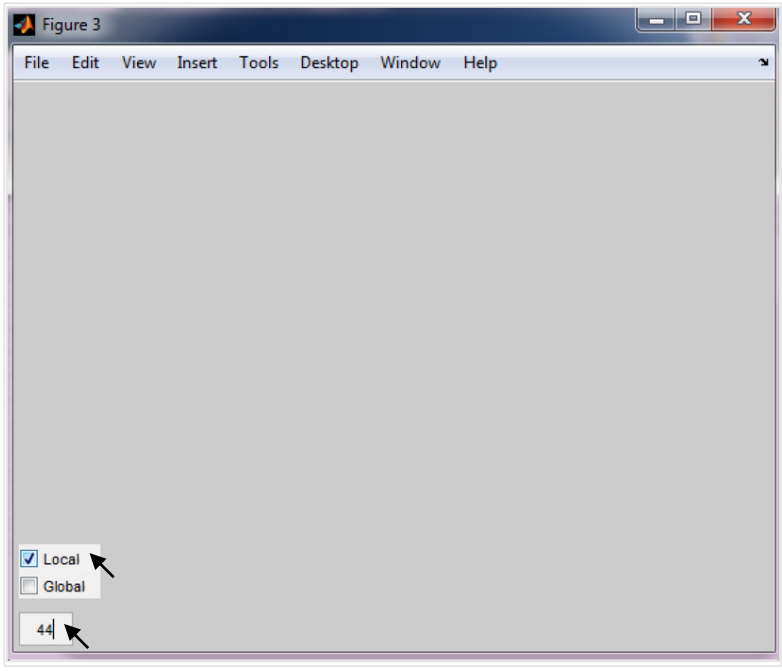

Fig. 4.36: Dynamic interface of step analysis command

As an example, in Fig. 4.36 we chose to analyse the step 44 in the *S-Local System*. Once set these two options, the step in 3D can be seen (Fig. 4.37), with the vectors representing the reactions that are activated for that step, and that verify the balance. The screen does

not display the vector relative to its weight of the step, considered applied in the centroid, but this value is still taken into account in the calculations. For each reaction, four numerical values are also reported:

- *r* : reaction module, expressed in N;
- *Rx* : projection of *r* on the x-axis of the selected reference system, expressed in N;
- *Ry* : projection of *r* on the y-axis of the selected reference system, expressed in N;
- *Rz* : projection of *r* on the z-axis of the selected reference system, expressed in N.

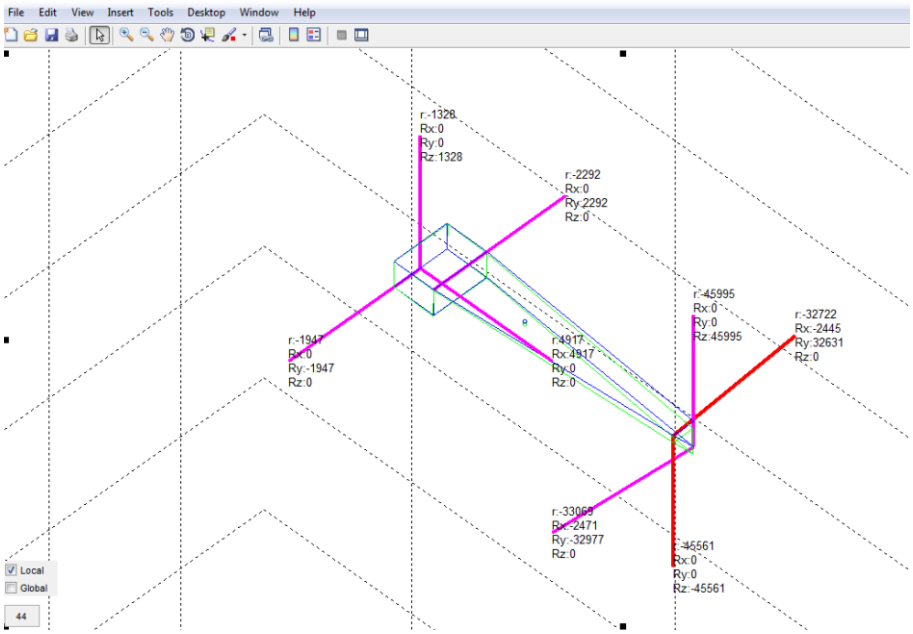

Fig. 4.37: View of the step in 3D

Stress

The last function (Fig. 4.38) is the most complex, as it aims to allow both the visualization and the stress analysis for all the steps.

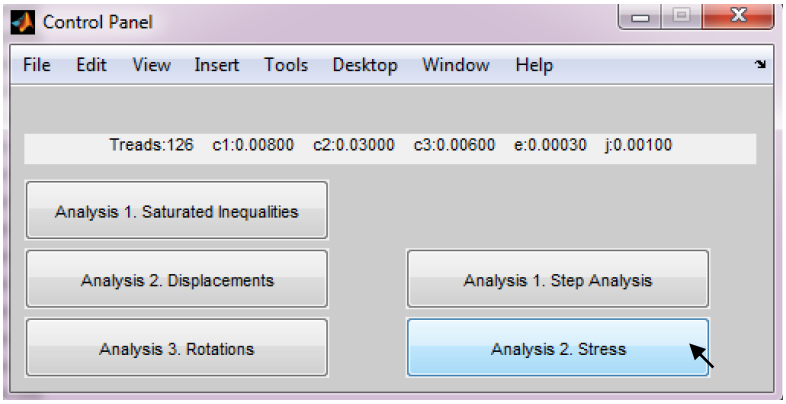

Fig. 4.38: Stress command

The complexity is due to the fact that our interest is both in the stress trend in a single step and in the global behaviour of the full stair. Since the step is partitioned in twenty control sections (Fig. 4.39), it is possible to refer the analysis results to one or more sections of the steps. In particular, the index 1 is referred to the section in correspondence to the wall, while the index 20 is referred to the section in correspondence of the internal rib, where the railing is present.

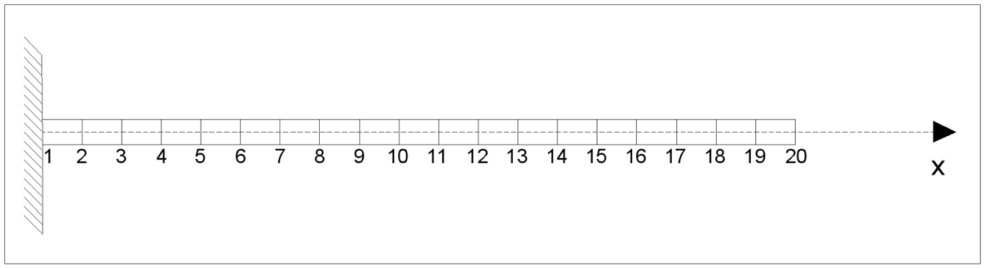

Fig. 4.39: Control sections

After selecting this function, it is then shown to the user a dynamic interface, where four options can be selected:

- *Step/s to select:* it can be either specified a single step, an interval 'from-to', or take into account all the steps (Fig. 4.40);
- *Section/s to select*: each step is divided into 20 sections. Here it can be selected, in the same manner of the steps, the section/s of interest (Fig. 4.41);
- *Reference system* to use for the results (Fig. 4.42);
- *Stress to analyze* with reference to the step/s and the section/s selected. This option allows us to analyze the values of axial force, shear, bending moment and torsional moment (Fig. 4.43).

Then, the resulting graph is a 3D graph, where the x-axis represents the step/s, the y-axis represents the section/s and the z-axis represents the stress. In special cases, for example for a single step or a single section, the graph becomes 2D. An example of 2D stress diagram is reported in Fig. 4.44, where the axial force, indicated with the notation 'r(1)' is reported, referring to the *S-Local System*, considering steps from 2 to 126, and the section 1 in correspondence to the wall is considered. Two examples of 3D stress diagram are reported in Fig. 4.45 and in Fig. 4.46, where the axial force and the torsional moment are drawn, considering all the control sections of the steps from 2 to 126 and referring to the *S-Local System*.

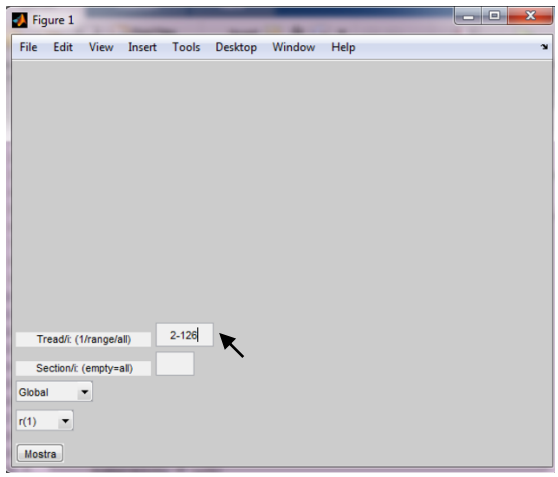

Fig. 4.40: Step selection

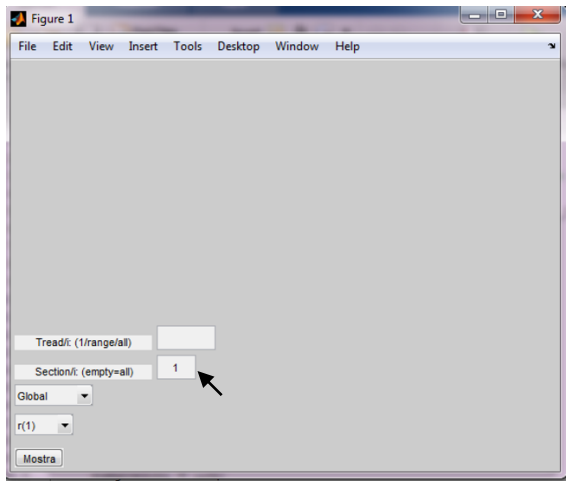

Fig. 4.41: Section selection

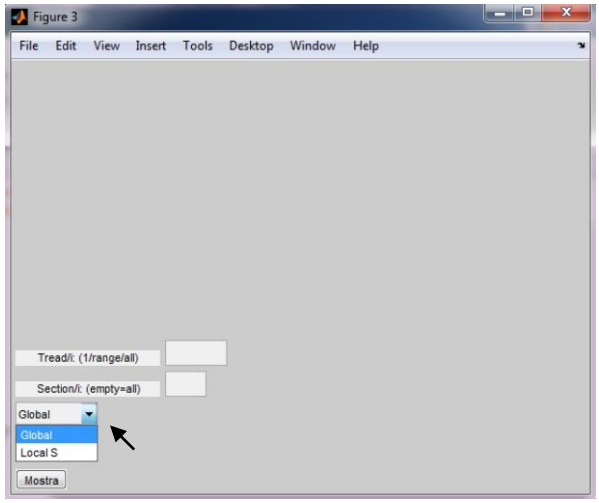

Fig. 4.42: Reference System selection

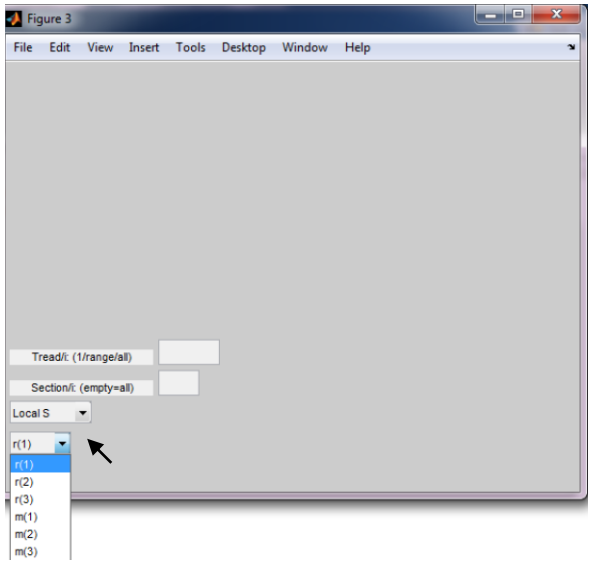

Fig. 4.43: Stress selection

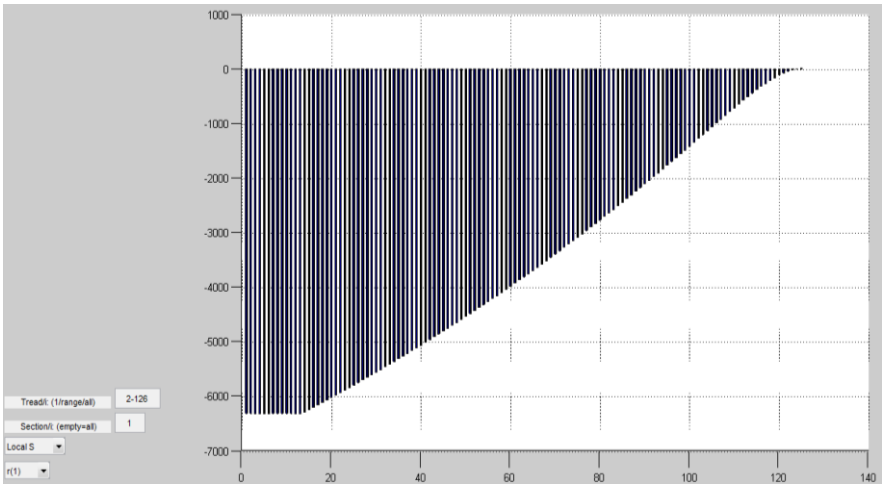

Fig. 4.44: Axial force for step from 2 to 126, section 1

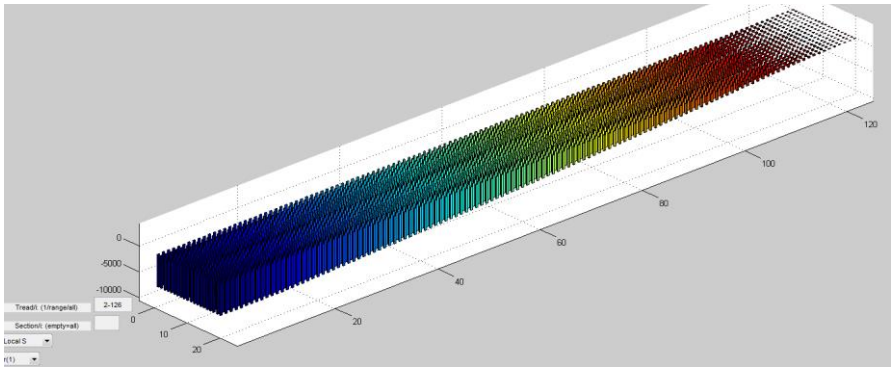

Fig. 4.45: 3D Diagram for Axial force for step from 2 to 126, for all the control sections

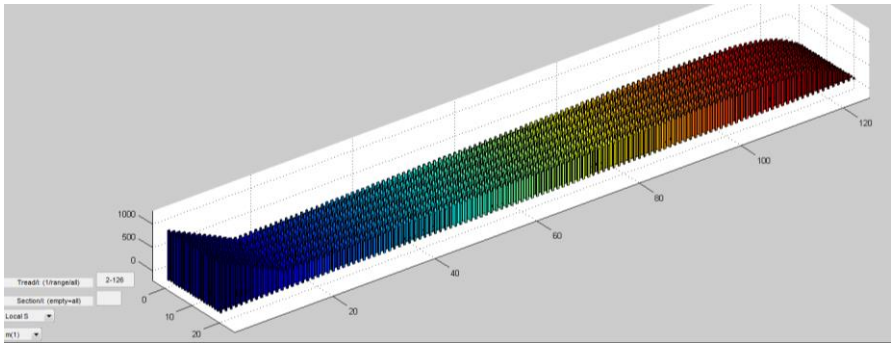

Fig. 4.46: 3D Diagram for Torsional moment for step from 2 to 126, for all the control sections

Chapter 5

CONCLUSIONS

5.1 Some remarks by Huerta

As noted by Huerta [16], the study of historic buildings deals with two main issues: 1) understanding their structural behaviour, by studying the possible states of equilibrium and 2) trace the origin and significance of their cracks, trying to imagine what kind of movements gave origin to the observed pattern of cracks.

In order to study the equilibrium of a structure, it is important to identify its structural parts, that is what can be considered structure and what not, since an inadequate identification of the structure and of its elements can be misleading. This issue can be addressed by referring to Heyman, who has already studied the most basic types of historic masonry structures.

Regarding the origin and significance of the cracks, the analogy between the typical cracking patterns and the kind of movement which could have originated them must be sought, although "complicated patterns produced by combined movements will demand the analyst experience and insight" [16].

Cracks represent the most evident manifestation of the nature of masonry material, due to the fact that masonry structures can adapt, while remaining safe, to small, unavoidable and unpredictable movements (e.g., soil settlements). For small movements we mean roughly 1/100 of the span, that is 100 mm for a 10 m span; in this case the state of equilibrium remains substantially unaltered and still "contained" within the distorted geometry. Hence, even if cracks could alarm a modern architect or engineer, they are in most cases irrelevant. Besides, since boundary conditions can vary at any time, the crack pattern may change, so there is no way to predict future movements, but, thanks to the Safe Theorem we learn that the structure will remain safe for any "small" movements in the future.

Of course, the modern computer programs may be of great help in the study of the equilibrium of arches, vaults and buttresses, working within the assumptions of Limit

Analysis. The complexity lies in the definition of the geometry, since every building, even within a certain studied type, presents different problems and there is not a unique way to approach the problem.

As noted by Huerta in [16], "the task is not easy; no computer program will give us a unique answer, but the problem presents itself with all its fascinating complexity and richness. Now the analyst is in the situation to ask relevant questions and give meaningful answers. It is not an amateur task; it needs long years of study, practice and reflection".

5.2 A short discussion about this PhD work

The present work extends previous research on the behaviour of masonry stairs. Its main purpose is the evaluation of the effect of settlements by employing a discrete model.

The behaviour of masonry stairs has been already studied by other authors. In particular, Heyman observes that the basic structural action for masonry stairs of small flight is represented by twist of individual treads, which lead to shear stresses and, consequently, to tensile stresses in the masonry.

In [46] the author shows how such stresses, which are low for short stairs, can become more harmful than direct compression for long flights, so that the strength of the material is violated and the equilibrium of the structure is compromised.

In [47] Angelillo proposes an analytical study of a real case, that is the triple helical stair of San Domingos de Bonaval, in which he overcomes this problem combining two different models. He models the helical stair, made of monolithic steps, built in torsionally at their external boundary and supported on an internal rib, as a continuum shell. His analysis is based on the assumption that the material of the stair is unilateral, namely a No-Tension material in the sense of Heyman and he employs the Safe Theorem of Limit Analysis in order to obtain a statically admissible stress field, combining concentrated stresses and 2d diffuse uniaxial stresses. With his continuous model, Angelillo combines the equilibrium solution proposed by Heyman with a sort of Ring-Like solution valid, by itself, only for a generic helical stair structure fixed at both ends. The combination of the two equilibrium solutions produces, in his analytical study, limited shear and tensile stresses into the steps and limited compressive stresses into the central rib.

The complementarity of the two equilibrium solutions proposed by Angelillo is here checked from a completely different point of view, on a case study, by employing an energy approach for a discrete model of the helical stair of San Domingos de Bonaval. The structure is treated as a system composed by an assembly of rigid blocks, that is it is assumed that each step behaves as a rigid body, whose behaviour, in terms of possible movements that can be exhibited, can be described by the displacements and the rotations of their centroids. It is assumed that the staircase is subject only to its own weight, that is the weight of each step is applied at its centroid; moreover, the rigid blocks are submitted to unilateral constraints, with no-sliding on interfaces.

While Angelillo refers to a static approach, that is applied for a continuous model of the masonry stair, in the present case we refer to a kinematic approach applied to a discrete model, in which we admit the presence of likely sets of given settlements of the

constraints. The effect of such settlements produces a piecewise rigid displacement field for the entire structure, which can be derived through an energy approach, by minimizing the potential energy of the loads. Since each individual step of the helical stair moves, the structure becomes statically determined as a whole, hence the corresponding statically admissible set of internal forces can be found, by invoking the static-kinematic duality. The whole calculation procedure and modelling are carried out with linear programming and implemented in the programming language Matlab.

The complexity related to a faithful reproduction of the stair geometry have been overcome by referring to a slightly simplified shape of the steps. Moreover, the longitudinal axis of the treads, which is actually curve, is assumed to be straight, being in this case negligible the error of approximation (0,2 ‰). In order to capture the behaviour of different parts of the step, that is the part of the step inserted into the wall and the part near the internal rib, and consequently confirm the Ring-Like stress regime, different local reference systems are considered. The choice of using three different reference systems is also useful to make the writing of constraint conditions and the analysis of results easier. The writing of the constraint conditions for the various nodes of the step is the result of long considerations and different hypothesis, made with the fundamental help, the intuitions and experience of Professor Angelillo, about the possible structural behaviour of the staircase as a whole.

Many attempts have been considered, taking into account different sets of possible settlements and clearances in correspondence of nodes along specific directions. The objective was to predict a possible scenario for the given settlements, which is able to mobilize the entire structure and, eventually, to identify a special set of internal and external reactions on each rigid piece composing the structure.

The fundamental difference with the original work by Angelillo consists in the fact that the search of the displacement field, as a solution of the kinematical problem, is here obtained by employing an energy approach, namely by minimizing the solely potential energy $\wp$ of the loads over the set of piecewise rigid displacements. In this case, the functional $\wp$ is linear in $\hat{\mathbf{u}}$ (vector of rigid body parameters) and it is subject to linear constraints, hence the problem can be set as a Linear Programming problem, whose solution is obtained, in Matlab, through the Interior Point algorithm, which is recommended when the problem contains many variables, that is it is a “large-scale” problem.

The interpretation of results, in terms of nodes displacements and of identification of reactive forces, is facilitated thanks to the concept of “saturated inequalities”: in this way, the visualization of steps behaviour is optimized and also the internal forces can be derived. Hence, the stress regime of the whole staircase can be obtained.

For what concerns the diagram of bending moment, the non-zero values at the ends are due to the fact that there is an eccentricity between the actual pressure line and the axis along which the bending moment is evaluated.

5.3 Potentiality of the method and future developments

By applying this method, which can also be employed for generic masonry structures, such as those made of bricks or small stones, the validity of the minimization procedure applied to masonry structures, discretized through rigid blocks, is checked. The solution obtained, in terms of internal forces, is qualitatively and quantitatively similar to that proposed by Angelillo in [47], who applies a static approach to an approximated continuous model of the staircase.

As a result, we find a force regime inside the structure which is compressive (that is compatible with the unilateral contact conditions on the interfaces) and determines stress levels inside the elements, well below the compressive and tensile strengths, showing the effectiveness of the discrete analysis, which can also be applied to different masonry structures.

With the present discrete model, a practical confirmation of the complementarity of Heyman and Ring-Like stress regime, for the case study of the triple helical stair of San Domingos de Bonaval, is obtained and a possible explanation of the reason why such bold structure is standing safely is given.

As said before, the power of the kinematic approach, presented in this work, is that it can also be applied to other types of masonry structures, through a discrete element modelling, by assuming that the masonry structure is constituted by an assembly of rigid blocks, which are in a unilateral contact among each other, and on whose interfaces sliding is prevented, according to Heyman's fundamental assumptions. This method could be easily extended to other cases just by defining, in a parametric form, the functions that describe the geometry of the structure and its blocks partition.

The work could be further improved by focusing on the following aspects:

- *Study of edge effects*: we observed a particular behaviour in correspondence of the floor, where there is an increment in terms of torsional moment, in particular for the first sixteen steps. This is probably due to a side effect of the system configuration and can be further explored, in order to understand all the possible implications and, consequently, refine the model.
- *Study of different constraint configurations*: during the model setup, we investigated different constraint configurations, and for two of them we evaluated all the possible results. Many other configurations can be explored, in order to understand better the correct way to model the constraints between adjacent blocks; for example, we can model edge-to-edge and surface-to-surface constraints, or introduce other convenient reference systems.
- *Settlements Sensitivity Analysis (and relative calibration)*: in this work, we consider just one main settlement in correspondence of the base of the stair, and clearances and tolerances values for all the other nodes. Other types and values of settlements are hypothetically possible and can be introduced in this model. The work of settlement calibration was done manually,

referring to the wide experience of Angelillo. It could be possible and interesting to automatize the process of settlement calibration, by introducing a new objective function, designed for this specific purpose, and consequently improve the Matlab program to accomplish this task.

Appendix A

LINEAR PROGRAMMING

Prologue. This section introduces the basic concepts of Linear Programming, following the approach set out in the lesson indicated in *point b* of web list and also referring to the Mathworks documentation (*point a* in the web list) for the solution of linear programming problem in Matlab.

* * *

Linear programming is a mathematical technique for finding optimal solutions to problems that can be expressed through linear equalities and inequalities. Although only few complex real-world problems can be expressed perfectly in terms of a set of linear functions, linear programs can provide reasonably realistic representations of many real-world problems, especially when a mathematical formulation of the problem is given in a creative manner (see *point b* in web sites list).

The many nonlinear and integer extensions of Linear Programming are collectively known as the Mathematical Programming field, which is defined by Dantzig as the *"branch of mathematics dealing with techniques for maximizing or minimizing an objective function subject to linear, nonlinear, and integer constraints on the variables."* Hence, Linear Programming represents a special case of Mathematical Programming, being *"concerned with the maximization or minimization of a linear objective function in many variables subject to linear equality and inequality constraints."* [62]

Linear programming can also be defined as *"a mathematical method to allocate scarce resources to competing activities in an optimal manner when the problem can be expressed using a linear objective function and linear inequality constraints"* (see *point b* in web sites list).

The essential elements of a linear program are:

- a set of variables;
- a linear objective function, indicating the contribution of each variable to the desired outcome;
- a set of linear constraints, describing the limits on the values of the variables.

The output of a linear program is a set of values, associated to the problem variables, which satisfy the objective function and are consistent with all the constraints.

The formulation of a linear program represents the hardest part of the process in which a real-world problem is translated into a mathematical model. Once a problem has been formulated as a linear program, a computer program can be used to solve the problem. When the problem is solved, another delicate part concerns with the interpretation of the result.

A.1 A brief introduction

Linear Equalities

When we deal with a linear program, all of the equalities and inequalities must be linear. A linear function has the following form:

$$a_0 + a_1x_1 + a_2x_2 + a_3x_3 + \cdots + a_nx_n = 0 \tag{A.1}$$

being *a* the coefficients of the equality, which are fixed values, related to nature of the problem, and *x* the variables of the equality, which can vary into a range of values within the limits defined by the constraints.

Linear equalities and inequalities are often written using summation notation, which makes it possible to write an equality in a much more compact form:

$$a_0 + \sum_{i=1}^{n} a_ix_i = 0 \tag{A.2}$$

in which the index *i* starts in this case at *1* and runs to *n*. There is a term in the sum for each value of the index.

The Decision Variables

The variables are the quantities that need to be determined in order to solve the problem, sometimes they are called decision variables because the problem is to decide what value each variable should take. The problem is solved when the best values of the variables have been identified.

Frequently, one of the hardest and/or most crucial steps in formulating a problem as a linear program is the definition of the variables of the problem. Sometimes creative variable definition can be used to dramatically reduce the size of the problem or make

linear an otherwise non-linear problem.

A variety of symbols, with subscripts and superscripts, can be used to represent the variables of an LP. For this general introduction, the variables are represented as $x_1, x_2, \dots, x_n$.

The Objective Function

The objective of a linear programming problem consists in the maximization or in the minimization of some numerical value and the objective function indicates how each variable contributes to the value to be optimized in solving the problem. The objective function takes the following general form:

$$maximize\ or\ minimize\ Z = \sum_{i=1}^{n} c_i X_i \tag{A.3}$$

being c_i the objective function coefficient corresponding to the ith variable, and X_i the ith decision variable. The coefficients of the objective function indicate the contribution to the value of the objective function of one unit of the corresponding variable. (It is noteworthy that the way the general objective function above has been written implies that there is a coefficient in the objective function corresponding to each variable. Of course, some variables may not contribute to the objective function. In this case, it can be either assumed that the variable has a null coefficient, or that the variable is not in the objective function at all).

The Constraints

Constraints define the possible values that the variables of a linear programming problem may take. They typically represent resource constraints, or the minimum or maximum level of some activity or condition. They take the following general form:

$$subject\ to \sum_{i=1}^{n} a_{j,i} X_i \leq b_j \quad j = 1,2, \dots, m \tag{A.4}$$

being X_i the ith decision variable, $a_{j,i}$ the coefficient on X_i in constraint j and b_j the right-hand-side coefficient on constraint j.

It can be noted that j is an index that runs from *1* to m, and each value of j corresponds to a constraint. Thus, condition (A.4) represents m constraints (equalities, or, more precisely, inequalities) with this form. Resource constraints are a common type of constraint. In a resource constraint, the coefficient $a_{j,i}$ indicates the amount of resource j used for each unit of activity i, as represented by the value of the variable X_i. The right-hand side of the constraint b_j indicates the total amount of resource j available for the project.

Moreover, while the constraint above is written as a less-than-or-equal constraint, greater- than-or-equal constraints can also be used. A greater-than-or-equal constraint can always be converted to a less-than-or-equal constraint by multiplying it by -1. Similarly, equality constraints can be written as two inequalities, that is a less-than-or-equal constraint and a greater-than-or-equal constraint.

A General Linear Programming Problem

All Linear Programming problems have the following general form:

$$\begin{aligned} &maximize\ or\ minimize\ Z = \sum_{i=1}^{n} c_i X_i \\ &subject\ to \sum_{i=1}^{n} a_{j,i} X_i \leq b_j \quad j = 1,2,\dots,m \\ &and\ X_i \geq 0 \quad i = 1,2,\dots,n \end{aligned} \tag{A.5}$$

being X_i the ith decision variable, c_i the objective function coefficient corresponding to the ith variable, $a_{j,i}$ the coefficient on X_i in constraint j and b_j the right-hand-side coefficient on constraint j.

A.2 Linear Programming Problem Formulation and graphic solution

The basic steps of the formulation are expressed as follows:

1. Identify the decision variables;
2. Formulate the objective function;
3. Identify and formulate the constraints.

Once a problem is formulated, it can be entered into a computer program to be solved. The solution is a set of values for each variable that are consistent with the constraints (i.e., feasible) and result in the best possible value of the objective function (i.e., optimal).

Not all Linear Programming problems have a solution, however. There are two other possibilities: *a)* there may be no feasible solutions (i.e., there are no solutions that are consistent with all the constraints); *b)* the problem may be unbounded (i.e., the optimal solution is infinitely large).

If the first of these problems occurs, one or more of the constraints will have to be relaxed. If the second problem occurs, then the problem probably has not been well formulated since few, if any, real world problems are truly unbounded.

Three key points that should be learned from the graphical solutions are:

1. the constraints should define a polygon in the case of two variables, or a n-dimensional polyhedron in the case of more than 2 variables, called the feasible region;
2. the objective function defines a set of parallel lines in the case of two variables, or a set of *n*-dimensional hyperplanes in the case of *n* variables, one for each potential value of the objective function;
3. the solution is the last corner or face of the feasible region that the objective function touches as the value of the objective function is improved.

This third point implies two important facts. First, the solution to a Linear Programming problem always includes at least one corner. Second, the solution is not always just a single point. If more than one corner point is optimal, then the face between those points is also optimal. The fact that the solution always includes a corner is used by the solution algorithm for solving Linear Programming problems. The algorithm searches from corner to corner, always looking for an adjacent corner that is better than the current corner. When a corner is found, which has no superior adjacent corners, then that is reported as the solution. Some of the adjacent corners may be equally good, however.

An important concept is whether a constraint is binding. A constraint is said to be binding at points where it holds as an equality. For example, in the case of a less-than-or-equal constraint representing a resource limitation, the constraint is binding when all of the resource is being used.

The graphical solution method can only be applied to Linear Programming problems with two variables. For problems that are larger than this, the solution can be obtained through a variety of computer programs.

A.3 The Fundamental Assumptions of Linear Programming

A problem can be realistically represented as a linear program if the following assumptions hold:

1. *Linearity*: the constraints and objective function are linear, this requires that the value of the objective function and the response of each resource expressed by the constraints is proportional to the level of each activity expressed in the variables; linearity also requires that the effects of the value of each variable on the values of the objective function and the constraints are additive. In other words, there can be no interactions between the effects of different activities.

2. *Divisibility*: the values of decision variables can be fractions. Sometimes these values only make sense if they are integers; then an extension of linear programming, called integer programming, is needed.

3. *Certainty*: the model assumes that the responses to the values of the variables are exactly equal to the responses represented by the coefficients.

4. *Data*: formulating a linear program to solve a problem assumes that data are

available to specify the problem.

A.4 Linear Programming in Matlab

A Linear Programming problem can be solved through the Matlab built in function *linprog*, which tries to find the minimum of a given problem, specified as follows:

$$\min_x f^T \; such\; that \begin{cases} A \cdot x \leq b \\ A_{eq} \cdot x = b_{eq} \\ l_b \leq x \leq u_b \end{cases} \tag{A.6}$$

being f, x, b, b_{eq}, l_b, and u_b vectors, and A and A_{eq} matrices. Being, indeed, Matlab a programming language that operates on matrices, the constraint equalities and inequalities are converted into matrix form.

The function *linprog* attempts to find an x that minimizes the objective function f, which in this work is represented by the potential energy of the loads.

Regarding to the inequalities:

A is an M-*by*-N matrix, related to linear inequality constraints, where M is the number of inequalities, and N is the number of variables (length of f). We recall that we have 6 variables for each step (3 rotations and 3 translations for each centroid), so the number of variables for the problem is 6n, and in our case the total number of variables is 6*126=756. The number of variable is important, since it has a direct impact on the possible algorithm that we can choose for the analysis. The matrix A can be passed as a sparse matrix, and it encodes the M linear inequalities $A \cdot x \leq b$, where x is the column vector of N variables, and b is a column vector with M elements. The vector b is an M-element vector related to the A matrix and it encodes the M linear inequalities $A \cdot x \leq b$, where x is the column vector of N variables, and A is a matrix of size M-*by*-N.

Regarding to the equalities:

A_{eq} is an M_e-*by*-N matrix, related to linear equality constraints, where M_e is the number of equalities, and N is the number of variables (length of f). The matrix A_{eq} encodes the M_e linear equalities $A_{eq} \cdot x = b_{eq}$, where x is the column vector of N variables, and b_{eq} is a column vector with M_e elements.

The vector b_{eq} is an M_e-element vector related to the A_{eq} matrix. The vector b_{eq} encodes the M_e linear equalities $A_{eq} \cdot x = b_{eq}$, where x is the column vector of N variables, and A_{eq} is a matrix of size M_e-*by*-N.

Lower bounds and upper bounds are specified as a real vector or real array.

The documentation of *linprog* function also contains some optimization options, some options apply to all algorithms, and others are relevant for particular algorithms (fig. A. 1)

`Algorithm`	Choose the optimization algorithm: • `'interior-point-legacy'` (default) • `'interior-point'` • `'dual-simplex'` For information on choosing the algorithm, see Linear Programming Algorithms.
Diagnostics	Display diagnostic information about the function to be minimized or solved. Choose `'off'` (default) or `'on'`.
`Display`	Level of display (see Iterative Display): • `'final'` (default) displays just the final output. • `'off'` or `'none'` displays no output. • `'iter'` displays output at each iteration. The `'iter'` option is unavailable for the `'active-set'` algorithm.
`MaxIterations`	Maximum number of iterations allowed, a positive integer. The default is: • 85 for the `'interior-point-legacy'` algorithm • 200 for the `'interior-point'` algorithm • `10*(numberOfEqualities + numberOfInequalities + numberOfVariables)` for the `'dual-simplex'` algorithm • `10*numberOfVariables` for the `'simplex'` algorithm • `10*max(numberOfVariables, numberOfInequalities + numberOfBounds)` for the `'active-set'` algorithm See Tolerances and Stopping Criteria and Iterations and Function Counts.
`OptimalityTolerance`	Termination tolerance on the dual feasibility, a positive scalar. The default is: • `1e-8` for the `'interior-point-legacy'` algorithm • `1e-7` for the `'dual-simplex'` algorithm • `1e-6` for the `'interior-point'` and `'simplex'` algorithms • The option is not used for the `'active-set'` algorithm
interior-point Algorithm	
`ConstraintTolerance`	Feasibility tolerance for constraints, a scalar from `1e-10` through `1e-3`. `ConstraintTolerance` measures primal feasibility tolerance. The default is `1e-6`.
Preprocess	Level of LP preprocessing prior to algorithm iterations. Specify `'basic'` (default) or `'none'`.
Dual-Simplex Algorithm	
`ConstraintTolerance`	Feasibility tolerance for constraints, a scalar from `1e-10` through `1e-3`. `ConstraintTolerance` measures primal feasibility tolerance. The default is `1e-4`.
`MaxTime`	Maximum amount of time in seconds that the algorithm runs. The default is `Inf`.
Preprocess	Level of LP preprocessing prior to dual simplex algorithm iterations. Specify `'basic'` (default) or `'none'`.

fig. A. 1: Optimization options for linprog function in Matlab (see *point a* in web sites list)

A.5 Time and Space complexity of the minimization problem

In the computer science, the amount of time and space required by an algorithm is quantified in a simplified form, providing the order of magnitude, expressed by the big O notation, where the argument of the big O is the complexity in two dimensions (time and space). The complexity is always given in relation to the *input* size, and it is useful to understand the behaviour of the algorithm when the *input* size changes.

For example, if a problem requires constant time to finish, whatever is the *input* of the problem, its time complexity is O(1). An example for this kind of time complexity is the *random* function, which, whatever is the input size, always picks a random element of the input and it always requires the same amount of time.

A slightly more complicated algorithm can require a O(n) complexity, and an example can be the *count* problem, where, in order to provide the *count* of all the element in the *input*, it must spend a small fixed amount of time on each of them.

In the case at hand, Matlab allows us to use two main different algorithms with different complexity in time:

- *Simplex*: which provides the most accurate results, but it finishes with exponential times $O(n^2)$;
- *Interior-point*: which provides a slightly worst approximate function (in some cases), but it is polynomial in the input size, then it can be used for very large

problems.

Hence, in the present work, the Simplex problem cannot be used, given the fact that it would require, even for relatively small problem with 756 variables, many weeks of calculation to complete (if it does not crash before) on a normal computer. For this reason, the *Interior-point* is applied, and the error of approximation is minimized by studying the initial value of the variables in the most appropriate way.

Appendix B

PLASTICITY

Prologue. This section introduces the basic concepts of plasticity, following the approach set out both in the course notes of Professor Nunziante (2005) and in his book [63].

B.1 Elastic-plastic constitutive law

Anelastic body and internal variables

Cauchy defines as *elastic* the body in which the stress in a certain instant is completely determined by the current strain field, whilst a body is *anelastic* when its deformation is defined by other parameters, related to the stress history (materials with memory) and other internal variables.

The theory that deals with these materials, in the linear case, is called *linear viscoelasticity*. An alternative way of representing the parameters on which depends the behaviour of an anelastic body, is to introduce a number of internal variables $\boldsymbol{\xi} = [\xi_1, \xi_2, \dots, \xi_n]^T$. Therefore, the strain $\boldsymbol{E} = [\varepsilon_{ij}]$ for these materials is expressed by the function:

$$\boldsymbol{E} = \boldsymbol{E}(\boldsymbol{T}, T, \boldsymbol{\xi}) \,, \tag{B.1}$$

or:

$$\boldsymbol{\varepsilon} = \boldsymbol{\varepsilon}(\boldsymbol{\sigma}, T, \boldsymbol{\xi}) \,, \tag{B.2}$$

$\boldsymbol{T} = [\sigma_{ij}]$ being the Cauchy stress tensor and where condition (B.1) and condition (B.2) represent the tensorial and the vectorial (Voight) formulation of the total strain, respectively. The presence of these additional variables requires additional constitutive equalities. For anelastic bodies, with infinitesimal deformation, the strain is additively decomposed into an elastic and an anelastic part as follows:

$$\boldsymbol{E} = \boldsymbol{E}^e + \boldsymbol{E}^a \,, \tag{B.3}$$
$$\boldsymbol{\varepsilon} = \boldsymbol{\varepsilon}^e + \boldsymbol{\varepsilon}^a \,, \tag{B.4}$$

where the elastic part of deformation is:

$$\boldsymbol{E} = \boldsymbol{C}^{-1}\boldsymbol{T} \,, \tag{B.5}$$
$$\boldsymbol{\varepsilon} = \boldsymbol{C}^{-1}\boldsymbol{\sigma} \,, \tag{B.6}$$

while the anelastic components depend on the internal variables.
The body is said to be in equilibrium, if it does not change spontaneously its state, when the external actions remain the same.
Since in this context the focus is on the plastic behaviour of materials and structures, the plastic strain $\boldsymbol{E}^p = \boldsymbol{E}^a$, representing the permanent deformation of the material, takes the role of an internal variable.
Therefore, we can express the deformation as follows:

$$\boldsymbol{E} = \boldsymbol{E}^e + \boldsymbol{E}^a \,, \tag{B.7}$$
$$\boldsymbol{\varepsilon} = \boldsymbol{\varepsilon}^e + \boldsymbol{\varepsilon}^p \,. \tag{B.8}$$

The Plastic Flow

The plastic behaviour of the material is non-conservative, in the sense that, during an increasing load process, part of the external energy is dissipated in other forms of energy, related to the development of irreversible deformations (or fractures) that arise within the material. On adopting the Voight notation, the strains $\boldsymbol{E}, \boldsymbol{E}^e, \boldsymbol{E}^p$ can be also expressed as column vectors of $\mathbb{R}^9$ as follows:

$$\boldsymbol{\varepsilon} = [\varepsilon_1, \varepsilon_2, \dots, \varepsilon_9]^T = [\varepsilon_{11}, \varepsilon_{12}, \dots, \varepsilon_{33}]^T \,, \tag{B.9}$$

as well as the stresses:

$$\boldsymbol{\sigma} = [\sigma_1, \sigma_2, \dots, \sigma_9]^T = [\sigma_{11}, \sigma_{12}, \dots, \sigma_{33}]^T \,. \tag{B.10}$$

We can also consider the tensor form for strains:

$$\boldsymbol{E} = \boldsymbol{E}^e + \boldsymbol{E}^p = \left[\varepsilon_{ij}^e\right] + \left[\varepsilon_{ij}^p\right] \,, \tag{B.11}$$

and for stresses:

$$\boldsymbol{T} = \left[\sigma_{ij}\right] \,. \tag{B.12}$$

If the load process is time dependent, conditions (B.7) and (B.8) can be rewritten in the following incremental forms:

$$\dot{\boldsymbol{E}} = \dot{\boldsymbol{E}}^e + \dot{\boldsymbol{E}}^p \,, \tag{B.13}$$

or:

$$\dot{\boldsymbol{\varepsilon}} = \dot{\boldsymbol{\varepsilon}}^e + \dot{\boldsymbol{\varepsilon}}^p \,, \tag{B.14}$$

Where, by denoting by t the time variable:

$$\dot{(-)} = \frac{d(-)}{dt} \,. \tag{B.15}$$

The experimental results show that anelastic strains in many structural materials generally arise when a certain limit level for stress $\boldsymbol{\sigma}$ and also a certain level for stress increase $d\boldsymbol{\sigma}$, are reached. In particular, the *plastic function* f_0,

$$f_0(\boldsymbol{\sigma}) = 0 \,, \tag{B.16}$$

defines a limit domain in the stress space in $\mathbb{R}^9$ (or in the principal stress space in $\mathbb{R}^3$, for isotropic materials), and describes all the limit stress states $\boldsymbol{\sigma}$ (fig. B. 1).

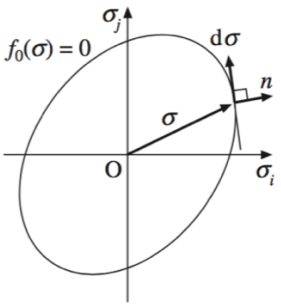

fig. B. 1: Limit domain [63]

It is usually assumed that the function f_0 is almost everywhere (a.e.) differentiable, in the sense that it does exist a hyperplane which is tangent to the surface at a.e. point $\boldsymbol{\sigma}$ satisfying condition (B.16).

From here on we restrict to consider "perfect plasticity" and then we use the notation $\boldsymbol{E}^p, \boldsymbol{\varepsilon}^p$ for the anelastic strain $\boldsymbol{E}^a, \boldsymbol{\varepsilon}^a$. In perfect plasticity, it is assumed that plastic deformations arise if the following conditions are met:

$$f_0(\boldsymbol{\sigma}) = 0\,, \tag{B.17}$$

$$df_0(\boldsymbol{\sigma}) = \left(\frac{df_0}{d\sigma_i}\right)_{\boldsymbol{\sigma}} = \nabla f_0 \cdot d\boldsymbol{\sigma} = 0\,. \tag{B.18}$$

In (B.17) it is expressed the fact that the stress vector $\boldsymbol{\sigma}$ belongs to the yield domain, while in (B.18) it is required that the stress increase d$\boldsymbol{\sigma}$ moves on the tangent plane to the limit domain at $\boldsymbol{\sigma}$, and then it is orthogonal to the normal **n**. The normal **n** is proportional to the quantity $\left(\frac{df_0}{d\sigma_i}\right)_{\boldsymbol{\sigma}}$, representing the components of the gradient vector of f_0. Through (B.18) it is ensured that the stress increase d$\boldsymbol{\sigma}$ is such that the tension $(\boldsymbol{\sigma} + d\boldsymbol{\sigma})$ satisfies condition (B.17), that is:

$$df_0(\boldsymbol{\sigma}) \cong f_0(\boldsymbol{\sigma} + d\boldsymbol{\sigma}) - f_0(\boldsymbol{\sigma}) = 0\,, \tag{B.19}$$

and consequently:

$$f_0(\boldsymbol{\sigma} + d\boldsymbol{\sigma}) = 0\,. \tag{B.20}$$

The points $\boldsymbol{\sigma}$ for which condition (B.17) occurs, belong to the limit domain f_0. The points internal to the surface f_0 are such that the following condition holds:

$$f_0(\boldsymbol{\sigma}) < 0\,, \tag{B.21}$$

and correspond to elastic states, while the stress states which are external to the limit domain $f_0(\boldsymbol{\sigma}) = 0$, are not admissible for elastic-perfectly-plastic materials, since they cannot be reached, such states are expressed by condition:

$$f_0(\boldsymbol{\sigma}) > 0\,. \tag{B.22}$$

The plastic strain increase dE_{ij}^p can be expressed in the following form:

$$dE_{ij}^p = d\lambda \pi_{ij}\,, \tag{B.23}$$

where $\boldsymbol{\pi} = [\pi_{ij}]$ is a second order symmetric tensor. The strain increase of the material can be characterized in the three following forms:

$$d\lambda \geq 0\,,\ f_0(\boldsymbol{\sigma}) = 0\,,\ df_0(\boldsymbol{\sigma}) = 0\,, \tag{B.24}$$

$$d\lambda = 0\,,\ f_0(\boldsymbol{\sigma}) = 0\,,\ df_0(\boldsymbol{\sigma}) < 0\,, \tag{B.25}$$

$$d\lambda = 0\,,\ f_0(\boldsymbol{\sigma}) < 0\,, \tag{B.26}$$

namely respectively *plastic state*, *elastic return* and *elastic state*.

Referring to condition (B.23), the quantities π_{ij} determine the *shape* of the plastic strain increase, while the infinitesimal scalar $d\lambda$ assigns the entity of the plastic strain increase. This assumption is made according to experimental results for a perfectly plastic material, for which plastic strains arise (if condition (B.18) is satisfied) when a limit stress state is attained along specific planes of plastic flow, depending on the material and the stress.

Moreover, the plastic strain increase does not depend neither on the direction nor on the magnitude of the stress increase $d\boldsymbol{\sigma}$, which needs to satisfy only condition (B.18).

Some metallic materials (such as steel) have, indeed, a structure made of polycrystalline aggregates. Each crystal is an assembly of atoms, with their own regular structure. These crystal aggregates, while presenting a macroscopic isotropic behaviour in elastic conditions, show plastic strains resulting from the relative motions, also said plastic slips, on special crystal planes, in response to shear stress therein. Such planes are those where the strength is minimal, and can thus define the mechanism.

Based on these experimental evidences, the direction of the strain increase is ruled by a function $P(\boldsymbol{T})$, called the *plastic potential*, which generates the quantities π_{ij} as a function of the stress:

$$\pi_{ij} = \frac{\partial P(\boldsymbol{T})}{\partial T_{ij}}, \tag{B.27}$$

For many materials, it is assumed that the plastic potential function $P(\boldsymbol{T})$ coincides with the yield function $f_0(\boldsymbol{T})$:

$$P(\boldsymbol{T}) = f_0(\boldsymbol{T}), \tag{B.28}$$

and this hypothesis enables to define the so called *Associated Plastic Potential* that holds true for standard or associated materials. Hence, the constitutive law, in the case of plastic condition, can be rewritten as follows:

$$d\boldsymbol{E}^p = d\lambda \frac{\partial f_0}{\partial \boldsymbol{T}}, \tag{B.29}$$

$$d\varepsilon_{ij}^p = d\lambda \frac{\partial f_0}{\partial \sigma_{ij}}. \tag{B.30}$$

Conditions (B.29) and (B.30), also known as *Normality Law* or *Normality rule*, states that the direction of $d\boldsymbol{E}^p$ and $d\boldsymbol{\varepsilon}^p$ is coincident with that of the normal **n** to the boundary or the yield domain f_0 at the stress point $\boldsymbol{\sigma}$.

If we overlap the vector space referred to $d\boldsymbol{\varepsilon}^p$ with that referred to $\boldsymbol{\sigma}$, both relating to $\mathbb{R}^9$, with coincident bases, we can represent in the same plane the vectors $\boldsymbol{\sigma}, d\boldsymbol{\sigma}, d\boldsymbol{\varepsilon}^p$ (fig. B. 2).

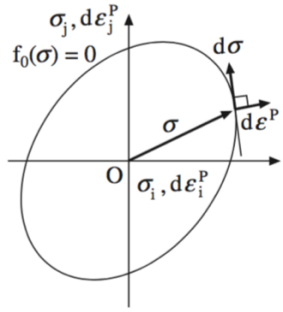

fig. B. 2: Normality Law [63]

The quantity $d\boldsymbol{\varepsilon}^p$ is not an exact differential, since if we consider two different transformations Γ_1, Γ_2 in the stress space, whose ends points $\boldsymbol{\sigma}_1, \boldsymbol{\sigma}_2$ are the same, we have in general different values of plastic strain increase $\Delta\boldsymbol{\varepsilon}^p$; hence, the increase $d\boldsymbol{\varepsilon}^p$ is not differentiable and the increase $\Delta\boldsymbol{\varepsilon}^p$depends on the effective history of the material (fig. B. 3).

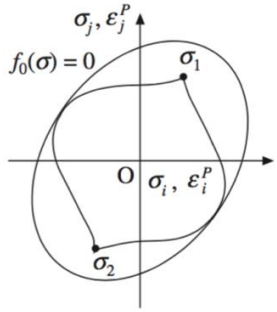

fig. B. 3: Different stress transformations [63]

When the increases are time-dependent, the condition (B.30) can be rewritten as follows:

$$\dot{\varepsilon}_i^p = \dot{\lambda}\left(\frac{\partial f_0(\boldsymbol{\sigma})}{\partial \sigma_i}\right)_{\boldsymbol{\sigma}}, \tag{B.31}$$

with:

$$\dot{\lambda} \geq 0 \quad if \quad f_0(\boldsymbol{\sigma}) = 0\,, \quad \dot{f}_0(\boldsymbol{\sigma}) = 0\,,$$

$$\dot{\lambda} \geq 0 \quad if \quad f_0(\boldsymbol{\sigma}) = 0\,, \quad \dot{f}_0(\boldsymbol{\sigma}) < 0\,, \tag{B.32}$$

$$\dot{\lambda} = 0 \quad if \quad f_0(\boldsymbol{\sigma}) < 0\,,$$

If the plasticization function f_0 is continuous but not differentiable at all points, we can assign a finite number *m* of functions $f_{01}(\boldsymbol{\sigma}), \dots, f_{0m}(\boldsymbol{\sigma})$, such that the strength domain is defined by the *m* inequalities:

$$f_{01}(\boldsymbol{\sigma}) \leq 0, \dots, f_{0m}(\boldsymbol{\sigma}) \leq 0\,, \tag{B.33}$$

and the yield condition, in this case, can be written as:

$$sup f_{0i}(\boldsymbol{\sigma}) = 0, \qquad i \in \{1, \dots, m\}\,, \tag{B.34}$$

Each function $f_{0i}(\boldsymbol{\sigma}) = 0$ represents a surface, within which the function f_{0i} is differentiable, while in the edge points the function f_{0i} is not differentiable (fig. B. 4).

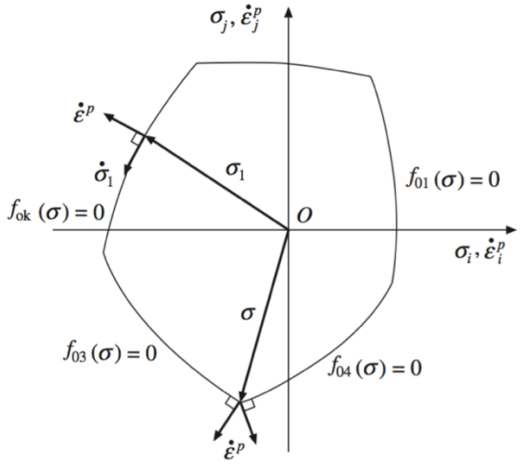

fig. B. 4: Limit domain defined by m functions [63]

When a stress state, said $\boldsymbol{\sigma}_1$, touches the limit domain in correspondence of the k-th plane, being $k \in \{1, \dots, m\}$, the following limit condition occurs:

$$f_{0k}(\boldsymbol{\sigma}_1) = 0\ ,\ \ f_{0i}(\boldsymbol{\sigma}_1) < 0\,, \qquad \forall\, i \in \{1, \dots, m\} - \{k\}\,, \tag{B.35}$$

In a similar way, when a stress state touches the intersection of *l* planes, with $1 < l < m$, the following plastic condition is valid:

$$\begin{aligned} f_{0j}(\boldsymbol{\sigma}) &= 0\ , \qquad \forall\, j \in \{n_1, \dots, n_l\} \subseteq \{1, \dots, m\}\,, \\ f_{0i}(\boldsymbol{\sigma}) &< 0\ , \qquad \forall\, i \in \{1, \dots, m\} - \{n_1, \dots, n_l\}\,, \end{aligned} \tag{B.36}$$

If condition (B.35) occurs together with condition (B.37):

$$\dot{f}_{0k}(\boldsymbol{\sigma}) = 0 \ , \ \ k \ \in \{1, \dots, m\} \, , \tag{B.37}$$

plastic strain can arise, expressed as follows:

$$\dot{\varepsilon}_i^p = \dot{\lambda}_k \left(\frac{\partial f_{0k}}{\partial \sigma_i} \right)_{\boldsymbol{\sigma}} \ , \qquad \dot{\lambda}_k \geq 0 \, , \tag{B.38}$$

If conditions (B.36) are satisfied together with condition (B.39):

$$\dot{f}_{0t}(\boldsymbol{\sigma}) = 0 \ , \ \ t \ \in \{n_1, \dots, n_l\} \, , \tag{B.39}$$

an increase of plastic strain can arise, expressed as follows:

$$\dot{\varepsilon}_i^p = \sum_{t=n_1}^{n_l} \dot{\lambda}_t \ \frac{\partial f_{0t}}{\partial \sigma_i} , \qquad \dot{\lambda}_t \geq 0 \, , \tag{B.40}$$

where the sum is referred only to the *l* active planes of the plastic domain. More generally, we can refer to the following relation:

$$\dot{\varepsilon}_i^p = \sum_{k=1}^{m} \dot{\lambda}_k \ \frac{\partial f_{0k}}{\partial \sigma_i} , \tag{B.41}$$

with:

$$\begin{gathered} \dot{\lambda}_k \geq 0 \; where \; f_{0k}(\boldsymbol{\sigma}) = 0 \, , \dot{f}_{0k}(\boldsymbol{\sigma}) = 0 \, , \\ \dot{\lambda}_k = 0 \; where \; f_{0k}(\boldsymbol{\sigma}) = 0 \, , \dot{f}_{0k}(\boldsymbol{\sigma}) < 0 \, , \\ \dot{\lambda}_k = 0 \; where \; f_{0k}(\boldsymbol{\sigma}) < 0 \, , \end{gathered} \tag{B.42}$$

where the multiplier $\dot{\lambda}_k$ is referred to the k-th plane of the plastic domain. The quantities $\frac{\partial f_{0t}}{\partial \sigma_i}$ define the gradient vector of the active planes f_{0t} in the stress space; thus, condition (B.41) expresses the vector of plastic strain increase as a non-negative linear combination ($\dot{\lambda}_t \geq 0$) of the gradient vectors of the active planes, for this reason the vector $\dot{\boldsymbol{\varepsilon}}^p$ belongs to the cone of the outward normal referred to the yield surfaces corresponding to the active stresses (fig. B. 4).
In this case, the elastic-plastic constitutive law can be written as follows:

$$\dot{\varepsilon}_i = a_{ij} \dot{\sigma}_j + \sum_{k=1}^{m} \dot{\lambda}_k \ \frac{\partial f_{0k}}{\partial \sigma_i} , \tag{B.43}$$

with:

$$\begin{aligned} \dot{\lambda}_k \geq 0 \; where \; f_{0k} = 0 \;\; , \;\; \dot{f}_{0k} = 0 \, , \\ \dot{\lambda}_k = 0 \; where \; f_{0k} = 0 \;\; , \;\; \dot{f}_{0k} < 0 \, , \\ \dot{\lambda}_k = 0 \; where \; f_{0k} < 0 \, . \end{aligned} \tag{B.44}$$

Stable material (Drucker postulate)

Referring to experimental test under one-dimensional stress regime (fig. B. 5),

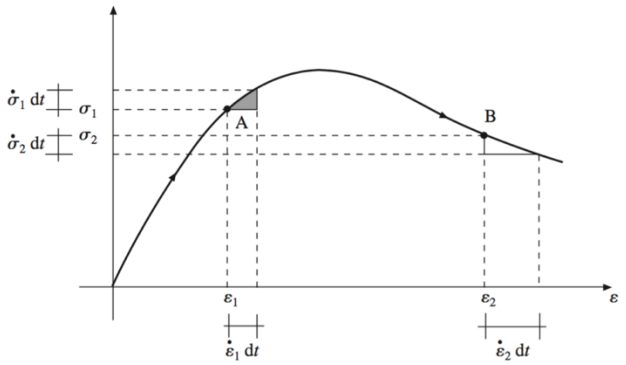

fig. B. 5: One-dimensional stress test [63]

if we consider the state A, characterized by values $(\sigma_1, \varepsilon_1)$, and we then apply the stress rate $\dot{\sigma}_1 dt > 0$, a strain rate $\dot{\varepsilon}_1 dt > 0$ arises, such that the specific power rate is a positive quantity:

$$\dot{\sigma}_1 \dot{\varepsilon}_1 > 0 \, , \tag{B.45}$$

which is depicted by a grey area in fig. B. 5.

Through this result, we can state that when the material is in the state A, it requires a stress increase $\dot{\sigma}_1 dt$ in order to exhibit the strain increase $\dot{\varepsilon}_1 dt$, such that the specific power increase $\dot{\sigma}_1 \dot{\varepsilon}_1$ is a positive quantity. In this case, the material is termed *stable*.

If we consider, instead, the state B, characterized by values $(\sigma_2, \varepsilon_2)$, and we then consider a strain rate $\dot{\varepsilon}_2 dt > 0$, a stress rate $\dot{\sigma}_2 dt < 0$ arises, such that the specific power rate is a positive quantity:

$$\dot{\sigma}_2 \dot{\varepsilon}_2 < 0 \, . \tag{B.46}$$

In this case, the material is called *unstable*.

According to the definitions just given, we obtain the stability postulate by Drucker, which gives rise to some implications, referring to the plastic behaviour of materials and structures.

A material is said to be stable, in a certain state depending on the previous load history and under the effect of external loads F, if the generic variation of these loads, applied through a loading and unloading cycle $\left(+\dot{F}, -\dot{F}\right)$, determines a stress variation cycle $(+\dot{\boldsymbol{\sigma}}, -\dot{\boldsymbol{\sigma}})$ in correspondence of the considered point, such that the consequent specific power variation is a non-negative quantity:

$$\oint \dot{\boldsymbol{\sigma}} \cdot \dot{\boldsymbol{\varepsilon}} \geq 0 \,. \tag{B.47}$$

Moreover, a stress state $\boldsymbol{\sigma}^a$ such that the condition $f(\boldsymbol{\sigma}^a) \leq 0$ is satisfied, being f the material yield function, is denoted ad *admissible stress state*.

If condition (B.43) occurs, referring to a stable material, the following properties descend:

1. Considering the elastic-plastic material with an associate plastic potential, and referring to a particular limit stress state $\boldsymbol{\sigma}$ with the corresponding vector $\dot{\boldsymbol{\varepsilon}}^p$, according with conditions (B.31) and (B.32), and to a generic admissible stress state $\boldsymbol{\sigma}^a$, such that the following condition occurs:

$$f(\boldsymbol{\sigma}) = 0 \;\; , \;\; f(\boldsymbol{\sigma}^a) \leq 0 \,, \tag{B.48}$$

condition (B.47), considering a single plastic strain rate $\dot{\boldsymbol{\varepsilon}}^p$, implies that:

$$(\boldsymbol{\sigma} - \boldsymbol{\sigma}^a)^T \cdot \dot{\boldsymbol{\varepsilon}}^p \geq 0 \,. \tag{B.49}$$

If we consider, indeed, the initial stress state $\boldsymbol{\sigma}^a$ and the generic load and unload cycle Γ, which increases the stress from the value $\boldsymbol{\sigma}^a$ to the value $\boldsymbol{\sigma}$, and then decreases the stress from the value $\boldsymbol{\sigma}$ to the value $\boldsymbol{\sigma}^a$ (fig. B. 6):

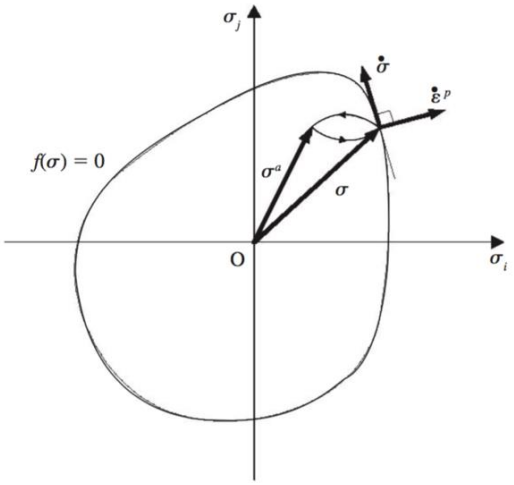

fig. B. 6: Load and unload cycle Γ [63]

condition (B.47), referring to the cycle Γ, can be rewritten as follows:

$$\oint_{\Gamma} \dot{\boldsymbol{\sigma}} \cdot \dot{\boldsymbol{\varepsilon}}\, dt = \oint_{\Gamma} \dot{\boldsymbol{\sigma}} \cdot \dot{\boldsymbol{\varepsilon}}^e\, dt + \oint_{\Gamma} \dot{\boldsymbol{\sigma}} \cdot \dot{\boldsymbol{\varepsilon}}^p\, dt \geq 0\,, \tag{B.50}$$

where the first integral at right-hand, referred to the elastic part of the strain, is zero, since the transformation Γ is a closed cycle; the second integral at right-hand, for a single rate $\dot{\boldsymbol{\varepsilon}}^p$ related to the stress state $(\boldsymbol{\sigma}, \dot{\boldsymbol{\sigma}} dt)$, reduces to the single term $\dot{\boldsymbol{\sigma}} \cdot \dot{\boldsymbol{\varepsilon}}^p$ and thus:

$$\dot{\boldsymbol{\sigma}} \cdot \dot{\boldsymbol{\varepsilon}}^p \geq 0\,. \tag{B.51}$$

For $\dot{\boldsymbol{\sigma}}$ such that $f(\boldsymbol{\sigma} + \dot{\boldsymbol{\sigma}} dt) < 0$, we have that $\dot{\boldsymbol{\varepsilon}}^p = 0$ and condition (B.49) is trivially valid in equality form. For $\dot{\boldsymbol{\sigma}}$ plastically admissible (plastic material), for which the condition $f(\boldsymbol{\sigma} + \dot{\boldsymbol{\sigma}} dt) = 0$ occurs, given a plastic strain rate $\dot{\boldsymbol{\varepsilon}}^p \neq 0$, the following condition holds true by virtue of the normality law:

$$\dot{\boldsymbol{\sigma}} \cdot \dot{\boldsymbol{\varepsilon}}^p = 0\,. \tag{B.52}$$

If the material has also a hardening behaviour, the following condition holds:

$$\dot{\boldsymbol{\sigma}} \cdot \dot{\boldsymbol{\varepsilon}}^p > 0\,. \tag{B.53}$$

Hence, the Drucker stability postulate is consistent with the definitions provided for both plastic and hardening materials.

2. *The plastic domain is convex*. Condition (B.49) implies that the admissible stress domain is convex, that is the stress states $\boldsymbol{\sigma}$ such that:

$$f(\boldsymbol{\sigma}) \leq 0. \tag{B.54}$$

From Convex Analysis, we recall the following theorem:
Theorem. Considering a limited, closed and non-empty set $S \subseteq \mathbb{R}^k$, if $\forall \mathbf{y} \in \mathbb{R}^k, \mathbf{y} \notin S$, a single $\bar{\mathbf{x}} \in S$ exists, having $\bar{\mathbf{x}}$ the minimum distance from $\mathbf{y}$, such that:

$$(\bar{\mathbf{x}} - \mathbf{x})^T (\mathbf{y} - \bar{\mathbf{x}}) \geq 0\,, \forall \mathbf{x} \in S\,, \tag{B.55}$$

the set S is convex. Condition (B.55), being $S \subseteq \mathbb{R}^9$, referring to the normality law and considering the following relations:

$$\begin{gathered} S = \{\mathbf{x} \in S \Leftrightarrow f(\mathbf{x}) \leq 0\}\,, \\ (\mathbf{y} - \bar{\mathbf{x}}) = \dot{\boldsymbol{\varepsilon}}^p\,, \\ \boldsymbol{\sigma} = \bar{\mathbf{x}}\ ,\ \boldsymbol{\sigma}^a = \mathbf{x}\,, \\ (\bar{\mathbf{x}} - \mathbf{x}) = (\boldsymbol{\sigma} - \boldsymbol{\sigma}^a), \end{gathered} \tag{B.56}$$

is coincident with condition (B.51) and implies the convexity of the set (B.54) (fig. B. 7a).

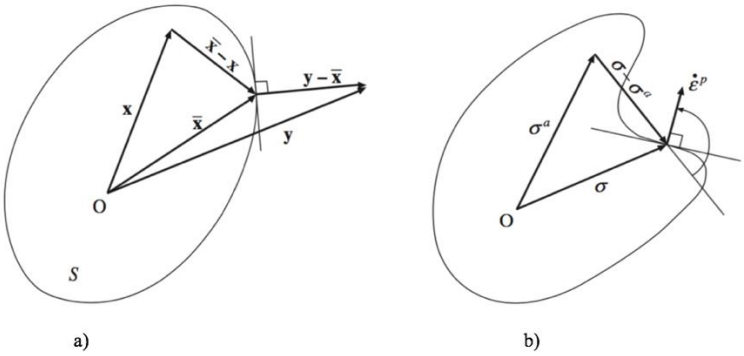

fig. B. 7: Limit domain: a) Convex domain, b) Non-convex domain [63]

Moreover, in fig. B. 7b it is shown how the non-convex domain contradicts condition (B.49), as shown by a geometric counterexample. If we consider, indeed, that exist the vectors $\boldsymbol{\sigma}, \boldsymbol{\sigma}^a, \dot{\boldsymbol{\varepsilon}}^p$ such that:

$$(\boldsymbol{\sigma} - \boldsymbol{\sigma}^a)^T \cdot \dot{\boldsymbol{\varepsilon}}^p < 0\,, \tag{B.57}$$

we prove, by contradiction, that condition (B.49) implies the convexity; if this does not happen, indeed, there would exist the vectors $\boldsymbol{\sigma}, \boldsymbol{\sigma}^a, \dot{\boldsymbol{\varepsilon}}^p$, which satisfies condition (B.57).

3. For a perfectly plastic material, in correspondence of the critical stress state $\boldsymbol{\sigma}^1$, such that:

$$f(\boldsymbol{\sigma}^1) = 0\,, \tag{B.58}$$

the corresponding plastic strain rate vector is:

$$\dot{\varepsilon}_i^{1p} = \dot{\lambda}_k \frac{\partial f_{0k}}{\partial \sigma_i}\,, \tag{B.59}$$

Now we consider, starting from the value $\boldsymbol{\sigma}^1$, the stress rate $\dot{\boldsymbol{\sigma}}' dt$, such that the following admissible condition is satisfied:

$$f(\boldsymbol{\sigma}^1 + \dot{\boldsymbol{\sigma}}' dt) \leq 0\,, \tag{B.60}$$

Thus, the stress $(\boldsymbol{\sigma}^1 + \dot{\boldsymbol{\sigma}}' dt)$ is admissible and, by virtue of the convexity of the limit domain, we have that:

$$\dot{\boldsymbol{\sigma}}' \dot{\boldsymbol{\varepsilon}}^p \leq 0\,, \tag{B.61}$$

denoting with $\dot{\boldsymbol{\sigma}}' dt$ all the possible admissible stress rates, starting from the stress state $\boldsymbol{\sigma}^1$.

4. Recalling condition (B.49), that we report in the following for convenience:

$$(\boldsymbol{\sigma} - \boldsymbol{\sigma}^a)^T \cdot \dot{\boldsymbol{\varepsilon}}^p \geq 0\,,$$

if we consider the stress state $\boldsymbol{\sigma}$, which is internal to the limit domain such that:

$$f(\boldsymbol{\sigma}) < 0\,,$$

we have that:

$$\dot{\boldsymbol{\varepsilon}}^p = 0\,,$$

If we suppose, indeed, that the stress state $\boldsymbol{\sigma}$ is internal to the limit domain, and we consider, by contradiction, that the corresponding plastic strain rate is denoted with $\dot{\boldsymbol{\varepsilon}}^p$, then there will exist a spherical neighbourhood $I(\boldsymbol{\sigma})$ that is entirely contained into the limit domain (fig. B. 8).

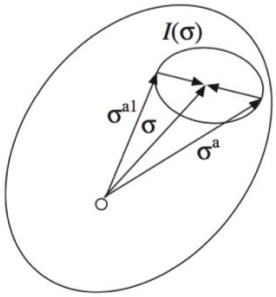

fig. B. 8: Spherical neighbourhood [63]

Now we consider any $\boldsymbol{\sigma}^a \in I(\boldsymbol{\sigma})$. Recalling the stability condition, expressed by condition (B.49), we refer to a different admissible stress $\boldsymbol{\sigma}^{a1}$ such that:

$$(\boldsymbol{\sigma} - \boldsymbol{\sigma}^{a1}) = -(\boldsymbol{\sigma} - \boldsymbol{\sigma}^a) \tag{B.62}$$

Hence the following condition holds:

$$(\boldsymbol{\sigma} - \boldsymbol{\sigma}^{a1})^T \dot{\boldsymbol{\varepsilon}} \geq 0 \Rightarrow (\boldsymbol{\sigma} - \boldsymbol{\sigma}^a)^T \dot{\boldsymbol{\varepsilon}}^p \leq 0\,, \tag{B.63}$$

Conditions (B.49) and (B.63) implies that the following condition holds:

$$(\boldsymbol{\sigma} - \boldsymbol{\sigma}^a)^T \cdot \dot{\boldsymbol{\varepsilon}}^p = 0\,,$$

which, due to the fact that the spherical neighbourhood is arbitrarily chosen, implies that:

$$\dot{\boldsymbol{\varepsilon}}^p = 0\,.$$

5. Referring to condition (B.49), with the stress $\boldsymbol{\sigma}$ that reaches the boundary of the limit convex domain, which is regular and differentiable, we have an associated plastic potential, by virtue of the normality law:

$$\dot{\varepsilon}_i^p = \dot{\lambda}\frac{\partial f}{\partial \sigma_i} \quad , \quad \dot{\lambda} \geq 0\,, \tag{B.64}$$

Let we consider, now, the hyperplane π, which is tangent to the limit boundary in correspondence of the stress value $\boldsymbol{\sigma}$, and which is such as to leave the limit domain into the negative half-space π^-, whose complementary part is denoted with π^+. It will exist a neighbourhood $I(\boldsymbol{\sigma})$ such that:

$$\forall \boldsymbol{\sigma}^a \in I(\boldsymbol{\sigma}) \cap D\,, \qquad f(\boldsymbol{\sigma}^a) \leq 0\,, \tag{B.65}$$

the vectors $(\boldsymbol{\sigma}^a - \boldsymbol{\sigma})$ can be projected into the negative half-space π^-; if, by contradiction, the plastic strain rate $\dot{\boldsymbol{\varepsilon}}^p$ does not have the same direction of ∇f (fig. B. 9), there would exist the vectors $\boldsymbol{\sigma}^a$ such that the product $(\boldsymbol{\sigma} - \boldsymbol{\sigma}^a)^{\boldsymbol{T}} \cdot \dot{\boldsymbol{\varepsilon}}^p$ is a negative quantity:

$$(\boldsymbol{\sigma} - \boldsymbol{\sigma}^a)^{\boldsymbol{T}} \cdot \dot{\boldsymbol{\varepsilon}}^p < 0\,, \tag{B.66}$$

and then condition (B.49) would be contradicted.

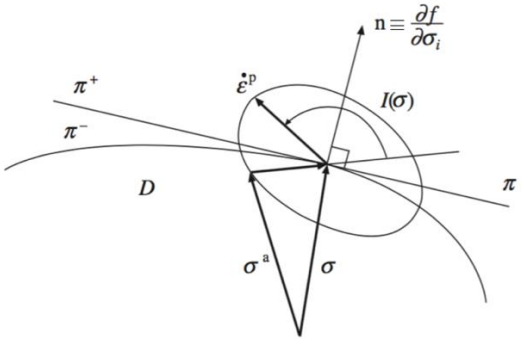

fig. B. 9: Hyperplane π [63]

Then, condition (B.64) must hold, and the condition of stability of the material, with the convexity of limit domain, implies the validity of the normality law.

6. Considering the stability condition (B.49), here repeated for convenience:

$$(\boldsymbol{\sigma} - \boldsymbol{\sigma}^a)^T \cdot \dot{\boldsymbol{\varepsilon}}^p \geq 0\,.$$

If the stress $\boldsymbol{\sigma}$ is a non-differentiable value on the limit boundary, the plastic strain rate $\dot{\boldsymbol{\varepsilon}}^p$ belongs to the outwards normals cone, that is $\dot{\boldsymbol{\varepsilon}}^p$ can be expressed as a linear combination of these outwards normals, through non-negative scalars (fig. B. 10).

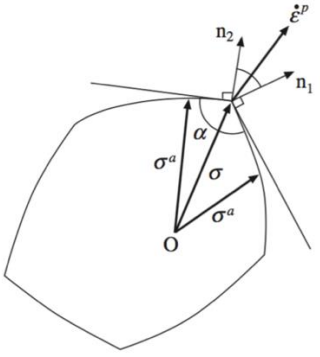

fig. B. 10: $\dot{\boldsymbol{\varepsilon}}^p$ belonging to the outwards normals cone [63]

By varying the stress $\boldsymbol{\sigma}^a$ among all the possible vectors of the limit domain, which satisfy the following condition:

$$f(\boldsymbol{\sigma}^a) \leq 0\,,$$

the vector $(\boldsymbol{\sigma} - \boldsymbol{\sigma}^a)$ describes the entire convex cone α. If we define the generic normal, which is external with respect to one of the hyperplanes tangent to the limit domain in correspondence of the stress state $\boldsymbol{\sigma}$, we have, recalling Farkas Theorem, the following condition:

$$\dot{\boldsymbol{\varepsilon}}^p = \dot{\lambda}_i \mathbf{n}_i \;\;, \dot{\lambda}_i \geq 0\,, \tag{B.67}$$

Thus, it is shown that the stability condition implies the existence of the Associated Plastic Potential, both in the case of differentiability and non-differentiability points on the limit domain.

7. Let we consider the stress $\boldsymbol{\sigma}$ on the limit domain, referred to an elastic and perfectly plastic material, such that the function $f(\boldsymbol{\sigma}) = 0$ is non-differentiable. Then we consider two different state of material, referred to two different stress increases, with the corresponding total strain increases (fig. B. 11):

$$(\boldsymbol{\sigma},\;\; d\boldsymbol{\sigma}^1,\;\; d\boldsymbol{\varepsilon}^1), \qquad (\boldsymbol{\sigma},\;\; d\boldsymbol{\sigma}^2,\;\; d\boldsymbol{\varepsilon}^2)\,,$$

which satisfy the plastic state equalities:

$$f(\boldsymbol{\sigma}) = 0, \qquad f(\boldsymbol{\sigma} + d\boldsymbol{\sigma}^1) = 0, \qquad f(\boldsymbol{\sigma} + d\boldsymbol{\sigma}^2) = 0.$$

Considering the elastic-plastic constitutive law, the virtual product $(d\boldsymbol{\sigma}^1 - d\boldsymbol{\sigma}^2)(d\boldsymbol{\varepsilon}^1 - d\boldsymbol{\varepsilon}^2)$ satisfies, in general, the following condition:

$$(d\boldsymbol{\sigma}^1 - d\boldsymbol{\sigma}^2)(d\boldsymbol{\varepsilon}^1 - d\boldsymbol{\varepsilon}^2) \geq 0, \tag{B.68}$$

which implies, for the plastic strains, the following condition:

$$(d\boldsymbol{\sigma}^1 - d\boldsymbol{\sigma}^2)(d\boldsymbol{\varepsilon}^{1p} - d\boldsymbol{\varepsilon}^{2p}) \geq 0. \tag{B.69}$$

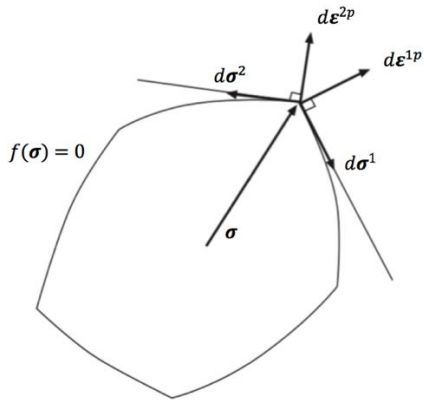

fig. B. 11: Different stress and strain increases [63]

8. Given the set of safe stress vectors $\boldsymbol{\sigma}^s$, such that:

$$f(\boldsymbol{\sigma}^s) < 0\,, \tag{B.70}$$

the set of vectors $\boldsymbol{\sigma}^s$ defines the set of admissible stress vectors $\boldsymbol{\sigma}^a$, such that:

$$f(\boldsymbol{\sigma}^a) \leq 0\,. \tag{B.71}$$

The convexity of the set $\boldsymbol{\sigma}^a$ holds as well as that of the set $\boldsymbol{\sigma}^s$.
If we refer to the vector $\boldsymbol{\sigma}$, belonging to the boundary of the yielding domain, such that:

$$f(\boldsymbol{\sigma}) = 0\,, \tag{B.72}$$

It can be shown the existence of a hyperplane D for the stress vector $\boldsymbol{\sigma}$, which is defined by an outwards normal vector **n** such that:

$$\mathbf{n} \cdot (\boldsymbol{\sigma}^a - \boldsymbol{\sigma}) \leq 0\ , \qquad \forall \boldsymbol{\sigma}^a : f(\boldsymbol{\sigma}^a) \leq 0\,, \tag{B.73}$$

and:

$$\mathbf{n} \cdot (\boldsymbol{\sigma}^s - \boldsymbol{\sigma}) < 0\ , \qquad \forall \boldsymbol{\sigma}^s : f(\boldsymbol{\sigma}^s) < 0\,, \tag{B.74}$$

By virtue of the normality law, for $\dot{\boldsymbol{\varepsilon}}^p$ corresponding to the stress vector $\boldsymbol{\sigma}$, we have:

$$(\boldsymbol{\sigma} - \boldsymbol{\sigma}^s)^T \cdot \dot{\boldsymbol{\varepsilon}}^p > 0\ , \qquad \forall \boldsymbol{\sigma}^s : f(\boldsymbol{\sigma}^s) < 0\,. \tag{B.75}$$

9. From the stability condition, here reported for convenience:

$$(\boldsymbol{\sigma} - \boldsymbol{\sigma}^a)^T \cdot \dot{\boldsymbol{\varepsilon}}^p \geq 0\,,$$

for a perfectly plastic material, we have that:

$$\boldsymbol{\sigma}^a \cdot \dot{\boldsymbol{\varepsilon}}^p \leq \boldsymbol{\sigma} \cdot \dot{\boldsymbol{\varepsilon}}^p \ , \qquad \forall \boldsymbol{\sigma}^a \ \ s.t. \ f(\boldsymbol{\sigma}^a) \leq 0 \, , \tag{B.76}$$

where $\dot{\boldsymbol{\varepsilon}}^p$ corresponds to the stress vector $\boldsymbol{\sigma}$.

B.2 Theorems of Limit Analysis

We refer to elastic-plastic materials, characterized by an associate plastic potential, according to the normality law and the stability postulate by Drucker: such materials are briefly defined as *normal materials* or *stable materials*.

When we consider an elastic-plastic material, stresses cannot grow indefinitely, since they cannot exceed the yielding limits; for this reason, the body loads **b** and the tractions $\underline{\mathbf{s}}$ cannot be indefinitely amplified.

We now introduce some definitions:

- We define *plastic collapse* the phenomenon in which, by increasing the load, the structure reaches a limit value for the load system (**b**, $\underline{\mathbf{s}}$), called *limit load*, which cannot be further amplified; the strains, however, can grow indefinitely, and consequently also the displacements of the whole structure or a part of it.
- The part of the displacement field, which indefinitely grows in correspondence of the collapse, and its consequent strains, define a *collapse mechanism*.
- The stress field $\boldsymbol{\sigma}^a$ is called *statically admissible stress field*, if it satisfies the equilibrium equalities (B.77) and the boundary equalities (B.78):

$$\frac{\partial \sigma_{ij}^a}{\partial x_i} + b_i = 0 \ , \qquad x \in V \, , \tag{B.77}$$

$$\sigma_{ij}^a n_j = s_i \ , \qquad x \in \partial V \, , \tag{B.78}$$

as well as the compatibility condition:

$$f(\boldsymbol{\sigma}^a) \leq 0 \, , \tag{B.79}$$

being n the outwards normal of the volume V, whose boundary is ∂V.

- We call *admissible loads* the load system $(\mathbf{b}, \underline{\mathbf{s}})$ which is in equilibrium with the admissible stress field $\boldsymbol{\sigma}^a$ so that the set $(\mathbf{b}, \underline{\mathbf{s}}, \boldsymbol{\sigma}^a)$ is said to be equilibrated. The collapse load system $(\mathbf{b}, \underline{\mathbf{s}})$ and the stress $\boldsymbol{\sigma}$ at collapse, represent the *admissible load-stress system* $(\mathbf{b}, \underline{\mathbf{s}}, \boldsymbol{\sigma})$ that occurs under the collapse of the structure.

- The stress field $\boldsymbol{\sigma}^s$ is called *statically safe stress field* or *safe stress field*, if it satisfies the equilibrium equalities (B.77) and the boundary equalities (B.78), and also the compatibility condition:

$$f(\boldsymbol{\sigma}^s) < 0\,, \tag{B.80}$$

and the load system $\left(\mathbf{b}^s, \underline{\mathbf{s}}^s\right)$ which is in equilibrium with this safe stress field is said *safe load system.*

- We consider the displacement rate field $\dot{\mathbf{u}}_\mathbf{0}$, which satisfies the kinematic conditions on the constrained boundary of the domain *V*:

$$\dot{\mathbf{u}}_\mathbf{0} = \underline{\dot{\mathbf{u}}}_\mathbf{0}\,, \qquad \mathbf{x} \in \partial V_D\,, \tag{B.81}$$

The corresponding infinitesimal strains rate field, which satisfies the kinematic conditions with $\dot{\mathbf{u}}_\mathbf{0}$, are expressed as follows:

$$\dot{\varepsilon}_{0ij} = \frac{1}{2}\left(\frac{\partial \dot{u}_{0i}}{\partial x_j} + \frac{\partial \dot{u}_{0j}}{\partial x_i}\right), \qquad \mathrm{x} \in \partial V\,. \tag{B.82}$$

The set $(\dot{\mathbf{u}}_\mathbf{0}, \dot{\varepsilon}_0)$ is said *kinematically admissible strain-displacement field*, or briefly *admissible kinematism*.

Static Theorem of Plastic Collapse

Part I. If a load program is assigned, the existence of a statically safe stress field $\boldsymbol{\sigma}^s$, for each instant of the load program, is a sufficient condition so that the plastic collapse will not occur.

Part II. The structure cannot bear an external load system if does not exist an admissible stress distribution $\boldsymbol{\sigma}^a$. In such a case, indeed, the equilibrium is not possible unless we violate the material yield limit. Hence, the existence of a statically admissible stress field $\boldsymbol{\sigma}^a$ is a necessary condition so that the plastic collapse will not occur.

Considering, indeed, the virtual work relation:

$$\int_V \dot{\mathbf{b}} \cdot \dot{\mathbf{u}} dV + \int_{\partial V} \dot{\mathbf{s}} \cdot \dot{\mathbf{u}} dS = \int_V \dot{\boldsymbol{\sigma}} \cdot \dot{\boldsymbol{\varepsilon}} dV = 0\,, \tag{B.83}$$

remembering that the strain can be decomposed in an elastic and a plastic part:

$$\boldsymbol{\varepsilon} = \boldsymbol{\varepsilon}^e + \boldsymbol{\varepsilon}^p\,,$$

we obtain:

$$\int_V \dot{\boldsymbol{\sigma}} \cdot (\dot{\boldsymbol{\varepsilon}}^e + \dot{\boldsymbol{\varepsilon}}^p) dV = 0 \,, \tag{B.84}$$

Referring to a perfectly plastic material, the following condition occurs:

$$\dot{\boldsymbol{\sigma}} \cdot \dot{\boldsymbol{\varepsilon}}^p = 0 \,, \tag{B.85}$$

even where $\dot{\boldsymbol{\varepsilon}}^p \neq 0$. Hence, condition (B.84) can be rewritten as follows:

$$\int_V \dot{\boldsymbol{\sigma}} \cdot \dot{\boldsymbol{\varepsilon}}^e dV = 0 \,. \tag{B.86}$$

Therefore, we can say that:

$$\int_V \dot{\boldsymbol{\sigma}} \cdot \dot{\boldsymbol{\varepsilon}}^e dV = \int_V \dot{\boldsymbol{\sigma}} \cdot (\mathbf{C}^{-1}\, \dot{\boldsymbol{\sigma}}) dV = \int_V \dot{\boldsymbol{\varepsilon}}^e \cdot (\mathbf{C}\, \dot{\boldsymbol{\varepsilon}}^e) dV = 0 \,, \tag{B.87}$$

being $\mathbf{C}^{-1}$ and $\mathbf{C}$ quadratic forms definite positive.
Hence, referring to the collapse mechanisms we have that the following conditions hold:

$$\dot{\boldsymbol{\sigma}} = \mathbf{0} \,, \qquad \dot{\boldsymbol{\varepsilon}}^e = \mathbf{0} \,, \qquad \dot{\boldsymbol{\varepsilon}} = \dot{\boldsymbol{\varepsilon}}^p \,, \tag{B.88}$$

that is the collapse mechanism exhibits only plastic strain rate $\dot{\boldsymbol{\varepsilon}}^p$, corresponding to the collapse rate $\dot{\mathbf{u}}$.
This theorem allowed the development of methods able to obtain lower bounds of the limit load, or to evaluate the safety structures under assigned loads. We can, indeed, immediately exclude the collapse for a structure under assigned load set $(\mathbf{b}, \underline{\mathbf{s}})$, only by determining a safe stress fields equilibrated with the external load set. Reference to the constitutive law or the elastic solution is not needed.

Kinematic Theorem of Plastic Collapse

Let we consider the admissible mechanism $(\dot{\mathbf{u}}^0, \dot{\boldsymbol{\varepsilon}}^0)$, the collapse load-stress set $(\mathbf{b}, \underline{\mathbf{s}}, \boldsymbol{\sigma})$ and the actual collapse mechanism $(\dot{\mathbf{u}}, \dot{\boldsymbol{\varepsilon}})$. Now we can write the virtual power equalities:

$$\int_V \boldsymbol{\sigma} \cdot \dot{\boldsymbol{\varepsilon}}^0 \, dV - \int_{\partial V} \underline{\mathbf{s}} \cdot \dot{\mathbf{u}}^0 \, dS - \int_V \mathbf{b} \cdot \dot{\mathbf{u}}^0 \; dV = 0 \,, \tag{B.89}$$

$$\int_V \boldsymbol{\sigma} \cdot \dot{\boldsymbol{\varepsilon}}\ dV - \int_{\partial V} \underline{\mathbf{s}} \cdot \dot{\mathbf{u}}\ dS - \int_V \mathbf{b} \cdot \dot{\mathbf{u}}\, dV = 0\,. \tag{B.90}$$

We know that the elastic strain rate is zero in correspondence of a kinematically admissible mechanism:

$$\dot{\boldsymbol{\varepsilon}}^0 = \dot{\boldsymbol{\varepsilon}}^{0p}. \tag{B.91}$$

Hence, conditions (B.89) and (B.90) can be rewritten as follows:

$$\int_V \boldsymbol{\sigma} \cdot \dot{\boldsymbol{\varepsilon}}^{0p}\ dV - \int_{\partial V} \underline{\mathbf{s}} \cdot \dot{\mathbf{u}}^0\ dS - \int_V \mathbf{b} \cdot \dot{\mathbf{u}}^0\ \ dV = 0\,, \tag{B.92}$$

$$\int_V \boldsymbol{\sigma} \cdot \dot{\boldsymbol{\varepsilon}}^{p}\ dV - \int_{\partial V} \underline{\mathbf{s}} \cdot \dot{\mathbf{u}}\, dS - \int_V \mathbf{b} \cdot \dot{\mathbf{u}}\, dV = 0\,. \tag{B.93}$$

Let we consider, now, a statically admissible stress state $\boldsymbol{\sigma}^0$, satisfying the normality law with respect to the $\dot{\boldsymbol{\varepsilon}}^{0p}$, such that:

$$\boldsymbol{\sigma} \cdot \dot{\boldsymbol{\varepsilon}}^{0p} \leq \boldsymbol{\sigma}^0 \cdot \dot{\boldsymbol{\varepsilon}}^{0p}\,, \tag{B.94}$$

By replacing condition (B.94) in conditions (B.92) and (B.93), we have:

$$\begin{aligned} \int_V \boldsymbol{\sigma}^0 \cdot \dot{\boldsymbol{\varepsilon}}^{0p}\ dV - \int_{\partial V} \underline{\mathbf{s}} \cdot \dot{\mathbf{u}}^0\ dS - \int_V \mathbf{b} \cdot \dot{\mathbf{u}}^0\ \ dV \\ \geq \int_V \boldsymbol{\sigma} \cdot \dot{\boldsymbol{\varepsilon}}^{p}\ dV - \int_{\partial V} \underline{\mathbf{s}} \cdot \dot{\mathbf{u}}\, dS - \int_V \mathbf{b} \cdot \dot{\mathbf{u}}\ \ dV\,. \end{aligned} \tag{B.95}$$

Where the first integral at the left-hand represents the power dissipation, or internal power, and can be denoted with $\dot{D}$:

$$\dot{D} = \int_V \boldsymbol{\sigma}^0 \cdot \dot{\boldsymbol{\varepsilon}}^{0p}\ dV\,, \tag{B.96}$$

the sum of the second and third integral at the left-hand represents the load power or external power, and is indicated with $\dot{W}$:

$$\dot{W} = \int_{\partial V} \underline{\mathbf{s}} \cdot \dot{\mathbf{u}}^0 \, dS - \int_V \mathbf{b} \cdot \dot{\mathbf{u}}^0 \, dV \,, \tag{B.97}$$

The left-hand term in (B.95) represents, hence, the total power dissipation and it is defined in the class of kinematically admissible mechanism.
Consequently, condition (B.95) can be shortly rewritten as:

$$\dot{D} - \dot{W} \geq 0 \,, \tag{B.98}$$

and represents the *kinematic theorem of plastic collapse*, which states that the functional power dissipation exhibits its minimum value in correspondence of the actual collapse mechanism. In particular, in correspondence of the actual collapse mechanism, the following condition occurs:

$$\dot{D} = \dot{W} \tag{B.99}$$

This condition is usually imposed in order to determine the optimal collapse load with reference to a class of kinematically admissible mechanisms.
Through the functionals $\dot{D}$ and $\dot{W}$, we can report the following statements:

- The existence of a kinematical admissible mechanism, for which the following condition occurs:

  $$\dot{D} < \dot{W} \,, \tag{B.100}$$

  represents a sufficient condition so that the plastic collapse will not occur.

- When the following condition, with reference to each kinematically admissible mechanism, occurs:

  $$\dot{W} \leq \dot{D} \,, \tag{B.101}$$

  it represents a necessary condition so that the structure is able to sustain the loads, and the plastic collapse will not occur.

- When the following condition, with reference to each kinematically admissible mechanism, occurs:

  $$\dot{W} < \dot{D} \,, \tag{B.102}$$

  it represents a sufficient condition so that the structure is able to sustain the loads.

References

[1] M. Como, Statica delle costruzioni in muratura, Aracne, 2010.

[2] J. Heyman, The stone skeleton, Cambridge University Press, 1995.

[3] S. Huerta, «Galileo was wrong: the geometrical design of masonry arches,» *Nexus Netw. J.*, vol. 8(2), pp. 25-52, 2006.

[4] F. Derand, L'architecture des voutes, Cramoisy, 1643.

[5] M. Angelillo, A. Fortunato, «Equilibrium of masonry vaults,» *Novel approaches in civil engineering*, pp. 105-111, 2004.

[6] P. Lenza, A. Ghersi, B. Calderoni, Edifici in muratura, Dario Flaccovio, 2011.

[7] P. Block, M. DeJong, J. Ochsendorf, «As Hangs the Flexible Line: Equilibrium of masonry arches,» *Nexus Netw. J.*, vol. 8, pp. 13-24, 2006.

[8] J. Heyman, «The stone skeleton,» *Int. J. Solids Struct.*, vol. 2(2), pp. 249-279, 1966.

[9] C. Formenti, La pratica del fabbricare, Hoepli, 1893-1895.

[10] G. Brandonisio, E. Mele, A. De Luca, «Limit analysis of masonry circular buttressed arches under horizontal loads,» *Meccanica*, pp. 1-19, 2017.

[11] M. Angelillo, Statica ed elementi di dinamica, Maggioli, 2016.

[12] S. Huerta, F. Foce, «Vault theory in Spain between XVIIIth and XIXth century: Monasterio's unpublished manuscript " Nueva Teórica de las Bóvedas",» *Proceedings of the First International Congress on Construction History, Madrid*, pp. 1155-1166, 2003.

[13] C. Cennamo, F. De Serio, A. Fortunato, A. Gesualdo, A. Iannuzzo, M. Angelillo, «The kinematical problem for masonry-like structures: an energy approach,» (submitted).

[14] J. Heyman, Structural analysis: a historical approach, Cambridge University Press, 1998.

[15] S. Huerta, «Structural design in the work of Gaudì,» *Architectural Science Review,* vol. 49(4), pp. 324-339, 2006.

[16] S. Huerta, «The analysis of masonry architecture: A historical approach: To the memory of professor Henry J. Cowan,» *Architectural Science Review,* vol. 51(4), pp. 297-328, 2008.

[17] A. Kooharian, «Limit Analysis of Voussoir (Segmental) and Concrete Archs,» *Journal Proceedings,* vol. 49(12), pp. 317-328, 1952.

[18] S. Huerta, «Geometry and equilibrium: the gothic theory of structural design,» *Struct. Eng.,* vol. 84(2), pp. 23-28, 2006.

[19] S. Huerta, «The debate about the structural behaviour of gothic vaults: From Viollet-le-Duc to Heyman,» *Proceedings of the Third International Congress on Construction History,* 20-24 May 2009.

[20] M. Como, «Equilibrium and collapse analysis for masonry bodies,» *Masonry Constructions,* pp. 185-194, 1992.

[21] A. Fortunato, E. Babilio, M. Lippiello, A. Gesualdo, M. Angelillo, «Limit Analysis for unilateral Masonry-like Structures,» *Open. Construct. Build. Tech.,* vol. 10(1), pp. 346-362, 2016.

[22] M. Gilbert, «Limit analysis applied to masonry arch bridges: state-of-the-art and recent developments,» *5th International Arch Bridges Conference,* pp. 13-28, 2007.

[23] M. Angelillo, Mechanics of Masonry Structures, Springer, 2014.

[24] A. Mauro, G. De Felice, M. J. DeJong, «The relative dynamic resilience of masonry collapse mechanism,» *Eng. Struct.,* vol. 85, pp. 182-194, 2015.

[25] R. Luciano, E. Sacco, «Homogenization technique and damage model for old masonry material,» *Int. J. Solids Struct.,* vol. 34(24), pp. 3191-3208, 1997.

[26] E. Sacco, «A nonlinear homogenization procedure for periodic masonry,» *Eur. J. Mech. A-Solids,* vol. 28, pp. 209-222, 2009.

[27] P. De Buhan, G. De Felice, «A homogenization approach to the ultimate strength of brick masonry,» *J. Mech. Phys. Solids,* vol. 45(7), pp. 1085-1104, 1997.

[28] E. Méry, «Sur l'équilibre des voûtes en berceau,» *Annales des ponts et chaussées,* vol. 19, pp. 50-70, 1840.

[29] M. Lucchesi, M. Silhavy, N. Zani, «Singular equilibrated stress fields for no-tension panels,» *Mechanical Modelling and Computational Issues in Civil Engineering,* vol. 23, pp. 255-265, 2005.

[30] M. Angelillo, A. Fortunato, A. Montanino, M. Lippiello, «Singular stress fields for masonry walls: Derand was right,» *Meccanica,* vol. 49(5), pp. 1243-1262, 2014.

[31] M. Gurtin, «The linear theory of elasticity,» in *Handbuch der Physik*, vol. VIa/2, Springer-Verlag, 1972.

[32] M. Angelillo, E. Babilio, A. Fortunato, «Numerical solutions for crack growth based on the variational theory of fracture,» *Comp. Mech.*, vol. 50(3), pp. 285-301, 2012.

[33] A. Gesualdo, M. Monaco, «Constitutive behaviour of quasi-brittle materials with anisotropic friction,» *Lat. Am. J. Solids Struct.*, vol. 12(4), pp. 695-710, 2015.

[34] M. Monaco, M. Guadagnuolo, A. Gesualdo, «The role of friction in the seismic risk mitigation of freestanding art objects,» *Nat. Hazards*, vol. 73(2), pp. 389-402, 2014.

[35] F. De Serio, M. Angelillo, A. Gesualdo, A. Iannuzzo, M. Pasquino, «Masonry structures made of monolithic blocks with an application to spiral stairs,» *Meccanica*, (submitted).

[36] C. Cennamo, A. Fortunato, A. Gesualdo, M. Lippiello, A. Montanino, M. Angelillo, «An energy approach to the analysis of unilateral masonry-like structures,» (submitted).

[37] A. Iannuzzo, M. Angelillo, E. De Chiara, F. De Serio, F. De Guglielmo, A. Gesualdo, «Modelling the cracks produced by settlements in masonry structures,» *Meccanica*, (submitted).

[38] C. Cennamo, M. Angelillo, C. Cusano, «Structural failures due to anthropogenic sinkholes in the urban area of Naples and the effect of a FRP retrofitting,» *Compos. Pt. B-Eng.*, vol. 108(1), pp. 190-199, 2017.

[39] R. K. Livesley, «Limit analysis of structures formed from rigid blocks,» *Int. J. Numer. Methods Eng.*, vol. 12, pp. 1853-1871, 1978.

[40] G. B. Dantzig, A. Orden, P. Wolfe, «The generalized simplex method for minimizing a linear form under linear inequality restraints,» *Pac. J. Math.*, vol. 5(2), pp. 183-195, 1955.

[41] S. Mehrotra, «On the implementation of a primal-dual interior point method.,» *SIAM J. Optim.*, vol. 2, pp. 575-601, 1992.

[42] Y. Zhang, «Solving large-scale linear programs by interior-point methods under the Matlab Environment,» *Optimization Methods and Software*, vol. 10(1), pp. 1-31, 1998.

[43] G. De Felice, «Out-of-plane seismic capacity of masonry depending on wall section morphology,» *Int. J. Archit. Herit.*, vol. 5, pp. 466-482, 2011.

[44] V. Sarhosis, K. Bagi, J. V. Lemos, G. Milani, Computational Modeling of Masonry Structures Using the Discrete Element Method, IGI Global, 2016.

[45] B. Rigo, K. Bagi, «Discrete element analysis of cantilever stairs,» (submitted).

[46] J. Heyman, «The mechanics of masonry stairs,» *WIT Transaction on The Built Environment*, vol. 17, 1970.

[47] M. Angelillo, «The equilibrium of helical stairs made of monolithic steps,» *Int. J. Archit. Herit.*, vol. 10(6), pp. 675-687, 2016.

[48] F. Fraternali, M. Angelillo, A. Fortunato, «A lumped stress method for plane elastic problems and the discrete-continuum approximation,» *Int. J. Solids Struct.,* vol. 39, pp. 6211-6240, 2002.

[49] F. Fraternali, M. Angelillo, G. Rocchetta, «On the Stress Skeleton of Masonry Vaults and Domes,» *PACAM VII,* pp. 369-372, 2002.

[50] F. Fraternali, «A thrust network approach to the equilibrium problem of unreinforced masonry vaults via polyhedral stress functions,» *Mech. Res. commun.,* vol. 37(2), pp. 198-204, 2010.

[51] M. Angelillo, E. Babilio, A. Fortunato, «Singular stress fields for masonry-like vaults,» *Continuum Mech. Termodyn.,* vol. 25, pp. 423-441, 2013.

[52] D. O' Dwyer, «Funicular analysis of masonry vaults,» *Comput. Struct.,* vol. 73, pp. 187-197, 1999.

[53] P. Block, «Thrust Network Analysis: exploring three-dimensional equilibrium. PhD Thesis,» *Massachusetts Institute of Technology,* 2009.

[54] P. Block, T. Ciblac, J. Ochsendorf, «Real-time limit analysis of vaulted masonry buildings,» *Comput. Struct.,* vol. 84(29), pp. 1841-1852, 2006.

[55] E. Vouga, M. Hobinger, J. Wallner, H. Pottmann, «Design of Self-supporting Surfaces,» *ACM Trans. Graph.,* vol. 31(4), n. 87, 2012.

[56] F. De Goes, P. Alliez, H. Owhadi, M. Desbrun, «On the equilibrium of simplicial masonry structures,» *ACM Trans. Graph.,* vol. 32(4), n. 93, 2013.

[57] P. Block, L. Lachauer, «Three-dimensional funicular analysis of masonry vaults,» *Mech. Res. Commun.,* vol. 56, pp. 53-60, 2014.

[58] M. Miki, T. Igarashi, P. Block, «Parametric self-supporting surfaces via direct computation of airy stress functions,» *ACM Trans. Graph.,* vol. 34(4), n. 89, 2015.

[59] F. Marmo, L. Rosati, «Reformulation and extension of the thrust network analysis,» *Comput. Struct.,* vol. 182, pp. 104-118, 2017.

[60] M. Angelillo, «Static analysis of a Gustavino helical stair as a layered masonry shell,» *Compos. Struct.,* vol. 119, pp. 298-304, 2015.

[61] A. Gesualdo, C. Cennamo, A. Fortunato, G. Frunzio, M. Monaco, «Equilibrium formulation of masonry helical stairs,» *Meccanica,* pp. 1-12, 2016.

[62] G. B. Dantzig, Linear Programming, 1: Introduction, Springer, 1997.

[63] L. Nunziante, Scienza delle Costruzioni terza edizione, McGraw-Hill, 2011.

Web sites

a. ***Linear programming in Matlab***

https://it.mathworks.com/help/optim/ug/linprog.html?requestedDomain=www.mathworks.com

b. ***Linear programming***

https://faculty.washington.edu/toths/Presentations/Lecture%202/Ch11_LPIntro.pdf

c. ***Photos of the stair of San Domingos de Bonaval***

http://www.alamy.com/stock-photo-spiral-staircase-in-the-convent-of-santo-domingo-de-bonaval-santiago-15614850.html

d. ***Photo of Basilica of Hagia Sophia***

http://haemus.org.mk/hagia-sophia-facts-history-architecture/

e. ***Photo of Partenone***

https://www.stoodi.com.br/blog/2016/09/22/filosofia-tudo-sobre-socrates/

f. ***Photo of Porta dei Leoni***

http://www.multytheme.com/cultura/multimedia/didattmultitema/scuoladg/storiarte/artemiceneaportaleoni.html

g. ***Photo of Pantheon***

http://www.travelsintranslation.com/2014/11/rome-wasnt-built-day-can-explored-one/

h. ***Photo of Castel del Monte***

http://autoservizieleonora.it/2016/04/13/castel-del-monte/

i. Photo of Notre Dame Cathedral
https://frenchmoments.eu/west-facade-of-notre-dame-cathedral-paris/

j. Photo of St. Peter's dome
https://historiaetageografia3.wordpress.com/aro-modernoko-europako-artea-errenazimendua-eta-barrokoa/errenazimenduko-artea/

k. Photo of façade of Sagrada Familia
https://jfistere.wordpress.com/2010/05/11/barcelona-day-2/

l. Photo of Gaudì's catenary
http://www.owitalia.org/sito/php/scheda.php?nazione=Spagna&libro=ow

m. Photo of hanging chain and catenary arch
https://plus.google.com/+LarryPhillipsTutor/posts/gDcBd42X3y9

n. Photo of Mutual contrast effect in voussoir arch
http://masonrydesign.blogspot.it/2012_07_01_archive.html

o. Photo of Trevi's arch
http://www.montiernici.it/arcoditrevi/acroditrevi.htm

p. Photo of Poleni's study about St. Peter's dome
https://sudu1construction.wordpress.com

q. Photo of Wedge Theory by De La Hire
http://www.ing.unitn.it/~cazzani/didattica/SdM/Materiale%20per%20relazioni/Contributi_italiani_alla_statica_dell'arco/Archi_volte_e_cupole.pdf

r. Photos of masonry fractures
http://www.monitoraggiofessure-mg.it/index.php?fbl=a3
http://www.assorestauro.org/it/progetti/da-qa-022015/la-domus-tiberiana-al-palatino.html
http://www.tbredcontractors.com/services/masonry-sealant-work/
http://www.archboston.org/community/showthread.php?p=247651
https://brickrestoration.com/repairs-restorations/
http://www.granitefoundationrepair.com/tag/crack/
http://www.concretecivil.com/professionalknow_view.php?id=213
http://db.world-housing.net/building/80/
http://www.promozioneacciaio.it/cms/it5400-rottura-a-taglio-dei-maschi-murari.asp#prettyPhoto

http://www.wikitecnica.com/author/coisson-eva/
http://www.controllofessure-mg.it/index.php?fbl=a3